Three-dimensional structural image analysis and mechanics of snow

Von der Fakultät Maschinenbau
der Technischen Universität Dortmund
zur Erlangung des Grades eines
Doktor-Ingenieurs
(Dr.-Ing.)
genehmigte Dissertation

von

Thiemo Theile

Davos 2010

Contents

Summary

This work deals with the problem of predicting the mechanical behaviour of dry snow based on the geometries and properties of its constituents. This approach is known as homogenisation. The main constituents of dry snow are ice and air. Their geometry, i.e. the microstructure, varies widely depending on the type of snow. The shape of individual, sintered snow grains varies and may take the form of stellar crystals, rounded and facetted grains or depth hoar crystals. The porosity (air fraction) ranges from 15% for dense firn to 95% for fresh snow. This wide range of microstructures and porosities is associated with a variety of mechanical properties. For example, the viscosity varies over six orders of magnitude for different snow types. This diversity of snow types and their associated properties complicates the study and description of snow and its mechanical properties. A large number of material tests would be necessary to capture the mechanical properties of all snow types. However, these tests are difficult to perform, especially with fragile snow types. Furthermore, the classical characterisation of snow, based on porosity, grain size and grain shape, describes the mechanical properties of snow only roughly. For example, a parameterisation according to porosity results in a scatter of factor 100 of the measured properties.

The aim of the research described here was to approach these problems by examining the connection between snow's microstructure and its macroscopic behaviour. The method used involved the following steps: 'capturing' and then simplifying the microstructure; simulating the macroscopic behaviour based on the properties of ice and the simplified microstructure; and finally verifying the model using measured values.

The microstructure was captured in a microcomputer tomograph (μCT). This device allowed the complex three-dimensional microstructure of snow to be recorded non-destructively. A challenge was then how to process these extensive, three-dimensional data. One focus of this work was on developing image-processing algorithms to simplify these data. The simplified microstructure was then used as input for micromechanical models.

Three different methods to simplify the real microstructure were developed and adjusted to the requirements of three different micromechanical models. The models describe the contact between a ski and snow; the creep of snow; and the brittle failure of snow. The first method to simplify the microstructure approximates the snow surface with spheres and the second approximates the complete microstructure with beams. The third method decomposes the microstructure where it tapers into grains. The different micromechanical models use the resulting simplifications and are explained below.

The contact model predicts the number and size of the contact spots between the ski and the snow. These are important parameters to determine the friction on snow. μCT images of the snow surface are captured before and after an impact experiment. The contact is modelled based on an approximation of the captured snow surface with spheres and the mechanical behaviour of the surface grains. The model is verified by comparing the measured and the modelled

force-displacement curves. However, it contains two free material parameters, which describe the behaviour of the surface grains. The creep and fracture models described below have, in contrast, no free material parameters.

The creep model simulates the viscous behaviour of snow. An in-situ creep experiment was performed inside a microcomputer tomograph to measure the macroscopic viscosities and obtain μCT images of the same sample. The microstructure from the μCT images was approximated with beams and simulated using the finite element method. Glen's creep law of monocrystalline ice was used as the material model. The approximation of the microstructure with beams permits the creep simulation of large snow volumes, which is otherwise computationally expensive. These volumes were large enough to ensure the behaviour of the volume corresponded to the macroscopic behaviour of snow. The validated model enables new insights into the deformation mechanisms in snow and raises doubts about the established theory in snow mechanics that grain boundary sliding is the dominant deformation mechanism. This mechanism is not considered in the creep model, and recent discussion in the literature also indicates that grain boundary sliding is not a dominant deformation mechanism. Another established theory is that snow is a kind of foam made up of ice. The creep model shows that the creation of new connections is an important mechanism during the compaction of snow, but this is not a mechanism that foam theories take into account.

The fracture model is nearly identical to the creep model, but it includes an additional fracture criterion based on the strength of monocrystalline ice. μCT images, captured before and after fracture tests with snow, are used as input to the model, which is then verified by the measured strengths. This model exemplifies how the beam model can be transferred to different load cases.

This thesis describes the first verified model of the macroscopic behaviour of snow to be made without free material parameters and based only on its microstructure and the behaviour of ice. The three-dimensional image processing methods described here make it possible to simplify and model the complex microstructure of snow. One method involved making, for the first time, μCT-Scans of a snow sample that had been experimented on, which enabled the verification of the micromechanical models. It was beyond the scope of this research to cover a wide range of load cases and snow types. In future research, these models should be tested with different load and snow types to determine more mechanical properties of a wider range of snow types and thus improve our understanding of snow mechanics.

Zusammenfassung

Diese Arbeit befasst sich mit dem Problem, das mechanische Verhalten von Schnee ausgehend von dem Verhalten seiner Bestandteile und deren geometrischer Anordnung zu bestimmen. Dieses Vorgehen wird auch Homogenisierung genannt. Die Hauptbestandteile in trockenem Schnee, auf den sich diese Arbeit beschränkt, sind Luft und Eis. Die geometrische Anordnung der Bestandteile (Mikrostruktur) variiert in verschiedenen Schneearten stark. Die Form der einzelnen, gesinterten Schneekörner variiert von sechseckigen, dendritischen Schneekristallen, über abgerundete oder kantige Körner bis zu Becherkristallen. Die Porosität (Luftanteil) reicht von 15% für dichten Firn bis 95% für Neuschnee. Mit dieser großen Bandbreite an geometrischen Anordnungen und Porositäten geht auch eine große Bandbreite an mechanischen Eigenschaften einher. Die Viskosität beispielsweise variiert für verschiedene Schneearten über sechs Größenordnungen. Diese große Vielfalt an Schneearten mit unterschiedlichsten Eigenschaften erschwert die Beschreibung und Untersuchung des mechanischen Verhaltens von Schnee. Eine große Anzahl an Experimenten zur Werkstoffprüfung wäre nötig, um die ganze Bandbreite an Schneearten zu erfassen. Besonders für die fragilen Schneearten sind solche Experimente allerdings äußerst schwierig durchzuführen. Außerdem hat sich im Laufe der Zeit gezeigt, dass die klassische Charakterisierung von Schnee aufgrund von Porosität, Korngröße und Kornform nur grob erfolgt. Eine Parametrisierung nur über die Porosität resultiert in einer großen Streuung (bis zu Faktor 100) der gemessenen Eigenschaften.

Die Motivation dieser Arbeit ist, einen Beitrag zur Lösung dieser Probleme zu leisten, indem der Zusammenhang zwischen Mikrostruktur und makroskopischen Schneeeigenschaften genauer untersucht wird. Die in dieser Arbeit benutzte Methode umfasst folgende Schritte: Erfassen der Mikrostruktur, Vereinfachen der Mikrostruktur, Simulation des makroskopischen Verhaltens ausgehend von der vereinfachten Mikrostruktur und dem mechanischen Verhalten von Eis, und schließlich der Verifikation mit gemessenen Werten.

Die Mikrostruktur wird im Mikrocomputertomographen (μCT) erfasst. Diese Technik erlaubt, die komplexe Mikrostruktur von Schnee dreidimensional und zerstörungsfrei zu erfassen. Ein zentrales Problem ist, wie aus diesen umfangreichen, dreidimensionalen Daten geeignete, möglichst einfache Modelle erstellt werden können. Das Vereinfachen der Mikrostruktur mit neuen dreidimensionalen Bildverarbeitungsmethoden ist ein Schwerpunkt dieser Arbeit.

Drei verschiedene Methoden zur Vereinfachung der realen Mikrostruktur wurden entwickelt. Die verschiedenen Methoden sind an die Anforderungen von drei unterschiedlichen Modellen angepasst. Die Modelle beschreiben Verformungen beim Kontakt zwischen Schnee und Ski, das Kriechen von Schnee und das spröde Versagen von Schnee. Ein Vereinfachungsalgorithmus approximiert die Schneeoberfläche durch Kugeln; ein zweiter approximiert die Schneestruktur durch Balken; und ein dritter zerlegt die Schneestruktur an Verjüngungen in einzelne Körner. In den verschiedenen Modellen zur Beschreibung des makroskopischen Verhaltens wurden diese Vereinfachungen benutzt und mit Experimenten verifiziert.

Das Kontaktmodell sagt die Anzahl und Größe der Kontaktpunkte zwischen Ski und Schnee voraus - wichtige Parameter für die Reibung auf Schnee. Vier verschiedene Deformationsmechanismen können durch Vergleich der Schneeoberfläche in μCT-Bildern vor und nach dem Skikontakt und in aufgenommenen Kraft-Weg-Kurven ausgemacht und im Modell implementiert werden. Die topographische Beschreibung der Schneeoberfläche gekoppelt mit dem mechanischen Verhalten der Oberflächenkörner simuliert den Kraft-Weg-Verlauf sehr genau. Allerdings sind in diesem Modell zwei freie Materialparameter, die das mechanische Verhalten der Oberflächenkörner beschreiben, enthalten. Die folgenden zwei Modelle dagegen kommen ohne freie Materialparameter aus: das Kriech- und Bruchmodell.

Das Kriechmodell simuliert das viskose Verhalten von Schnee. Ein in-situ Kriechexperiment im Computertomographen liefert gemessene, makroskopische Viskositäten und μCT-Bilder von derselben Schneeprobe. Die Mikrostruktur aus den μCT-Bildern wird mit Balken approximiert und mit der Finite Elemente Methode simuliert. Als Materialmodell wird dabei das Glen'sche Fließgesetz von monokristallinem Eis angenommen. Die Vereinfachung der Struktur durch Balken ermöglicht die rechenaufwändige Kriechsimulation von Ausschnitten der Mikrostruktur, die großgenug sind, um das makroskopische Verhalten widerzuspiegeln. Aus dem validierten Modell lassen sich wichtige Schlußfolgerungen über die Verformungsmechanismen in Schnee ziehen und etablierte Theorien der Schneemechanik in Frage stellen: Korngrenzengleiten, das als dominanter Deformationsmechanismus in Schnee gilt, wird in dem Modell nicht berücksichtigt. Neben anderen Argumenten gegen Korngrenzgleiten aus der Literatur wird somit die Lehrmeinung des Korngrenzengleitens in Frage gestellt. Außerdem wird gezeigt, dass der etablierte Ansatz, Schnee als offenporigen Schaum zu betrachten, unvollständig ist. Die Bildung neuer Kontakte innerhalb der Struktur spielt im Schnee bei der Kompression eine wichtige Rolle und erklärt die Verfestigung von Schnee. In mikromechanischen Modellen von Schaummaterialien dagegen wird die Bildung neuer Kontakte nicht berücksichtigt.

Das Bruchmodell ist identisch mit dem Kriechmodell, nur dass zusätzlich noch ein Versagenskriterium für die Balken zugefügt wurde. Das Versagenskriterium basiert auf der Bruchfestigkeit von monokristallinem Eis. Zur Verifikation wurden Schneeproben im μCT gescannt und deren Bruchfestigkeit in Zugversuchen ermittelt. Die Simulationsergebnisse stimmen gut mit den gemessenen Werten überein. Das Bruchmodell zeigt somit, dass das Balkenmodell auf andere Belastungszustände übertragen werden kann.

Obwohl in dieser Arbeit nur wenige Belastungsfälle und Schneearten berücksichtigt werden, konnte erstmals das makroskopische Verhalten von Schnee ausgehend von der Mikrostruktur und dem Verhalten von Eis ohne freie Materialparameter modelliert und verifiziert werden. Die Stärken dieser Arbeit liegen in der Entwicklung von 3D Bildverarbeitungsmechanismen, die es erlauben die 3D μCT-Bilder von Schnee zu vereinfachen und zu modellieren. Zudem wurden erstmals mechanische Experimente und μCT-Scans mit ein und derselben Schneeprobe durchgeführt. Dadurch können die entwickelten Mikrostrukturmodelle sehr gut verifiziert werden. Dass die Modelle erfolgreich auf andere Belastungszustände übertragen werden können, läßt hoffen, dass in zukünftigen Arbeiten mithilfe dieser Modelle die mechanischen Eigenschaften für verschiedene Schneearten und Belastungszustände bestimmt werden.

Chapter 1

Introduction

1.1 Snow as a material and its microstructure

Snow forms in the atmosphere. However, we are interested in snow as a material, which forms when snow accumulates on the ground. Snow can be classified very generally as a heterogeneous material since it consists of clearly distinguishable constituents: mainly ice, water and air. More narrowly defined snow is a porous medium. Porous media are heterogeneous materials which contain pores (voids) and a solid skeleton (ice matrix). The porosity of snow ranges from 95% for fresh snow to 10% for dense firn. Snow with a porosity larger than about 30% is a bicontinuous porous medium. This means that both the ice matrix and the pore space are continuous volumes. For lower porosities single pores are closed off. Furthermore snow is a sintered, polycrystalline material, consisting of sintered, monocrystalline ice grains. Snow that has not sintered yet or snow where the sintered bonds broke is a granular material.

Beside these structural classifications snow is a high temperature material. This might sound strange as snow feels cold to the touch. However, ice and snow in nature are mostly found near their melting point. The homologous temperature T/T_{melt} is larger than 0.9 for temperatures warmer than -27°C. In this sense, snow is a high-temperature material. It has been shown that there is a wide field of categories snow can be assigned to. Snow is a sintered, polycrystalline, bicontinuous, porous, high-temperature material and sometimes granular. Since snow shows characteristics of all these different types of materials, snow is a multi-faceted, fascinating and interesting material on the one hand but on the other hand challenging to investigate.

Snow on the ground consists of snow crystals which formed in the atmosphere when supercooled cloud droplets start freezing from a nucleus and grow by deposition of water vapour. The shape of the snowflake depends on temperature and humidity at which it formed (Figure 1.1). Stellar crystals with six arms (Figure 1.2 a) are the most common form of crystals during snowfall events. Once the snow crystals reach the ground the snow cover starts to densify due to gravity (settlement), to sinter and to change their form (metamorphism). These transformations depend on environmental conditions like temperature, temperature gradients and forces on the snow. For different environmental conditions and different initial shapes a high variety of different snow types with different microstructures and properties forms. The shapes of snow grains range from stellar crystals (Figure 1.2 a), to facetted (Figure 1.2 c), depth hoar crystals (Figure 1.2 d) and rounded grains (Figure 1.2 b) and densities range from 30 kg/m^3 (fresh snow, see Figure 1.3) to ultimately 915 kg/m^3 (solid ice). All these different snow types can occur in the same snow pack due to different environmental conditions during different snowfall events and due to different environmental conditions at different locations in the snow pack. A snow pack therefore is a layered material (Figure 1.4) with highly varying properties

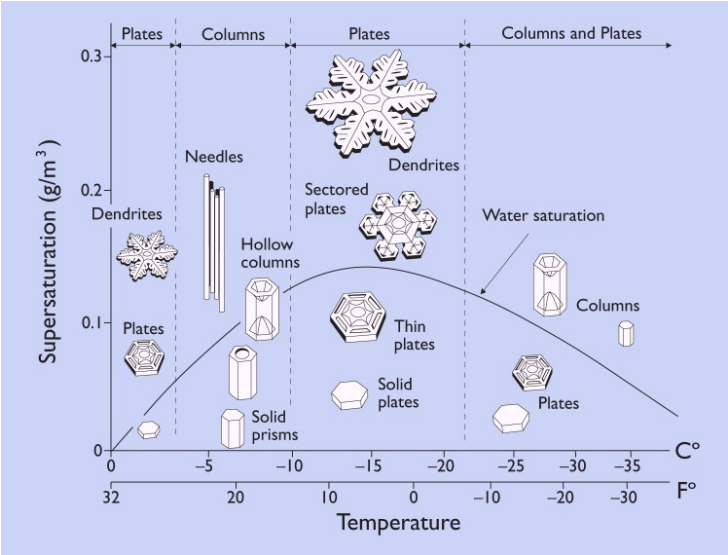

Figure 1.1: Morphology diagram of snowflakes. The shape and size of snow crystals depends on temperature and supersaturation. Diagram from http://www.snowcrystals.com

from layer to layer. Weak layers (Figure 1.5) in a snow pack play a major role in the release of avalanches. Typical layers in an alpine snow pack consist of rounded or facetted grains and have a density between 150 and 400 kg/m^3. Compacted snow on roads or on hard ski slopes has densities between about 400 and 600 kg/m^3. Snow older than one year is called firn. Firn has a density between 500 and 800 kg/m^3. For higher densities it is called porous ice.

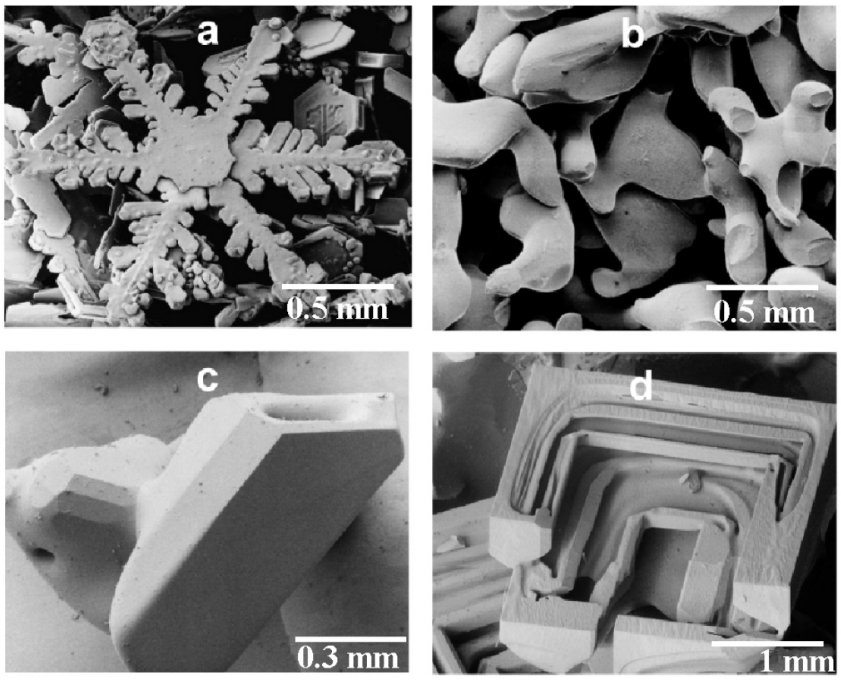

Figure 1.2: Examples of snow crystals: a) Stellar snow crystal, b) Rounded snow crystals, c) Faceted snow crystal, d) Depth hoar. Low temperature scanning electron microscope images from http://emu.arsusda.gov/

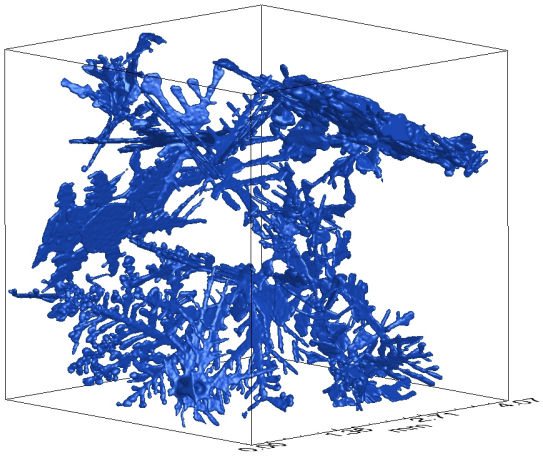

Figure 1.3: Fresh snow with a very low density of 30 kg/m^3 imaged by micro computer tomography.

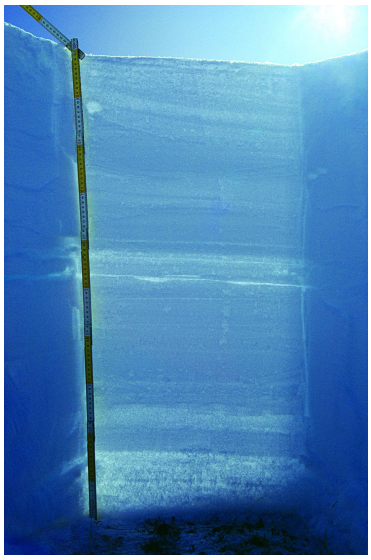

Figure 1.4: Shine-through-profile of a 1 meter deep snow pack. Different layers can clearly be distinguished by different brightness. Photo from SLF archive

Figure 1.5: Weak layer in a snow pack consisting of snowed in surface hoar. Photo from SLF archive

Two different types of metamorphism produce the different grain shapes and layers: equilibrium and kinetic metamorphism. Kinetic metamorphism is driven by strong temperature gradients which induce high vapour fluxes in the snow structure. Grains with angular shapes, sharp edges and flat faces or facets (Figure 1.2) form in a few hours or days during kinetic metamorphism. In contrast to this, equilibrium metamorphism results in rounded grains (Figure 1.6). The initial shapes - usually dendritic - change after a few days into rounded particles, to reduce their specific surface area, followed by the slow growth of larger particles at the expense of smaller particles. This process is driven by the vapour pressure gradient causing a vapour flux from surfaces with high curvature to low curvature. The dominant mechanism during both equilibrium and kinetic metamorphism is vapour diffusion. The high equilibrium vapour pressure of ice near its melting point is responsible for the fast structural changes by vapour diffusion (Pinzer, 2009). In addition to the fast metamorphism of snow the high homologous temperature explains another important characteristic of snow: the creep behaviour. Like other crystalline materials near its melting point ice and snow exhibit a pronounced creep behaviour. Creep deformation is the ongoing deformation of a material under the influence of a load. Snow creep enables the fast and ongoing densification under relatively small loads and thus the wide range of densities of natural snow and even the densification to ice of glaciers.

To sum up, snow is a highly dynamic material, which quickly changes its appearance. This is caused by two important properties of ice typical for high temperature materials: the high equilibrium vapour pressure and the creep behaviour. If snow consisted of gold chips, no densification, sintering or metamorphism would take place and the appearance and thus the properties of this "gold snow" would remain the same. However, densification, sintering and metamorphism take place in snow and continually change its microstructure and cause the high variability of snow types. With the changing microstructure also the properties of snow change. The properties of snow depend on the microstructure and on the properties of the constituents of snow; this is mainly ice and air for dry snow. In this thesis only dry snow and its mechanical properties are considered. For most mechanical properties the contribution of air is negligible and thus the mechanical properties depend only on microstructure and ice properties. All characteristics of ice are passed on to snow like the earlier mentioned creep behaviour or elastic properties, ductile to brittle transition, strength and so on. When snow density approaches the density of ice all properties approach the respective property of ice as well and the variation of the properties approaches zero. Thus for high densities (denser than about 650 kg/m^3) the properties of snow are well described by the respective property of ice and density. However, for lower densities the arrangement of the ice, i.e. the microstructure, becomes more important. Since the microstructure varies considerably in snow, the physical properties scatter significantly even for the same density. The viscosity of snow with a density of 250 kg/m^3 for example varies by a factor 100 (Kojima, 1967). Thus the properties of low-density snow cannot be described by the respective property of ice and density alone. Microstructure must be considered as well. This shows the importance of microstructure for the understanding of the material behaviour of snow. The question which arises is how the material behaviour depends on microstructure and how the microstructure of snow can be characterised.

Despite the great variability of snow microstructures there are some characteristics snow types of all microstructures have in common. Snow microstructures are disordered: Even

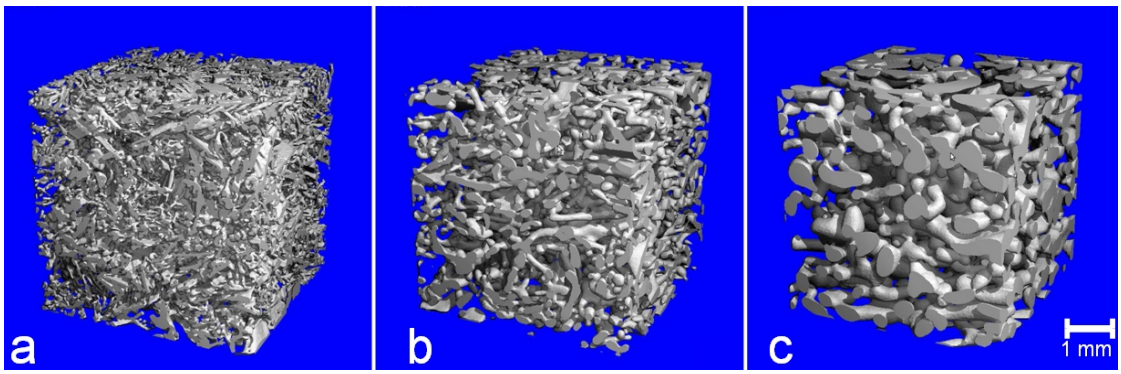

Figure 1.6: Changing microstructure during equilibrium metamorphism captured by micro computer tomography. Dendritic forms (a) change to rounded forms (b) and become larger (c).

though snow flakes are famous for their regularity and beauty (Libbrecht, 2005) snow on the ground is not regular. The ice matrix which builds the snow can be seen as a connected random graph. In this graph many dead ends exist, which do not contribute to mechanical properties. Small portions of the ice matrix carry most of the loads. Thus, loads are unevenly distributed in snow. Furthermore highly tortuous paths in the matrix decrease strength, viscosity and stiffness of snow. Compared to other porous materials which are optimised for good mechanical stability at a low weight like bones, metallic foams or honeycomb structures, snow has a more complex microstructure and poor mechanical stability. The microstructure of the optimised materials usually shows some regularity or even periodicity (like for honeycombs) which simplifies its characterisation.

Besides density, snow is traditionally characterised by grain size, bond size and grain shape. These are parameters which can be identified using magnifying glasses in the field. However, important information about the connectivity of the ice network is missing in these parameters. With micro-computed tomography we have a new technique at hand which enables us to capture the complete three-dimensional microstructure of snow (Figure 1.3 and Figure 1.6). Still, the problem how to characterise the microstructure and how to find the connection between microstructure and macroscopic properties remains. Three-dimensional image processing algorithms are necessary to determine structural and topological parameters and to break down the complex microstructure into simpler structural units and their connections (Figure 1.7). Such simplifications are useful to approach the goal to characterise snow and to describe the properties of snow as accurately as possible with the smallest possible amount of microstructural information. The motivation and importance of this goal will be described in more detail in section 1.3. But first, a more fundamental question will be answered in the next section: Why are we interested in snow and its mechanical properties at all?

1.2 Snow mechanics and its relevance

Snow mechanics studies how snow deforms and eventually fails under given loads or stresses. There is a wide field of applications for snow mechanics. The most famous application of snow mechanics is the prediction of avalanches. Avalanches are a natural hazard occurring in

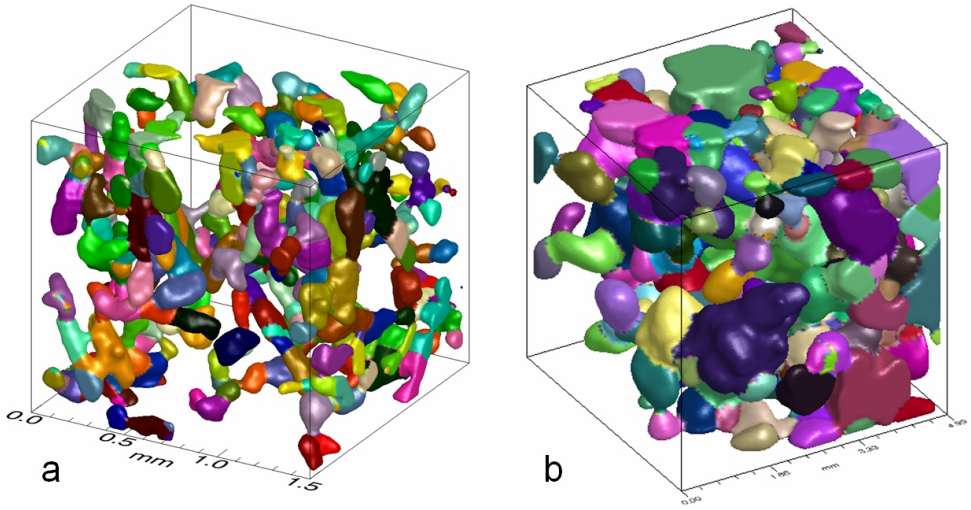

Figure 1.7: Micro-CT images of round grained (a) and wet snow (b) decomposed into single grains by image processing algorithms. The single grains are labelled in different colours.

mountain regions where snow and steep terrain come together. Avalanches do not only threaten infrastructure like roads, railways, or buildings but also the increasing number of recreationists spending their time in snow-covered mountainous areas (Figure 1.8 a). On average, 25 people die in avalanches per year in Switzerland, 90% of these fatalities can be attributed to skiing or snowboarding beyond controlled ski runs (Tschirky et al., 2001). Avalanche forecasting includes the prediction of the release and of the flow of avalanches. The release of avalanches is studied by fracture mechanics to understand under which load a snow pack fails. Here, snow behaves like a solid body. Avalanche flow is a different problem. Snow in an avalanche becomes dispersed and can be regarded as a granular material. Hydrodynamic approaches are used to estimate velocities, forces on obstacles and run out lengths of avalanches (Figure 1.8 b).

Apart from avalanche forecasting only infrequent use is made of snow mechanics (Shapiro et al., 1997). However, many possible applications of snow mechanics exist. Further possible applications include the calculation of forces on constructions in contact with snow like snow fences, roofs, cables, walls, etc. (Figure 1.8 c); the improved design of equipment for snow removal (Figure 1.8 d) or ski piste preparation; snow as a construction material for building roads or airstrips; settlement of the seasonal snow pack; densification from snow to ice with regard to the estimation of the age of ice cores; contact and friction of wheels or skis on snow (Figure 1.8 e).

From all these applications a clear demand for constitutive equations of snow follows. According to Shapiro et al. (1997) the infrequent application of snow mechanics originates in the lack of exact constitutive equations, which allow confident predictions. This is possibly caused by the lack of funding for research on snow mechanics. For sure, the knowledge of snow properties is not as valuable for commercial activities as for typical construction materials. Another reason is the difficulty to determine the constitutive equations of snow. Especially the wide variety of snow types with different microstructures and properties complicates matters. Up to now the properties of snow have been determined only for a few cases.

Different approaches to better cover the wide variety of snow types are possible. Approaches

which consider snow as a continuum and neglect its microstructure are inappropriate and inaccurate. In fact, snow is a heterogeneous material and its microstructure influences the macroscopic behaviour. Thus, more experiments which determine macroscopic properties and characterise the microstructure of the same snow are needed to determine the properties for more cases and thus advance snow mechanics. Another maybe even more important approach is to improve the understanding of how the microstructure influences the macroscopic behaviour of snow, with the goal to model snow behaviour and thus replace experiments. These problems are discussed in micromechanics and will be described in the next paragraph.

Figure 1.8: Examples of possible applications of snow mechanics: a) prediction of avalanche release; b) prediction of avalanche run-out length and forces on obstacles; c) forces on constructions in contact with snow; d) design of equipment for snow removal; e) the friction of wheels on snow. Image from www.c3overlays.com

1.3 Micromechanics and its benefits for snow mechanics

Mechanics of materials studies how materials deform and eventually fail under given loads or stresses. Micromechanics is a branch of mechanics of materials and deals with heterogeneous materials. Heterogeneous materials, such as composites, solid foams, polycrystals or snow, consist of clearly distinguishable constituents that show different mechanical and physical properties. Given the material properties of the constituents one important goal of micromechanics

is predicting the macroscopic mechanical behaviour of the heterogeneous material on the basis of the geometries and properties of the individual phases, a task known as homogenisation. Homogenisation provides a powerful tool to predict the behaviour of a heterogeneous material, thus replacing expensive or difficult experiments. For example, optimum microstructures can be forecasted rather than found by trial and error in engineering design (e.g. Schladitz et al., 2006; Shu and Huang, 2009). Besides homogenisation a second main task in micromechanics is localisation: the evaluation of the local stress and strain fields for a given load. This results in a better understanding and description of material damage and failure. However, to rely on micromechanics, the particular micromechanics theory must be validated through comparison to experimental data.

Since snow is a heterogeneous material, micromechanics can be applied to study snow. The benefits of homogenisation are attractive in snow mechanics as the experimental determination of snow behaviour is not always possible. E.g. the Young's modulus of snow is notoriously difficult to measure. So far no reliable measurements of the Young's modulus of low density snow (density lower than about 400 kg/m^3) exist (Kirchner et al., 2001). Also the measurement of slope stability for avalanche prediction is difficult. On one hand it is dangerous and difficult to perform meaningful experiments in the field (Föhn et al., 1998; Jamieson and Johnston, 2001) and on the other hand it is difficult to reproduce a natural snow pack in cold laboratories for controlled experiments. Furthermore, the handling and preparation of weak layers (Figure 1.5), which play an important role in avalanche release, is very troublesome. Such snow is very fragile and samples are easily destroyed before measuring. Therefore most data of mechanical properties exist for round-grained snow (Figure 1.6), which is much easier to handle. Only in two studies layered samples including a weak layer were tested under controlled laboratory conditions (Fukuzawa and Narita, 1993; Joshi et al., 2006). Homogenisation can be useful to better capture the wide range of mechanical properties for different densities and snow types and can therefore replace many experiments. Also the understanding of the mechanisms on the microstructural scale could be improved by micromechanics: localisation enables us to analyse the local stress and strain fields in the snow microstructure and helps to better understand and describe the failure of snow. This is important to understand the release of avalanches.

These possible benefits from micromechanics are promising. Therefore there are many approaches to model the mechanical behaviour of snow under consideration of the microstructure. However, meaningful micromechanical models must be validated through comparison to experimental data and a useful representation of the microstructure is required. As will be seen in the next paragraph these are the main problems in micromechanical modelling of snow.

1.4 Present state of snow mechanics

The goal of snow mechanics is the prediction of forces on objects interacting with snow and the prediction of deformation and failure of snow under given loads. To this end, the mechanical properties of snow, like elasticity, viscosity or strength, need to be determined and then described by constitutive equations and fracture criteria. Fracture criteria give the critical relationship of stresses at yield or rupture. And constitutive equations describe the relationship between stress, strain and strain rate tensor and parameters like temperature, density and snow

type. The challenge hereby is to find as universal as possible relations and to define the extent of validity. A non-linear stress - strain rate relation for example observed over a small stress range can be described by a linear constitutive equation. However, this constitutive equation is not very useful as it cannot be applied to cases which exceed the small stress range. The ultimate goal is to determine a theory of everything for snow: a constitutive equation which is valid for a wide range of stresses, temperatures, densities and snow types or alternatively a 'dictionary' which piecewise covers the wide range of parameters (stresses, temperatures, densities, snow types) as Salm (1982) proposed in his review of snow mechanics. However, up to now most pages of the 'dictionary' are still white. The properties of snow have been determined only for a few cases as Shapiro et al. (1997) agrees in his review paper about snow mechanics from the year 1997 with Brown (1994). This has basically not changed in the last 13 years, even though some more cases have been determined. Here the work of Scapozza and Bartelt (2003) has to be pointed out who described the viscous behaviour of snow for a wide range of parameters. However, only one snow type (round-grained snow) was considered in their work.

Basically two different approaches are useful to better cover the wide range of cases and thus advance snow mechanics: experimental work to determine and describe the mechanical behaviour of snow or micromechanical modelling as described in the previous paragraph. Salm (1982) calls these two approaches 'constitutive equations based on continuum theories' and 'constitutive equations based on the structure'. And Shapiro et al. (1997) distinguish 'descriptive and experimental studies' and 'microstructural studies'. These distinctions mean more or less the same. The first approach is simple: The behaviour of snow is observed and then described. No knowledge about the mechanisms in snow is necessary and the results are valid for the range of experimental conditions. The second approach is more complicated. The behaviour of snow is modelled based on its microstructure. Knowledge about the mechanisms and the geometry of the microstructure are necessary. Furthermore the model needs to be verified by experiments. One potential advantage of the second approach is that a good model can be applied to a wide range of problems. The present state of research for the two approaches will be presented in the following. The focus will be on the second approach as this thesis also focuses on this approach.

Methods to observe the microstructure of snow are the basis for both approaches. The visualisation of the microstructure is necessary to observe processes and changes in snow and to characterise snow. The technological progress from magnifying glasses to computed tomography plays a significant role in snow mechanics. With new methods new insight can be gained. Therefore, first a short overview of different methods to observe the microstructure is presented.

1.4.1 Methods to observe and characterise the microstructure of snow

The oldest method to observe the microstructure of snow is by magnifying glasses. Because of its simplicity it is still the most-used method to characterise the microstructure of snow in the field. Under magnifying glasses the grain size and grain shape are estimated. Information about the connectivity of the grains cannot be obtained by this method, since single grains are quarried out of the snow structure and observed separately. Furthermore, the precision of this method is low. The classification of snow (Fierz et al., 2009) is mainly based on this observation technique - grain size and shape are the most important characteristics beside density in traditional

snow classification. However, since this classification contains only limited information about the microstructure, this classification is not entirely reliable. Macroscopic properties vary by up to factor 10 for snow with the same density and snow type (Kojima, 1967). The earliest method to analyse the connectivity of the microstructure is by thin sections. Already in the beginning of snow research, in the 1930s, thin sections of snow were used to analyse the microstructure of snow more precisely. Thin sections are obtained by first casting and then cutting snow samples into thin slices (Bader et al., 1939). Under polarised light even the crystallographic texture of snow in thin sections can be analysed. Since 1975 stereology has been applied to thin sections to obtain three-dimensional structural parameters (Kry, 1975a). However, this method is based on assumptions about the three-dimensional structure, and thus the results are imprecise (Shapiro et al., 1997). The first 3D reconstruction of the microstructure was prepared by Good (1987) using serial sectioning. He successively cut and photographed sections of casted snow samples to obtain a series of parallel 2D slices of the microstructure. The series of parallel slices can then be reconstructed to a 3D image. However, this method was rarely applied, because it is very time-consuming. Furthermore, computer hard- and software for further processing of the large amount of data was not available at that time. In the year 1999 micro-computed tomography was used for the first time to capture the three-dimensional microstructure of snow (Brzoska et al., 1999). With computed tomography a snow sample can be scanned in about one hour. This method is much less time- and labor-consuming than serial sectioning. Furthermore it is non-destructive and thus enables the observation of changes in the microstructure of snow. Computer hardware was developed to the extent required for analysis of the three-dimensional data. However, even though the complete microstructure of snow is captured by computed tomography, this data is useless without methods to evaluate the 3D images. Methods to characterise the snow or to determine macroscopic properties from the 3D images are necessary. A few such methods exist as will be shown later. But the connection between microstructure and macroscopic properties is still in large part unclear. More research is needed to make use of the possibilities this new technology offers; especially methods to interpret the 3D images of the snow microstructure are needed. Another problem with computed tomography is that it is not suitable for outdoor use. It is bound to a laboratory. To analyse snow from the natural snowpack, snow samples have to be casted (Heggli et al., 2009). This way fragile snow samples can be transported to the cold laboratory without destroying the microstructure. However, this method is very laborious.

The stratigraphy of the snowpack and the mechanical properties of the single layers play an important role in avalanche release. The determination of the mechanical properties in the field is difficult and imprecise (e.g. Föhn et al., 1998; Jamieson and Johnston, 2001) but necessary to determine the stability of a snowpack. The stratigraphy of the snowpack is mainly analysed by magnifying glasses in a snow profile. But the precision of this method is low and thin layers are easily missed by the observer. Furthermore, mechanical properties cannot reliably be correlated to the simple structural parameters like grain size or grain shape. New methods to characterise the stratigraphy were recently developed. By near-infrared photography of a snow profile the specific surface area of the different layers can be determined (e.g. Matzl and Schneebeli, 2006). Furthermore a device was developed which measures the penetration resistance of a probe which vertically penetrates the snow pack (Schneebeli and Johnson, 1998). From the

force-displacement signal conclusions about snow type and snow pack stability can be drawn (Bellaire et al., 2009; Satyawali et al., 2009). However, the reliability of this analysis is not yet satisfactory and thus more development work is necessary to characterise the stratigraphy and to draw reliable conclusions about the stability of the snowpack. The step from snow characterisation to stability assessment requires knowledge about the mechanical properties and fracture criteria of the different snow types. The present state of research of this knowledge is described in the following two paragraphs.

1.4.2 Descriptive and experimental studies

The systematic investigation of the mechanical properties of snow was started in the 1930s by Swiss researchers motivated by the wish to understand, predict and prevent avalanches (Bader et al., 1939). Early studies followed the descriptive approach of snow mechanics. They measured the macroscopic behaviour of different snow types with different densities under different loads at different temperatures. Thus, the major parameters were already considered. In review papers of Mellor (1975), Salm (1982), Brown (1994) and Shapiro et al. (1997) the most important results of snow mechanics up to the year 1997 are summarised.

A considerable part of the studies deal with the long-term creep and failure behaviour of snow. These properties are relevant to the most important applications of snow mechanics, like settlement of the snow cover, forces on constructions in contact with snow or the release of avalanches. Snow properties important to describe how snow behaves under fast loading are investigated to a lesser extent. Still, a few studies deal with the ductile-to-brittle transition of the failure behaviour. The elastic properties of snow have also been investigated. However, according to Kirchner et al. (2001) so far no reliable data for the elastic properties of snow exist as they are very difficult to measure. More research is needed to measure the elastic behaviour and primary creep of snow. Primary creep is the initial phase of creep deformation which shows a different behaviour than the long-term creep deformation.

A general problem that often appears is that many studies determine mechanical properties of snow and its density but do not characterise its microstructure. This results in a large scatter of properties when correlated to density. However, even if the microstructure is characterised in terms of snow type, results still scatter. This indicates that the classical characterisation by snow type is not sufficient to describe snow. Besides these problems the main problem here is that only a few cases were investigated. As mentioned earlier, most experimental data exist for round-grained snow, which is easier to handle than other snow types. Unfortunately, results cannot easily be carried over to different conditions, like different densities, snow types or load cases. To achieve this, a better understanding of the mechanisms on the microstructure scale is necessary. Also the three latter review authors conclude that more work is needed to determine the connection between microstructure and macroscopic behaviour: “First we must understand what really happens when snow deforms and fractures.” (Salm, 1982); “More research is needed to provide a better correlation between microstructure and properties.” (Brown, 1994); “developing a method of using microstructural properties as an indicator of deformational response to load still remains to be done.” (Shapiro et al., 1997).

1.4.3 Micromechanical studies

We distinguish micromechanical studies which focus on the observation of mechanisms on the microstructure scale and studies which aim to model the snow behaviour based on its microstructure. Without understanding the processes and mechanisms in the microstructure a useful micromechanical model of snow cannot be developed. Therefore it is essential to first investigate the dominant mechanisms during snow deformation. This can be done either by observing the changes in the microstructure or by models which use assumptions about the mechanisms. Possible mechanisms during the deformation of snow are: breaking and sintering of bonds; deformation of the grains by stresses; deformation of the grains by vapour diffusion; relative movement of the grains (e.g. grain rearrangement by grain boundary sliding). The importance of the understanding of the mechanisms for useful modelling shall be illustrated by an example where the correct mechanism was not considered in the model: Kirchner et al. (2001) suggested considering snow as a foam of ice. Basically this is a promising approach since snow has some similarity with foam materials. Therefore for certain properties this approach might be useful, but Kirchner also applied foam theory to model the densification of snow. Here, foam theory is not suitable. The formation of new bonds is not considered in foam theories. But new bonds play a major role during snow densification (e.g. Kry, 1975b).

Micromechanical mechanisms

Important studies about the changes in the snow microstructure during deformation were performed by Wakahama (1960a,b, 1974), Kinosita (1967), Voitkovsky et al. (1974), Kry (1975a,b), Fukue (1979), Gubler (1978), Edens and Brown (1991).

The creation and growth of bonds in snow have a huge impact on its mechanical properties. Voitkovsky et al. (1974) and Fukue (1979) observed that the bonds between the single snow grains grow due to sintering and that new bonds are created during deformation. The strength of the same snow with constant density can increase by one order of magnitude with increasing age and thus stronger bonding (Fukue, 1979). Voitkovsky et al. (1974) showed that the cohesion force is linearly related to the bond area but independent of density. Thus they recommended using specific bond area, i.e. the total area of all bonds in a certain snow volume, instead of density as a structural parameter to characterise snow. However, the method to determine the bond area is not trivial and insufficiently explained. Kry (1975b) speculated that the formation of new bonds must occur primarily during the relaxation process after the densification stress is removed. This is doubtful. In experiments presented in this thesis new bonds were created during the densification under a constant stress.

Number and size of the bonds alone are not enough to explain the mechanical properties of snow. Kry (1975b) observed a 15-fold increase in mechanical properties which could not be directly explained by a measured 1.5- to 2-fold increase in the number of grain bonds. The spatial arrangement of bonds is another important factor. Kry developed the hypothesis that chains, defined as series of stress-bearing grains, are the basic units of snow structure. With this definition, the importance of individual bonds is combined with the connectivity of snow grains. Important conclusions of the chain hypothesis are that not all grains and thus not all bonds are load-bearing and that the tortuosity of the chain determines its mechanical response.

Furthermore the problem with traditional snow characterisation becomes apparent, which does not contain any information about the connectivity of the snow grains. The idea of tortuosity of the snow structure was picked up by Kaempfer et al. (2005) to describe the heat conductivity of snow. The hypothesis that only a small fraction of the grains is load-bearing was indirectly proven by heat conductivity simulations of three-dimensional snow structures by Pinzer (2009). He found that 80% of the heat is transported by 40% of the ice mass in snow with a density of around 300 kg/m^3. Agrawal and Mittal (1994) found that the chains are optimised during deformation. The number of bonds perpendicular to the load direction increases during deformation. This results in apparent strain hardening of snow, since these bonds are more effective in supporting the axial stresses.

A fundamental question in snow mechanics is which deformation mechanism dominates during deformation. Two basic behaviours of snow are distinguished depending on the deformation rate. For low strain rates the deformation is ductile: high strains are obtained under small loads without failure. For high strain rates the deformation is brittle. The transition from ductile to brittle behaviour takes place for tensile deformations at strain rates of about 10^{-4} 1/s increasing with temperature and snow density (Narita, 1983). For shear deformation the transition from ductile to brittle behaviour occurs at strain rates of about 10^{-3} 1/s (Schweizer, 1998). The deformation mechanisms in snow under fast deformation are not well known. Elastic deformations of the grains, grain boundary sliding, or primary creep are possible. Elastic deformations seem not to be dominant even for high strain rates, since the Young's modulus of snow could not be measured reliably up to now (Kirchner et al., 2001). After brittle failure snow can be treated like a granular material. Friction and interaction of the loose grains with each other and grain rearrangement determine the mechanical response of granular snow. Granular snow occurs under snowcats, in snow removal equipment, or in avalanches for example.

The ductile deformation of snow shows a substantially different behaviour and different deformation mechanisms are active. Up to now it is not clarified which deformation is dominant during the ductile deformation of snow. Basically two different deformation mechanisms are discussed: intracrystalline deformation by basal slip and intercrystalline deformation by grain boundary sliding. Basal slip takes place due to the motion of basal dislocations in ice (Schulson and Duval, 2009). The basal plane is a crystal plane in the ice lattice. Ice basically only creeps if there is a shear stress acting on the basal plane (Schulson and Duval, 2009). Grain boundary sliding is a process in which grains slide past each other along their common boundary. This is a typical deformation mechanism in polycrystalline materials, especially active in high temperature materials (Ree, 2000). In polycrystalline ice grain boundary sliding was identified as an accommodation process for intracrystalline creep deformations (Barnes et al., 1971; Sinha et al., 1979). This means that the deformation of polycrystalline ice requires both intracrystalline deformations by basal glide and intercrystalline deformations by grain boundary sliding (Goldsby and Kohlstedt, 2002). However, with increasing porosity the mobility constraints from neighbouring grains are removed and so intra- and intercrystalline deformation mechanisms become less strongly coupled. For low density snow (density less than 550 kg/m^3) particle rearrangement by grain boundary sliding is believed to be the dominant deformation mechanism (e.g. Johnson and Hopkins, 2005). For higher densities particles are too closely packed to allow further particle rearrangement and intracrystalline deformation becomes dom-

inating like in polycrystalline ice. However, the established picture of particle rearrangement and grain boundary sliding as dominant deformation mechanism for low density snow was recently doubted by Meysonnier et al. (2009). In fact, only few observations of grain boundary sliding exist: Wakahama (1960a, 1974) analysed thin sections of snow under polarised light during compression. He observed grain boundary sliding in wet snow (Wakahama, 1974). In dry snow he found that basal slip (intracrystalline deformation) and grain boundary sliding are the dominant mechanisms (Wakahama, 1960a). Nakaya and Matsumoto (1954) observed grain boundary sliding at temperatures up to -7°C but the deformation rate is not specified; Hansen and Brown (1988a) observed grain rearrangement for strain rates between 10^{-3} and 10 1/s. However, at these strain rates the rearrangement is caused by bond rupture. On the other hand Kinosita (1967) concluded from Wakahamas and own experiments that intracrystalline deformation dominates. Furthermore Steinemann (1958) and Ignat (1987) found in experiments on bicrystals of ice that grain boundary sliding is not a dominant deformation mechanism and that ice prefers to deform intracrystalline. Therefore it is not unambiguously clear if grain boundary sliding is an exception or the dominant ductile deformation mechanism in snow.

Another deformation mechanism somewhere between brittle and ductile behaviour is deformation by continuous breaking and creation of bonds. This mechanism enables large strains during shear deformation without macroscopic failure. De Montmollin (1982) explained these observations by the hypothesis that microscopic stress accumulation is avoided by fast metamorphism of the bond system, i.e. the growth of existing bonds and creation of new bonds. Reiweger et al. (2009) has described such a deformation mechanism by a fibre bundle model based on the two competing processes: bond fracture and bond formation. Experimental stress-strain curves for different strain rates were successfully modelled.

Micromechanical models

The attempts to model snow behaviour based on its microstructure started in the 1980s when the analysis of the microstructure was facilitated by improvements in data acquisition systems, image analysis system and theory of stereology. This topic was also pushed by the generally accepted opinion that snow mechanics can be advanced only by improving the understanding of how microstructure influences macroscopic properties (Brown, 1994; Salm, 1982). The most important models up to the year 1997 are summarised in the review paper by Shapiro et al. (1997). All of these early models are based on microstructural parameters determined by stereologic work. Shapiro concluded in his review paper that critical microstructural properties cannot be established by stereologic work, because the accuracy to determine three-dimensional parameters by this method was too low. Further he summarised that "developing a method of using microstructural properties as an indicator of deformational response to load still remains to be done." Stereologic work was the only method to determine three-dimensional parameters of the microstructure up to then. Shortly after, in the year 1999, micro-computed tomography (Brzoska et al., 1999) was introduced in snow research to capture the three-dimensional microstructure of snow. This enabled new possibilities and new insights into snow microstructure. While up to then almost all approaches to model snow behaviour concentrated on the bonds, a new picture of the snow microstructure arose. The picture of a granular material which consists of bonded grains was challenged by the picture of a homogeneous ice skeleton or foam-like ma-

terial (Kirchner et al., 2001). One reason might be that the crystallographic grain boundaries are not directly visible in CT-images, in contrast to thin-section images. Another reason might be that for the first time the complex three-dimensional microstructure could be visualised, which suggests that its tortuosity and its topology must play an important role with respect to snow properties. Compatible with this new picture Kirchner et al. (2001) suggested to consider snow as a foam of ice based on the general ideas of cellular materials by Gibson and Ashby (1988). By applying foam theory to snow he was able to describe the relation between strength and density. However, as mentioned before, important mechanisms of snow deformation are not considered in foam models. The foam model implies properties which solely depend on the volume fraction, leaving the geometry of the unit cell invariant. Topological changes of the ice matrix are not accounted for. This seems questionable for snow over a wide density range. As described in the previous paragraph topological changes were observed in many studies, for example when bonds break or form.

Another type of models which came up together with micro tomography applied finite element methods. The full 3D representation of microstructure from the CT images and the material behaviour of ice are used to model the macroscopic behaviour of snow. These simulations are computationally expensive. Therefore only small sub volumes of snow samples can be simulated. However, the sub volumes need to be large enough to represent the macroscopic properties of snow. Srivastava et al. (2010) determined the necessary size of the sub volume, i.e. the representative elementary volume (REV), to be at least 1.5^3 mm^3 for finite elements simulations of Young's modulus for snow with a density of about 400 kg/m^3. Kaempfer et al. (2005) determined a REV of at least 5^3 mm^3 for finite element simulations of heat conductivity in snow with densities of about 250 kg/m^3. Thus the size of the REV seems to depend on density and presumably on snow type. The REV of fine-grained snow for example is expected to be smaller than for coarse-grained snow.

Schneebeli (2004) and Srivastava et al. (2010) applied finite element models to simulate the Young's modulus of snow. Schneebeli simulated a series of images from a kinetic metamorphism experiment to study how metamorphism changes the mechanical properties of snow. The snow changed from round-grained to faceted during the metamorphism experiment but the density remained constant at 243 kg/m^3. The simulations permit for the first time to visualise and quantify the stress distribution inside the microstructure and the stress concentrations inside the bonds. The simulated Young's modulus decreased from 226 MPa for the round-grained snow to 62 MPa for the faceted snow. Measured Young's moduli from literature with similar snow are 3-100 times smaller than these simulation results. Schneebeli explains this difference with strain-rate effects of the measurements. According to Kirchner et al. (2001) no reliable measurements of the Young's modulus of snow exist due to this strain-rate effect. Therefore it is not possible to verify the simulations of Young's modulus. Thus the reliability of the simulation results is somewhat reduced. Still, this type of modelling is a powerful tool, which can be used to replace experiments. Srivastava et al. (2010) have applied finite-element simulations instead of experiments to obtain a macroscopic property of snow, which they compared with several structural parameters. This way they determined a set of structural parameters which best correlates with the simulated Young's modulus. Like Schneebeli they used a series of CT images obtained from a kinetic metamorphism experiment. The snow changed from round-

grained to faceted during the metamorphism experiment, and density ranged from about 350 to 400 kg/m^3. They simulated the Young's modulus for different orientations of the snow sample. The simulated Young's modulus parallel to the direction of the temperature gradient increased from about 500 MPa to 1000 MPa. In directions perpendicular to the temperature gradient the Young's modulus remained constant at 500 MPa. Thus the behaviour of snow becomes anisotropic during kinetic metamorphism. Srivastava et al.'s results differ from Schneebeli's results: For Srivastava et al.'s simulations the Young's modulus increases while it decreases for Schneebeli's simulations. Srivastava et al.'s results seem more reliable. They simulated sub volumes larger than the representative volume element, while Schneebeli did not consider size effects of the simulated sub volume. Schneebeli and Srivastava et al. agree that the simulated Young's moduli are larger than measured Young's moduli. However, Srivastava et al.'s simulation results are only about 3 times larger than measured Young's moduli. Even though finite element simulations of snow were not verified so far, the power of this type of modelling is promising. Finite element models could be applied for creep simulations as well; for example to verify or contradict the assumption that intracrystalline deformation mechanisms dominate. For finite element models the whole ice matrix is assumed to behave homogeneously like ice. No special behaviour at the bonds is considered. Thus, only intracrystalline deformations can be modelled.

To consider a different behaviour at the bonds, like intercrystalline deformation by grain boundary sliding, discrete element modelling is suitable. Discrete element models are applied to simulate granular materials. Johnson and Hopkins (2005) developed a discrete element model for snow. The single grains are represented by randomly oriented cylinders of random length with hemispherical ends. The cylinders are rigid and cannot be deformed. The macroscopic deformation is only generated by relative displacements of the cylinders. Sintering, sliding, rotation, compaction and breaking of the bonds are considered. Frozen and unfrozen contacts between pairs of cylinders are distinguished. The forces necessary for sliding or rotation are determined by a friction coefficient for the unfrozen contacts and by a grain boundary viscosity for the frozen contacts. The model was applied to simulate the ductile compression behaviour of snow, like during snow settlement. As mentioned earlier, basically two different mechanisms are discussed to be dominating during the ductile deformation of snow: inter- and intracrystalline deformations. The discrete element model is based on the assumption that intercrystalline deformation mechanisms dominate. However, even though the simulated bulk viscosity increases with density like measured bulk viscosities of snow, the discrete element model contains too many uncertainties to be able to prove the assumption of dominating intercrystalline deformation. The model lacks in two important points: the representation of snow microstructure and the material parameters. The applicability of representing the microstructure by randomly arranged cylinders is doubtful. It was not analysed whether the random arrangement of cylinders in the model resembles the arrangement of grains in real snow. However, this is an important point, since the arrangement of grains, i.e. the microstructure, determines the mechanical properties of snow. The second criticism affects the material parameter. The most important material parameter of the simulation is grain boundary viscosity. This parameter is not a measured material parameter but a free parameter. Alley (1987) developed a firn densification model which is also based on grain boundary viscosity. While Alley found best-fit

viscosities between 30 and 700 MPa s, Johnson and Hopkins underestimate measured bulk viscosities by four orders of magnitude using a grain boundary viscosity of 55 MPa s. Because of these uncertainties a verification of the model and its assumptions is not possible. However, the discrete element model is a promising approach to simulate processes in snow where intercrystalline deformations dominate. For the ductile behaviour this is not clear, but for the brittle and granular behaviour of snow intercrystalline deformations dominate and thus discrete element modelling should be applicable.

The main advantage of finite element or discrete element modelling is that arbitrarily complex structures can be simulated. Some limitations exist in discrete element modelling for the shape of the grains. But basically the complex microstructure of snow can be included in these models. If furthermore the correct mechanisms and material behaviour on the microscale are considered, the model should be able to simulate the macroscopic behaviour of snow.

However, the exact representation of the microstructure also has disadvantages. On one hand these simulations, especially finite element simulations, are computationally intensive and limit these models to snow volumes of a few mm^3 and on the other hand the capturing of the three-dimensional microstructure is problematic. It can only be captured by expensive laboratory equipment. Therefore, models which further simplify the microstructure are useful. Firstly, to decrease the computation times, and secondly, to obtain models which are based only on a few significant structural parameters, which are easy to capture.

Many models use strong simplifications of the snow structure: Brown's 'neck growth model' (1980); Alley's 'grain-boundary sliding model' (1987); Kirchner's 'foam-model' (2001) or Nicot's 'granular-model' (2004) for example. All of these models are able to represent certain properties of snow and thus can be applied to certain cases. However, the simplification of the microstructure can be justified in none of these models. The error due to the structural simplifications cannot be quantified because the models contain too many uncertainties: assumptions about the mechanisms, free parameters, empirical adjustments and arguable structural simplifications. As a consequence the models cannot be applied to problems differing from the reference conditions, which were used to adjust the model. Different models are based on different mechanisms even though the models aim to model the same behaviour. Alley assumes grain-boundary sliding as the dominant deformation mechanism while Nicot's and Brown's models are based on compression of the bonds. Also the simplification and description of the snow structure differs fundamentally between different models. Alley and Brown use parameters like grain size, bond size and coordination number, while Kirchner uses beam length, beam cross-section and an assumption about the arrangement of beams to describe the microstructure of snow. Due to missing confident verifications, it is difficult to judge which models are more realistic. This shows that a lack of clarity about the deformation mechanisms and the description of the microstructure exists. This leads to the next paragraph which summarises the open questions and research objectives in snow mechanics.

1.5 Open questions and research objectives in snow mechanics

From the review of literature many open questions and research objectives in snow mechanics become apparent. Here I summarise these points.

The main problem of snow mechanics is the lack of exact constitutive equations that allow confident predictions for a wide range of snow types and load cases. The most important approach to improve the constitutive equations is to investigate how the microstructure influences the mechanical properties of snow. To this end, tools are needed to capture the three-dimensional microstructure of snow. Up to the year 1999 this was the main problem of microstructural studies. The methods were not precise enough to determine reliable structural parameters. However, since the year 1999 with micro-computed tomography a new tool is available, which permits capturing the complete three-dimensional microstructure of snow. To make use of this technology new methods are needed to process the three-dimensional data.

One approach is to determine three-dimensional structural parameters from this data and to correlate them with macroscopic properties. The goal is to describe snow properties by a set of simple, significant parameters and thus to improve the characterisation of snow. Up to now this approach was applied in a study by Srivastava et al. (2010). More studies with different snow types and densities are needed to confirm his interesting results. However, a drawback of this approach is that the interpretation of the physical meaning of structural parameters is often difficult.

A more promising approach to make use of the three-dimensional images of snow microstructure is micromechanical modelling. Three prerequisites need to be fulfilled for successful modelling: a meaningful representation of the microstructure, correct deformation mechanisms at the microscale and verification with measured values. However, most models lack in at least one of these points.

The microstructure of snow is up to now best represented in finite element models. However, further simplifications of the microstructure are desirable to obtain controllable and manageable models. Many models use strong simplifications of the snow microstructure. But the error due to the structural simplifications was quantified in none of these models. Especially for low density snow (density lower 400 kg/m^3) the influence of microstructure on snow properties is large and thus also the error due to structural simplifications can be large. The second prerequisite for micromechanical models is to consider the correct deformation mechanisms. However, the deformation mechanisms during snow deformation are in large part unclear. For example, during the ductile deformation of snow, it is not clear whether deformations in the crystals or in the grain boundaries dominate. There are different models which are based on different, contradictory deformation mechanisms. More research is needed to clarify which mechanisms dominate during snow deformation.

The third prerequisite to obtain a reliable model is verification with measured values. A drawback of the finite element models is that a verification is still missing. This reduces the credibility of the model and should be improved in future studies. Furthermore, in many studies measured values from literature are used for verification. Due to problems with snow characterisation these values scatter and do not allow confident verifications.

Finite element models and computed tomography have only rarely been applied in snow mechanics, even though these methods offer new possibilities to answer some of the open questions in snow mechanics. Finite element simulations could be applied to simulate how further and further simplifications of the microstructure affect the simulation results. Deformation mecha-

nisms could be observed in-situ in the computer tomograph. Or datasets of three-dimensional images of snow and its mechanical properties could be created to improve the understanding of how the microstructure influences mechanical properties of snow. Models based on the three-dimensional images, like discrete or finite element models, could be verified using this dataset. Structural parameters determined from the 3D images could be compared with the mechanical properties to obtain a set of parameters which describe snow and its properties.

It has been shown that there is a strong demand to investigate the connection between microstructure and mechanical properties of snow in more detail. Micromechanics seems to be a fruitful approach to better understand the mechanical behaviour of snow. However, especially the following two important points must be clarified to advance snow micromechanics: a better understanding of the deformation mechanisms on the microscale and meaningful simplifications of the microstructure are needed. Furthermore, the verification of micromechanical models must be improved.

1.6 Contribution of the present work

The work presented in this thesis deals with some open questions in snow mechanics, which were pointed out in the last paragraph. The general goal of this work is to bring together the microstructure and mechanical properties of snow, i.e. to describe the macroscopic behaviour based on the microstructure of snow (homogenisation). Two important prerequisites to achieve this goal are necessary: an appropriate simplification of the microstructure and a data set which contains mechanical properties and information about the microstructure of the same snow. In the last paragraph it was shown that earlier studies have deficits in these two points. The strength of this work compared to earlier approaches is that improvements in these two points were achieved. This was possible especially due to micro-computed tomography, which permits for the first time to capture the three-dimensional microstructure of snow non-destructively. Furthermore, the development of 3D image-processing algorithms enabled us to make use of the three-dimensional data.

Still not resolved is complete clarity about the deformation mechanisms in snow and the lack of exact constitutive equations for a wide range of snow types and load cases. Only a small range of snow types and load cases are considered in this thesis. Furthermore only little effort was put into the important question, which mechanisms dominate snow deformation. Here, uncertainties still remain. However, the proposed methods and models could be applied to improve the understanding of these two points. Assumptions about different mechanisms can be tested or the models can be transferred to different problems with different snow types and different load cases. This remains to be done in future work. In Chapter 5 the potential of this approach is exemplified where a model, originally built for creep simulations, is used to simulate the brittle failure of snow.

1.6.1 Organisation of the thesis

This work consists of a collection of manuscripts accepted and submitted for publication in peer-reviewed journals. The work presented in the manuscripts was done in collaboration with the co-authors, but mainly by myself. All manuscripts deal with the problem how the microstructure

of snow can be simplified and used to model the macroscopic behaviour of snow. A dataset to verify the models was obtained by three different experiments. The contents of the manuscripts and their connections to the topic are described in the following.

Chapter 2 - Algorithm to decompose three dimensional complex structures at the necks: tested on snow structures

Snow consists of mono-crystalline ice grains which are sintered together. The proposed algorithm is able to detect single grains and grain boundaries from 3D CT images of snow. Thereby the complex snow structure is simplified into an assembly of single grains allowing discrete element simulations of snow for example. Furthermore, important parameters of the snow structure like grain size, grain boundary size and coordination number can now be determined.

Accepted for publication in IET Image Processing, 2010. Authors: Theile, T., Schneebeli, M.

Chapter 3 - Simulation of snow densification using a beam model

The observation of the snow structure during creep deformation using micro-computed tomography provides new insight into the deformation mechanisms of snow. We successfully simulated creep behaviour of snow with densities between 200 and 400 kg/m^3 using a finite element model. The model uses the snow microstructure from 3D CT-images as geometric input and monocrystalline ice in secondary creep as material model. The microstructure was approximated by beam elements. By using beam elements the number of elements is reduced by two orders of magnitude compared to common meshes and therefore the computationally expensive creep simulation of large snow structures is possible. For the first time a model which is based only on the microstructure of snow and the material properties of ice could be verified. The model was used to explain the hardening mechanism during snow deformation.

Submitted to Acta Materialia, 2010. Authors: Theile, T., Schneebeli, M., Löwe, H.

Chapter 4 - Mechanics of the ski-snow contact

The deformation of hard snow in a short-time impact of a ski has been measured. The changes in the snow microstructure and snow surface have been captured by micro tomography. Four types of deformation have been identified: brittle fracture of bonds, plastic deformation of ice at the contact spots, elastic and delayed elastic deformation of the ice matrix. The latter is the dominant deformation in the ski-snow contact. Based on 3D CT-images a micromechanical model is proposed. The model is able to simulate the deformation of snow in the ski-snow contact. The microstructure of snow is included in the model by the complete topographical description of the snow surface obtained from the 3D images. The surface grains are modelled as ice spheres supported by rheological elements (a nonlinear spring in series with a Kelvin element). The model predicts the number and area of contact spots between ski and snow.

Published in Tribology Letters, Volume 36, 223-231, 2009. Authors: Theile, T., Szabo, D., Luthi, A., Rhyner, H., Schneebeli, M.

Chapter 5 - Modelling the brittle failure of snow

Unpublished, preliminary results of fracture tests with snow are presented in Chapter 5. The motivation for these tests is to improve the understanding of the fracture process of snow on the microscale. The microstructure was captured in the CT before and after the tests. This data is used to observe where snow fractures. Furthermore the CT-images are used as input for a fracture model. The model is adapted from the beam model from Chapter 3. Additionally, a fracture criterion based on the strength of ice was added to the model. The first results show good agreement between simulation and experiment. However, for the confident application of this model more experiments for verification are necessary.

Chapter 2

Algorithm to decompose three dimensional complex structures at the necks: tested on snow structures

The separation of overlapping particles in 3D images is an image processing task with many fields of application. However, commonly used image processing algorithms have difficulties to identify the single particles and their connections in certain structures. Here we present an alternative algorithm for part decomposition which performs better on some structures than common algorithms. This algorithm is a special case of part decomposition, as it decomposes a structure at the necks into single particles. The necks are detected based on their characteristic negative Gaussian curvature. The algorithm itself consists of three steps: cutting at negative Gaussian curvature, region growing and intersecting plane minimisation. We tested the performance of the algorithm by comparison with two state-of-the-art algorithms for part decomposition, the watershed and a skeleton based algorithm on strongly differing geometries, taken from natural snow samples. The two test algorithms are known for having difficulties to decompose certain structures. As the new algorithm uses a different characteristic to decompose the structure, the new algorithm is a good alternative to the existing algorithms. The new algorithm decomposes 72% of the reference structure correctly. This is a better performance than by the two other algorithms.

2.1 Introduction

Today many techniques exist to capture the 3D-structure of multiphase materials (e.g. Brzoska et al., 1999; Oswald et al., 1997; Yeong and Torquato, 1998). Whenever this complex structure shall be characterised or simplified, it is necessary to decompose the structure into simpler particles, like the grains in concrete or the pores in sandstone for example. Size, shape, orientation, spatial arrangement or the connection of the single particles or pores can then be obtained. This information is related to physical characteristics of the material. Of particular interest in oil- and water- related geosciences is how the network of single pore bodies and their connections control the permeability and drainage in porous media (e.g. Culligan et al., 2004; Liang et al., 2000b; Mowers and Budd, 1996; Oswald et al., 1997; Solymar and Fabricius, 1999). While the pore space is related to the permeability of the structure, the solid phase determines mainly the mechanical properties of the structure. Decomposing the solid phase into particles can be used as an input for discrete element simulations for example (Johnson and Hopkins, 2005; Stroeven et al., 2009).

We applied and tested the proposed algorithm on the porous material snow. Snow is a sin-

tered material consisting of monocrystalline ice grains, which are bonded together (Colbeck, 1998). These bonds are crystallographic grain boundaries and therefore of fundamental importance to many processes in snow. The absorption of chemicals in snow for example depends on the grain boundaries as the chemicals are deposited there (Abbatt, 2003; Huthwelker et al., 2006). This is of great relevance to atmospheric chemistry (Grannas et al., 2007). A technical problem in this context is the detection of the grain boundaries in snow. The technique to directly capture grain boundaries is time consuming and destructive (Arnaud et al., 1998). The proposed algorithm will simplify matters: As most of the grain boundaries in snow form necks, they can be identified by the proposed algorithm from 3D volume images. These 3D images of snow are captured by in-situ X-ray micro tomography (Schneebeli and Sokratov, 2004). We used a desktop microcomputer tomograph (μCT) from Scanco Medical, which is placed in a cold chamber.

The structure of snow varies in a wide range: porosities range from less than 0.3 for firn to more than 0.9 for fresh snow and the particle shapes vary from plates over spheres to faceted particles (Libbrecht, 2005). This great variety of snow structures was the reason for the development of the new algorithm. Implementations of neck detection respectively particle separation algorithms found in literature were not general enough to successfully decompose all different or mixed snow types. In the following some of these algorithms and their limits are described.

The 3D watershed algorithm combined with the distance function is able to decompose connected particles (Ohser and Schladitz, 2009; Soille, 1999). Each local maximum of the distance values is a seed for one particle. Usually this will separate the particles at necks. The problem with the watershed algorithm is that the shape of the single particles should not deviate too much from spheres. While over-segmentation can be reduced by filtering and region merging, there are certain necks that will not be detected in principle. A neck between two plate-shaped grains for example will not be detected by this algorithm, because there is no local maximum of the distance values in each grain (Figure 2.1).

Another class of algorithms directly tries to detect necks in the structure. One approach breaks down the problem from 3D to 2D by identifying necks in several different oriented 2D-sections through the 3D volume (Kwiecien et al., 1990). This method is not very reliable in detecting necks, as discussed by Zhao et al. (1994). Another approach to detect necks involves skeletonisation or morphological thinning (Baldwin et al., 1996; Ioannidis and Chatzis, 2000; Liang et al., 2000a). Here Liang et al. (2000a) determined cross sections perpendicular to the skeleton for each skeleton point. The local minima of these cross sections are the necks. The fundamental problem with the latter algorithms is that they are based on a restrictive definition of necks. This definition reads as follows: necks are planes where the hydraulic radius of the pore space exhibits local minima (Kwiecien et al., 1990; Liang et al., 2000a). The restriction of necks to planes is not generally valid. In contrast to the 2D case, where a neck is always a straight line, a neck in 3D is an arbitrary curved surface. This is illustrated in Figure 2.2b). Here the curved necks between three overlapping spheres are shown. However, in many structures most necks form planes, so that algorithms based on this definition are appropriate. But we will show denser multi-particle structures where these algorithms fail.

Another type of 3D part decomposition is based on the minima rule from cognitive theory.

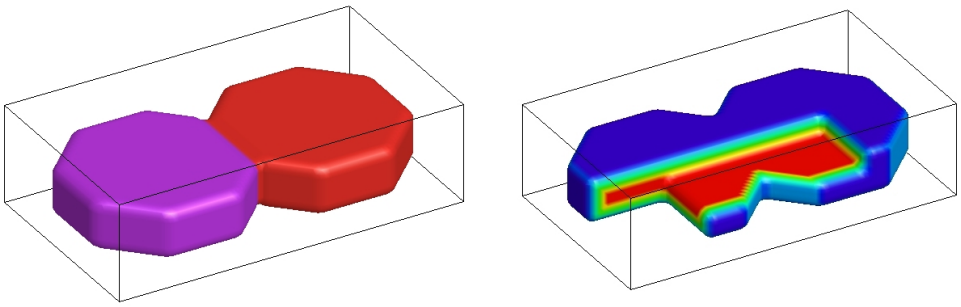

a) b)

Figure 2.1: Two overlapping plates decomposed by the curvature or skeleton based algorithm (a). Figure (b) shows the distance transformation of the overlapping plates (red - high distances to the background; blue - small distances). The watershed algorithm fails to decompose the two plates, because there is no local maximum of the distance values in each plate.

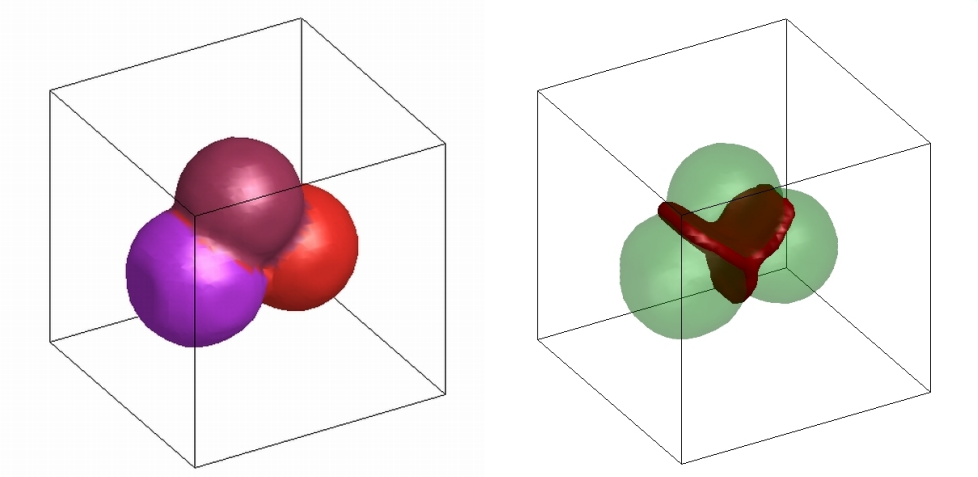

a) b)

Figure 2.2: Three overlapping spheres decomposed by the curvature based or watershed algorithm (a). The skeleton based algorithm fails to decompose these spheres, because the necks form curved surfaces here (b). In contrast to the 2D case, where a neck always is a straight line, a neck in 3D is an arbitrary curved surface.

This rule states that the human visual system divides three-dimensional shapes into parts at negative minima of curvature (De Winter and Wagemans, 2006; Hoffman, 1997). Methods based on this rule aim to decompose 3D geometries into meaningful, simple parts with applications in skeleton extraction (Katz et al., 2005), 3D morphing (Gregory et al., 1999), shape matching and reconstruction (Zuckerberger et al., 2002). A human body would be decomposed into something like torso, head, legs and arms. The advantage of this approach is that arbitrarily shaped, complex geometries can be decomposed into meaningful parts. But this is not necessarily decomposition at necks. The Gaussian curvature of a point on a surface is the product

of the principle curvatures of the given point. A point has a negative Gaussian curvature if one principle curvature is positive while the other is negative, like at saddle points. Since each neck has at least one surface point with negative Gaussian curvature, negative Gaussian curvature is a strong indication for a neck. But not each surface point with negative Gaussian curvature is necessarily part of a neck as shown in Figure 2.3. So the minima rule provides only a necessary but not sufficient condition for necks.

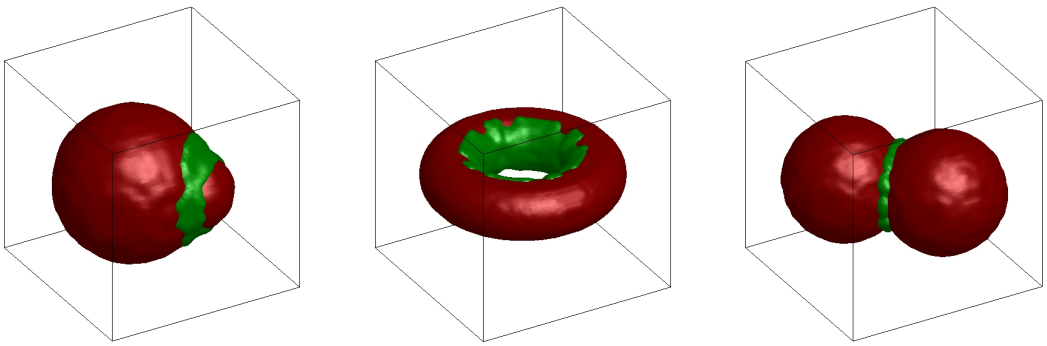

a) b) c)

Figure 2.3: Examples for points with negative Gaussian curvature (green) that form a neck (c) and that do not form a neck (a,b).

The algorithm we propose in this paper combines this necessary condition and the definition of necks to optimise their detection. The necessary condition provides neck candidates which are then selected by checking which ones fulfil the following definition of a neck: a neck is the cross section of the structure with local minimal area. Finally, this algorithm is applied to several snow types and compared with implementations of two algorithms from literature, namely the watershed and the skeleton based algorithm. To avoid confusion with these two algorithms, we call the new algorithm *curvature based algorithm*.

2.2 Methods

The proposed algorithm is implemented using the programming language IDL (IDL 6.4, ITT Visual Information Solutions) and works on binary 3D voxel data. This means the geometric data of the porous medium has to be provided in a 3D array of 0's and 1's, where 0 represents the void space and 1 the solid space.

The algorithm consists of three major steps: cutting at negative Gaussian curvature, region growing and intersecting plane minimisation. These steps are illustrated in Figure 2.4-2.6 and detailed below. The Gaussian curvature of the surface is estimated using a voxel-based approach by Ogawa et al. (2006). The Gaussian curvature G of a surface point p can be exactly calculated using the following expression:

$$G = \vec{n} \cdot \left(\frac{\partial \vec{n}}{\partial u} \times \frac{\partial \vec{n}}{\partial v} \right) , \tag{2.1}$$

where $\vec{n}$ is the normal vector of the surface at point p and $\vec{u}$, $\vec{v}$, $\vec{n}$ form orthonormal coordinates. This expression cannot efficiently be used on a voxel grid, because it is difficult to calculate $\frac{\partial \vec{n}}{\partial u}$

and $\frac{\partial \vec{n}}{\partial v}$, if $\vec{u}$ and $\vec{v}$ are not parallel to the grid coordinates (X,Y,Z). But the exact expression can be converted to the following expression which is suitable for a voxel grid:

$$G = \vec{n} \cdot \left(\frac{\partial \vec{n}}{\partial U} \times \frac{\partial \vec{n}}{\partial V} \right) n_{\mathrm{w}} \ , \tag{2.2}$$

where $\vec{n}$ is the normal vector of a surface voxel.

The original coordinate system (X,Y,Z) is rotated to the form (U,V,W) such that the following expression is fulfilled:

$$n_{\mathrm{w}} = max(|n_{\mathrm{X}}|, |n_{\mathrm{Y}}|, |n_{\mathrm{Z}}|) \ , \tag{2.3}$$

where n_{X}, n_{Y}, n_{Z} are the components of $\vec{n}$ in the original coordinate system (X,Y,Z).

The voxel grid remains unchanged after this rotation, only the indices of the axes are changed. Therefore this rotation is very efficient.

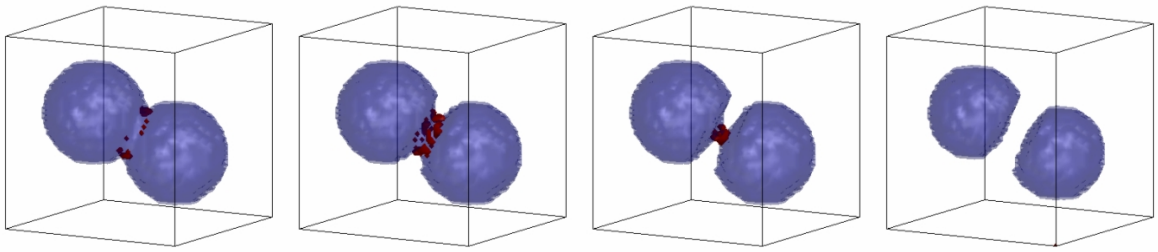

a) b) c) d)

Figure 2.4: step 1 - cutting at negative Gaussian curvature. By successively deleting voxels with negative Gaussian curvature (in red in image a - c), seed particles (d) are obtained.

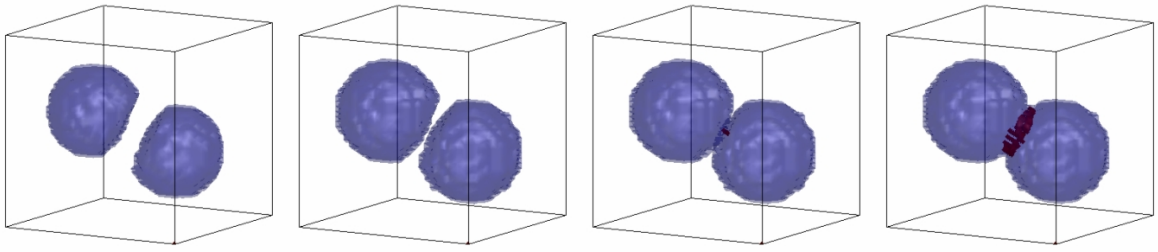

a) b) c) d)

Figure 2.5: step 2 - region growing. The seed particles from step 1 are successively dilated until the original structure is filled (image a - d). Where two growing particles touch, an intersecting plane forms (in red). This intersecting plane is a neck candidate.

The normal vector of a surface voxel is determined by subtracting the position of the center of mass of a 26-voxel neighbourhood around the voxel from the position of the voxel. The mass of each solid voxel is 1 and the mass of each void voxel is 0. Before calculating the normal vectors the image is smoothed using a simple 3x3x3 box filter. By smoothing, singularities of the curvature, like at edges, are removed. Hence for each surface voxel a curvature value can be determined. The cutting is done by successively deleting voxels with negative Gaussian

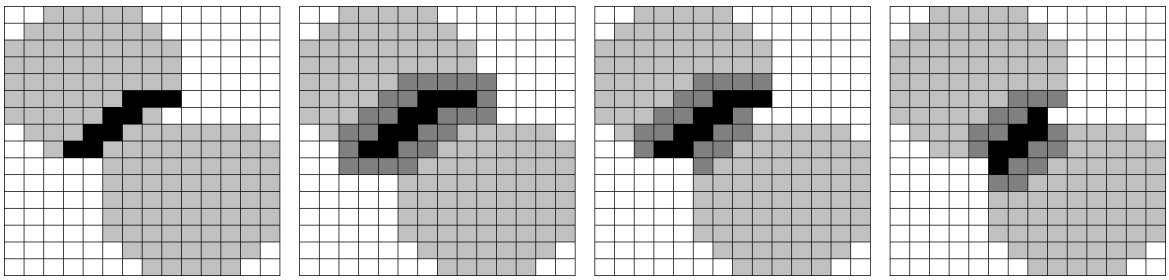

Figure 2.6: 2D sketch of step 3 - intersecting plane minimisation. The neck candidate from step 2 (in black in image a) is compared with parallel intersecting lines (in dark grey in image c) until an intersecting line with local minimal length (i.e. a neck) is found (in black in image d).

curvature and recalculating the curvature at the new surface voxels until there are no more voxels with negative Gaussian curvature. This kind of cutting can be seen as a fire front's propagation from surfaces with negative Gaussian curvature. Too avoid that the fire spreads too much, the criteria for a voxel to be burned in fact needs to be stricter than negative Gaussian curvature, rather the Gaussian curvature has to be smaller than a certain threshold. The need for this threshold is illustrated in Figure 2.7. It shows the surface points with negative Gaussian

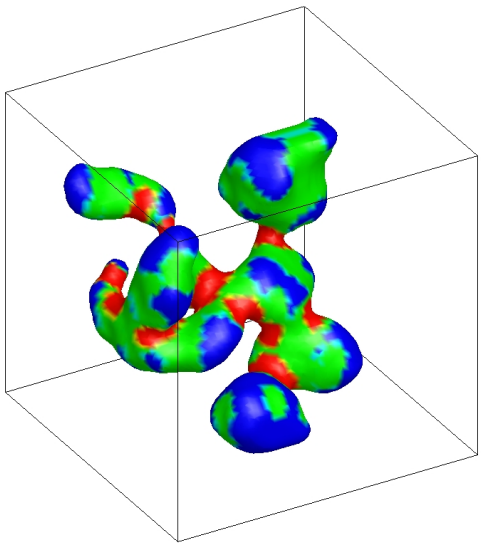

Figure 2.7: Different thresholds to identify necks from the Gaussian curvature: negative Gaussian curvature in green and red; Gaussian curvature smaller than the defined threshold in red. While the red surfaces are good indicators for necks, the green surfaces are too big as indicators for necks.

curvature (in green and red) and the surface points with a Gaussian curvature smaller than a threshold (in red). While the green points are scattered over the whole surface, the red points are good indicators for necks. If we cut the structure at the green points, this would result in over-segmentation. By cutting at the red points the structure is mainly cut at the necks. The threshold is defined so that 20% of the surface voxels with negative Gaussian curvature have a smaller Gaussian curvature than the threshold. The red surfaces in Figure 2.7 are obtained by this threshold. The absolute value of the threshold is therefore automatically adapted to

different structures depending on the Gaussian curvature distribution of the structure. Still the choice of the parameter is somewhat arbitrary. Figure 2.7 shows indeed that it makes sense to use a threshold, but the threshold could instead of 20% just as well cover 5% or 50% of the surface voxels with negative Gaussian curvature. So why should we use this 20% value? It is an empirical value, which gives the best results on a wide variety of different structures. And fortunately, the sensitivity of the results to this threshold is small, as will be discussed in the "Results and Discussion" section.

From the cutting procedure we do not obtain nice intersecting planes. Instead it removes a volume. The remaining volume consists of meaningful seed particles. Between these seed particles neck candidates are located. These neck candidates are found in the second step (Figure 2.5). To this end the original structure is filled by successively dilating the seed particles using a cubic 3x3x3 structuring element. Dilation is a basic morphological operation (Serra, 1983; Soille, 1999). Here layer by layer of voxels is wrapped around the particles until the original structure is filled. This method is called geodesic dilation (Soille, 1999), with the seed particles as the marker set and the original structure as the geodesic mask. The voxels, where two growing particles touch, form an arbitrarily curved intersecting plane of the structure. The method used is similar to the Voronoi tessellation or the Skeleton by Influence Zones (SKIZ) (Soille, 1999). The resulting planes are the intersection between the SKIZ and the original structure. In a last step it is checked whether these intersecting planes are necks or not. A neck is an intersecting plane with local minimal area; therefore transformations (translation, rotation or deformation) of a neck will always increase the area of the intersecting plane. For simplicity we only apply translations on the intersecting planes. The translation of an intersecting plane is realised by geodesic dilation (Soille, 1999) illustrated in 2D in Figure 2.6 a) - c):

1. Dilate the intersecting line using a 3x3 square structuring element and subtract the intersecting line from the result. This gives the dark grey region in Figure 2.6b).

2. Intersect this region with the original structure. This gives the dark grey regions in Figure 2.6c). These regions are two intersecting lines which are parallel to the neck candidate.

The same procedure works in 3D with intersecting planes instead of intersecting lines in the same way using a cubic 3x3x3 structuring element. After finding the shifted intersecting planes, the areas of the three parallel intersecting planes can be compared. The areas are estimated by counting the number of voxels in the planes. This approximation is sufficiently precise to compare the parallel boundary areas. If the original intersecting plane is a neck, its area would be the smallest amongst the three planes. Otherwise we can reject this neck candidate. But for the case that there is a neck close to the neck candidate (like in Figure 2.6), we do not just reject this candidate; instead we repeat this step up to eight times with the intersecting plane having the smallest area. Thereby we do not only check the neck candidates, furthermore the candidates can be moved to necks, like in Figure 2.6d). This is useful as the neck candidates often are positioned a few voxels next to the necks due to inaccuracies in the region growing step. Preliminary intersecting planes that touch each other form multiple-junctions (Figure 2.2b). These junctions are more complicated to handle and basically treated as a set of single boundaries.

As references for our algorithm we implemented two common algorithms for part decomposition found in literature: the watershed algorithm (Ohser and Schladitz, 2009) and a skeleton based algorithm (Baldwin et al., 1996; Ioannidis and Chatzis, 2000; Liang et al., 2000a).

We implemented the skeleton based algorithm in the following way: The skeleton is determined using a fully parallel 3D thinning algorithm (Tao and Anup, 2007). A thinning algorithm is a connectivity preserving process which is applied to erode an object layer by layer until only a skeleton is left. In a next step for each skeleton voxel a minimal intersecting plane of the original structure is determined. This intersecting plane intersects the skeleton voxel and cuts the original structure. It is found by choosing the smallest intersection between the original structure and one of 13 planes, which intersect the skeleton voxel. By repeating this for the whole skeleton, an intersecting plane area is assigned to each skeleton voxel. Necks are the intersecting planes with local minimal area, this means the intersecting planes of the forerunner and follower skeleton voxel is bigger than the intersecting plane at the neck. To reduce the over-segmentation of the structure the intersecting plane areas which are assigned to each skeleton voxel need to be smoothed. This is done by three times repeating simple averaging of each voxel with its two neighbouring voxels.

For the watershed algorithm we implemented a modified watershed version called *volume constrained pre-flooded* watershed (Ohser and Schladitz, 2009): First the Euclidean distance transform (Soille, 1999) is applied to the image. Then starting from the voxels with the highest distance values the image is "flooded". During the "flooding" process the regions around these maximum distance values grow. Voxels where two growing regions meet are watershed or neck voxels. The special thing about the pre-flooded watershed is that watersheds are build only if the two meeting regions each have a volume greater than a threshold volume. Otherwise the two regions are merged to form one region, reducing over-segmentation. The correct choice of volume threshold is crucial for the correct segmentation. We simply varied the threshold until the best result was obtained.

The goal of the decomposition of snow is the detection of crystallographic grain boundaries. To verify whether the detected necks are in fact crystallographic grain boundaries in snow, we compared the results of the algorithms with directly captured grain boundaries in a snow sample. The method to directly capture grain boundaries is time consuming and destructive (Arnaud et al., 1998). It works as follows: by sublimating a cross section of snow for a few minutes a groove forms at the grain boundaries. This groove can be imaged. Figure 2.8a) shows the 3D reconstruction of 60 cross sections with a distance of 30 m between each cross section. The different colours represent single grains.

2.3 Results and discussions

The impact of the curvature threshold on the results is the most crucial point about the curvature based algorithm. Therefore we will first analyse the sensitivity of the threshold to the results. Then we compare the different algorithms. To illustrate the differences and weaknesses of the algorithms we first apply them to specific test geometries and then to snow. Furthermore we compare the results with a 3D-image of real crystallographic grains to show the capability of the algorithm to detect crystallographic grain boundaries in snow. To show that the algorithm

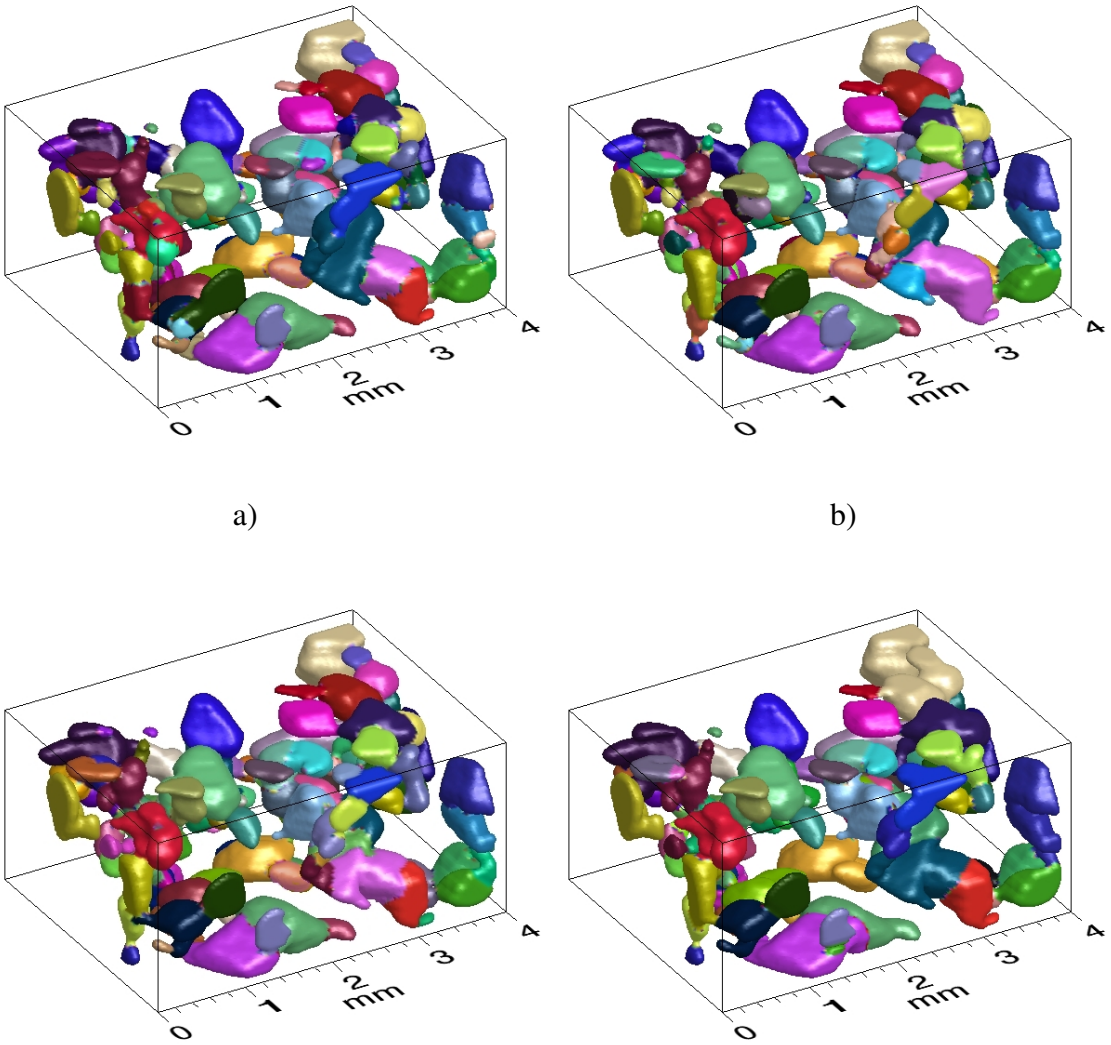

Figure 2.8: 4 mm x 3 mm x 1.8 mm - cut-out of round grained snow decomposed by sublimation (a), curvature based algorithm (b), watershed algorithm (c) and skeleton based algorithm (d). The grains detected by sublimation are the real crystallographic grains and serve as a reference for the algorithms. The skeleton based algorithm labels 58% of the voxels correctly; the watershed algorithm labels 68% correctly; and the curvature based algorithm labels 72% correctly.

can also be used to decompose other structures than snow, we finally segment the connected pore space of a shell into single pores using the curvature based algorithm.

In the methods section we stated that the impact of the curvature threshold on the results is small. However, if the threshold value is too small, some necks will not be detected; and if the threshold is too large (like the threshold used for the green surfaces in Figure 2.7), the structure will be over segmented. But what means too small or too large? The sensitivity of the results to this threshold is shown in Figure 2.9 for the structure displayed in Figure 2.8. The green

curve shows how the number of detected grains increases with an increasing threshold when running the algorithm without the "intersecting plane minimisation"-step. Especially if the

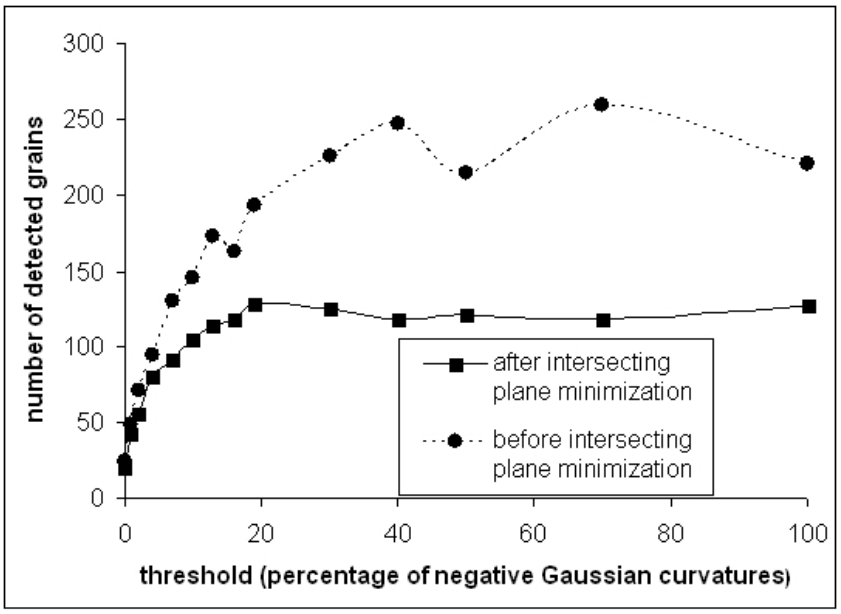

Figure 2.9: Sensitivity of the curvature based algorithm to the threshold for the structure shown in Figure 2.8. The circles show the number of detected grains for different thresholds before executing the last step of the algorithm (intersecting plane minimisation). The squares represent the number of detected grains after running all steps of the algorithm.

threshold value is large, the structure is also cut at non-necks. These cuts are filtered out by the "intersecting plane minimisation" and only the cuts at the necks remain. The blue curve shows the number of detected grains after the "intersecting plane minimisation"-step. The difference to the green curve is explained by the cuts which were filtered out during this step. For a threshold value bigger than 10% the number of detected grains varies between 105 and 128. This is a reasonable sensitivity to the threshold. So even if the threshold value is too large, the structure will be segmented correctly at the necks. Nevertheless, too large threshold values should be avoided for two reasons: Firstly, the larger the threshold the more neck candidates need to be filtered by the "intersecting plane minimisation"-step, which is computationally intensive. Secondly, the larger the threshold the less precise is the cutting step. Imprecise cutting leads to neck candidates, which are beside the true neck and therefore not detected. Therefore we recommend a threshold value of 20%, which gives the best results on all tested structures. For other structures it is possible that a different threshold is appropriate. As the sensitivity of the results to this threshold is small, the correct choice of the threshold is not crucial.

The skeleton based algorithm and the watershed algorithm are state-of-the-art algorithms to decompose structures into single particles. As mentioned in the introduction these algorithms have some weaknesses and are not universally suitable. We will show these weaknesses now on simple test geometries.

The necks between three overlapping spheres form a curved surface (Figure 2.2b). While the watershed and the curvature based algorithm succeed in detecting the necks (Figure 2.2a), the skeleton based algorithm fails. The skeleton based algorithm is restricted to necks which form

planes; curved necks cannot be detected.

The watershed algorithm is known for having difficulties in decomposing particles with shapes far from spheres (Soille, 1999). There are approaches to overcome over-segmentation of these structures with special filtering techniques, like the pre-flooded watershed (Ohser and Schladitz, 2009) for example. However, certain structures cannot be decomposed by the watershed algorithm in principle. Always if the largest distance transform values in the neck are greater or equal to the largest distance transform values in the center of a neighbouring particle, this neck will not be detected. This is illustrated for two overlapping plates in Figure 2.1. The largest distance transform values in the neck are equal to the largest distance transform values in the plates. Therefore there is only one maximum of the distance values. Thus the watershed algorithm detects only one particle containing both plates. Both the curvature and skeleton based algorithm successfully detect two particles in this test structure (Figure 2.1a).

Beside the test structures we applied the algorithms on different snow structures. Figure 2.10 shows the result of the three algorithms applied on wet spring snow. The image shows a cube with a side length of 5 mm; the resolution is 0.048 mm. This snow is characterised by its low porosity of around 0.5 and the round shape of the single grains, which are melted together and form agglomerates. This type of snow forms when snow melts during the day and freezes over night. The skeleton based algorithm is able to decompose the structure only into the single agglomerates. The watershed algorithm and the curvature based algorithm are able to detect most of the single grains.

There are structures where the weaknesses of the different algorithms do not matter. Figure 2.8 shows the result of the three algorithms applied on round grained snow. The image was captured by serial sectioning, as described in the methods section. Fresh snow, which has a finer structure, transforms to this type of snow after a few weeks. The process is called decomposing metamorphism and is driven by temperature gradients and surface energy minimisation. This type of snow is characterised by its high porosity of around 0.8 and the round shape of the single grains; the necks usually form planes. All algorithms succeed in decomposing the structure at the necks into similar particles. The image of the real crystallographic grains, captured by serial sectioning, serves as a reference for the algorithms (Figure 2.8a). By comparing the images qualitatively it is clear that indeed most grain boundaries in snow are located at the necks and therefore are detected correctly with the different algorithms. Still there are some differences, which can be explained either by drawbacks of the algorithms or by grain boundaries which are not located at necks. As a simple quantitative analysis of the resemblance of the images we count the portion of voxels which are labelled identically to the reference image. Furthermore the number of detected grains, the coordination numbers (i.e. the number of contacts per grain), and the total grain boundary area of all decomposed structures is compared (Table 1). These parameters are important in snow physics. The coordination number, the grain size and grain boundary size are important parameters to model the physical properties of snow (Lehning et al., 2002). All these parameters can now be derived from μCT images. Up to now these parameters were determined from 2D images. The new method is more precise, especially for the coordination number. In almost all parameters the curvature based algorithm shows the best performance, respectively the best resemblance to the real crystallographic grains. Only for the calculation time the watershed algorithm shows a better performance. The curvature based

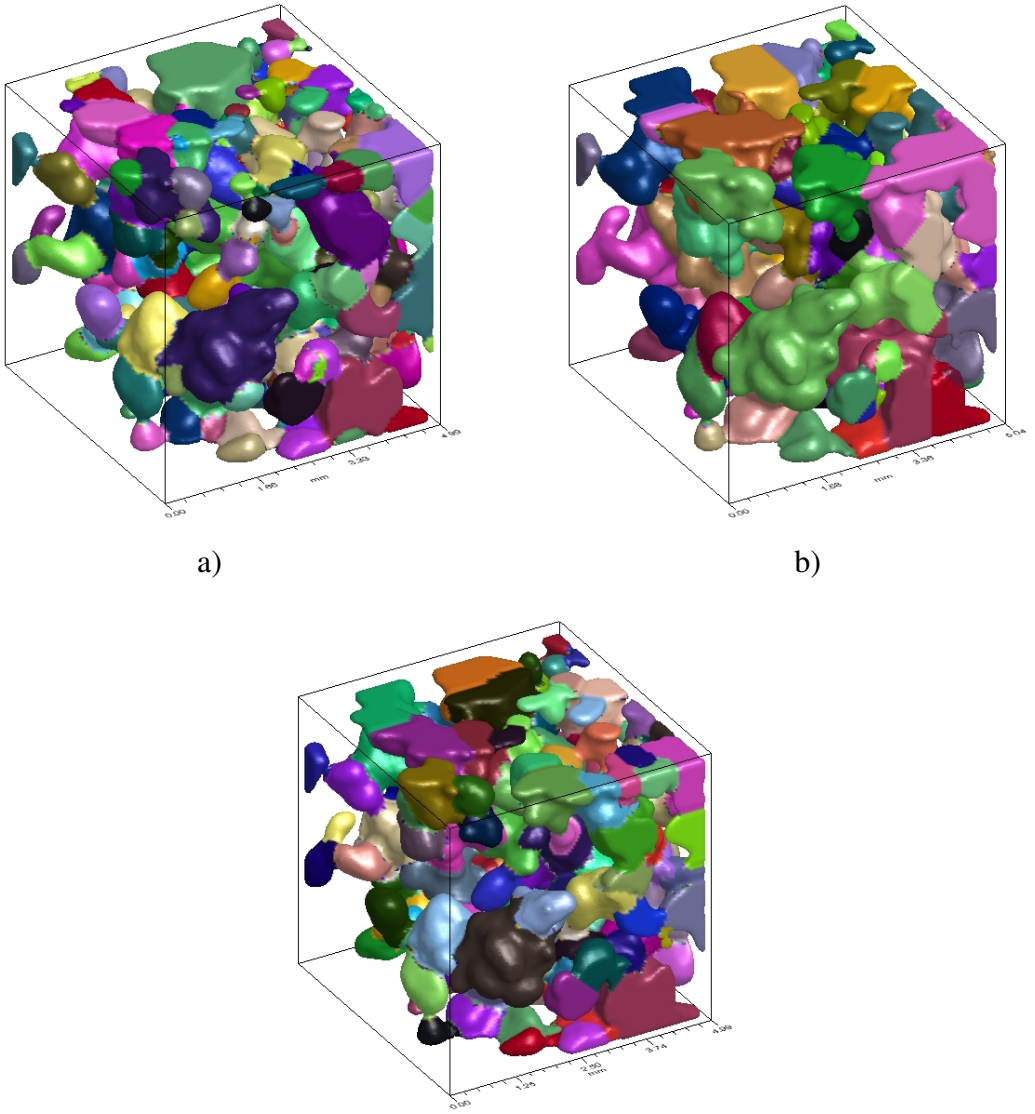

a) b)

c)

Figure 2.10: Wet snow decomposed by the curvature based (a), skeleton based (b) and watershed algorithm (c). The best result is obtained by the curvature based algorithm, because most single grains are detected. The two other algorithms can only detect the grain agglomerates.

algorithm does not emphasise on low computational cost. The focus is on the correct detection of necks. It takes about 200 s to decompose the structure shown in Figure 2.8 comprising 130x100x60 voxels on a 2.66 GHz Intel Pentium processor with 1 GB memory. The watershed algorithm is about twice as fast to decompose the same structure.

The curvature based algorithm is also applicable to other structures than snow. Figure 2.11 shows a sectional view of fossilised foraminifer (Speijer et al., 2008). Foraminifera are single celled organisms surrounded by a calcium carbonate shell. The shell consists of multiple chambers, which are connected to each other. The single chambers are colour coded in Figure 2.11 and were identified by the curvature based algorithm. The chambers are created by the same single organism, which keeps on moving to a larger chamber as it grows bigger and bigger.

	Real grains	Curvature-based algorithm	Watershed algorithm	Skeleton-based algorithm
resemblance with real grains, %		76	72	58
number of grains	137 (100%)	128 (93%)	115 (84%)	78 (57%)
coordination number	2.28 (100%)	2.34 (103%)	2.35 (103%)	2.54 (111%)
grain boundary area, mm^2	4.35 (100%)	6.14 (141%)	6.53 (150%)	2.68 (62%)
calculating time, s		208	122	759

Table 2.1: Comparison of different algorithms. Parameters were calculated on the images shown in Figure 2.8.

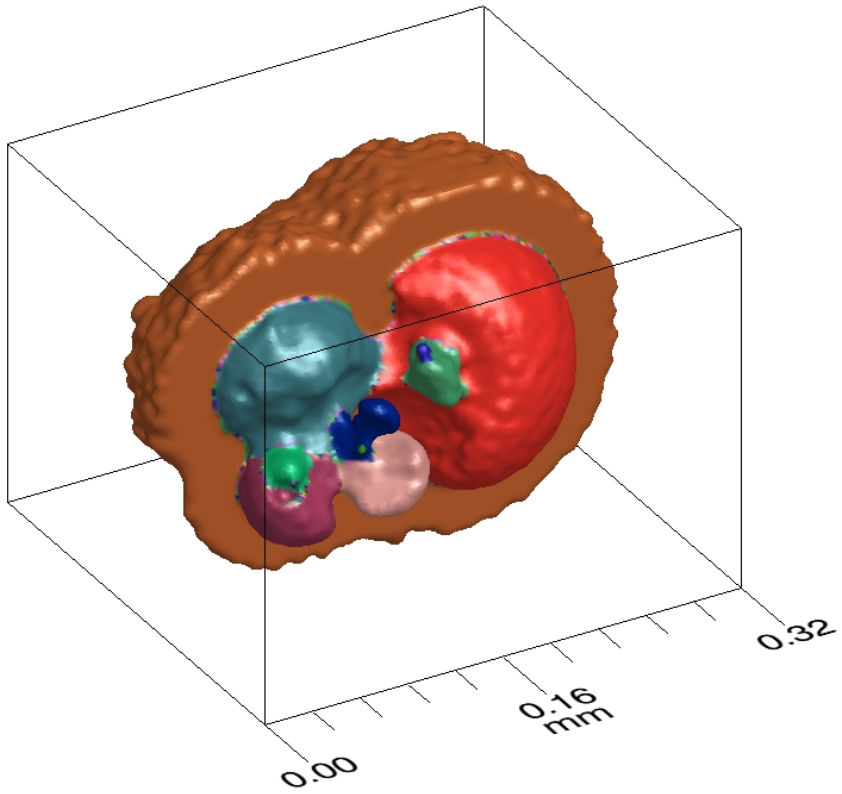

Figure 2.11: Sectional view of a fossil of foraminifer decomposed by the curvature based algorithm. Foraminifera are single celled organisms surrounded by a calcium carbonate shell (in brown). The shell consists of multiple chambers (colour coded), which are connected to each other. The single chambers were identified by the curvature based algorithm.

Foraminifera are commonly used as a dating method for rocks. They are also very interesting in studies involving paleoclimatology. The segmentation of the single chambers enables to

determine the size and the growth rate of the foraminifera.

2.4 Conclusions

In this paper a curvature based algorithm for neck detection respectively part decomposition was presented. This algorithm was compared with two common algorithms for part decomposition - a watershed and a skeleton based algorithm. The new algorithm is an alternative to these two algorithms, with a better performance on certain structures. The watershed algorithm is known for having problems in decomposing structures composed of non-spherical particles. And the skeleton based algorithm fails to detect curved necks. The new algorithm overcomes these problems. For the examined structures the new algorithm shows the best results. But on different structures and when calculation time is critical, the watershed algorithm might be the better choice.

We applied the algorithm on 3D-images of snow. We have shown that crystallographic grain boundaries in snow are located at the necks and therefore can be identified by the new algorithm. These grain boundaries are of essential importance to snow chemistry and snow mechanics.

Chapter 3

Simulation of snow densification using a beam model

The micro mechanics of ductile snow deformation are not well understood. The observation of the snow structure during creep deformation using micro tomography provides new insights into the deformation mechanisms of snow. We successfully simulated the creep behaviour of snow with densities between 200 and 400 kg/m^3 using a beam model. The model uses the snow microstructure from the 3D CT-images as geometric input and monocrystalline ice in secondary creep as material model. By using beam elements the number of elements is reduced by two orders of magnitude compared to common meshes and therefore the computationally expensive creep simulation of large snow structures is enabled. Established theories about snow mechanics are challenged: Grain boundary sliding which is believed to be the dominant deformation mechanism cannot be supported by our results. Furthermore we doubt the idea of snow as foam of ice. In foam theory the creation of new connections in the structure during deformation is not considered. However, for snow the creation of new connections seems to be the most important mechanism which causes the pronounced hardening behaviour during its densification. Furthermore we can conclude that the hardening of ice as a possible mechanism responsible for the hardening of snow can be neglected.

3.1 Introduction

Snow is a porous material consisting of crystalline ice grains, which are bonded together (Colbeck, 1998). The ice crystals form in the atmosphere. After they fall to the ground they immediately start to sinter together and quickly form a tenuous ice network that we call snow. On the ground the structure densifies itself by gravity and metamorphism. Thereby a wide spectrum of densities is covered from 50 kg/m^3 (fresh snow) to 600 kg/m^3 (ice). The densification of snow has been investigated extensively (e.g. Alley, 1987; Arnaud et al., 1998; Ebinuma and Maeno, 1987; Golubev and Frolov, 1998; Scapozza and Bartelt, 2003), because of its importance to applied problems like settlement of seasonal snow (Lehning et al., 2002) or estimation of the age of ice cores used to determine past climate conditions (e.g. Goujon et al., 2003). The underlying problem is however of general importance, namely how macroscopic material behaviour emerges from properties of the base material and the microstructure in which the base material is arranged.

The base material in snow is ice. The creep behaviour of mono- or polycrystalline ice is quite well understood (Schulson and Duval, 2009). However, the role of ice in creep of snow is not clear. The creep behaviour of monocrystalline ice is highly anisotropic. Ice basically only

creeps if there is a shear stress on the basal plane (Schulson and Duval, 2009). A single crystal where the basal plane is rotated 45° with respect to the force direction deforms five orders of magnitude faster than in case where the basal plane is parallel or perpendicular to the force direction. In polycrystalline ice the single grains have different orientations and therefore a different response to a given load. As the grains have to deform in a body, the deformation of each grain is constrained by the neighbouring grains. The macroscopic behaviour of a polycrystal can be computed from volume averaging based on the behaviour of the single crystals (Lebensohn et al., 2009). The deformation of polycrystalline ice requires both intracrystalline deformations by basal glide and intercrystalline deformations by grain boundary sliding (Goldsby and Kohlstedt, 2002). However, with increasing porosity the mobility constraints from neighbouring grains are removed and so intra- and intercrystalline deformation mechanisms become less strongly coupled. For low density snow (density less than 550 kg/m^3) particle rearrangement by grain boundary sliding is believed to be the dominant deformation mechanism (e.g. Johnson and Hopkins, 2005). For higher densities particles are too close packed to allow further particle rearrangement and intracrystalline deformations become dominating like in polycrystalline ice. However, Meysonnier et al. (2009) question the established picture of rearrangement of particles and grain boundary sliding as dominant deformation mechanism for low density snow. In fact, observations of grain boundary sliding are very sparse and prone with experimental difficulties: Wakahama (1960b; 1974) observed thin sections of snow under polarised light during compression. He observed grain boundary sliding in wet snow (Wakahama, 1974). In dry snow he found that basal slip (intracrystalline deformation) and grain boundary sliding are dominant mechanisms (Wakahama, 1960b). Nakaya and Matsumoto (1954) observed grain boundary sliding at temperatures up to -7°C but the deformation rate is not specified; Hansen and Brown (1988b) observed grain rearrangement for strain rates between 10^{-3} and 10 1/s caused by bond rupture. On the other hand Kinosita (1967) concluded from Wakahama's and own experiments that intracrystalline deformation dominates. Furthermore Steinemann (1958) and Ignat (1987) found in experiments on bicrystals of ice that grain boundary sliding is not a dominant deformation mechanism and that ice prefers to deform intracrystalline. Therefore the importance of grain boundary sliding in snow is uncertain. Another important question about the base material in snow is whether the ice behaves like mono- or polycrystalline ice. Monocrystalline ice creeps up to three orders of magnitude faster than polycrystalline ice (Schulson and Duval, 2009). To consider the ice as polycrystalline the length scale of the crystallographic grains is required to be much smaller than typical length scales of the ice network. Artificial snow and wind pressed snow consists quite often of polycrystalline particles (Figure 3.1 b). However, most snow types are quasi-monocrystalline (Figure 3.1 a). Here the crystallographic grains correspond reasonably to snow grains (see Chapter 2). Also for natural snow and firn analysed by Arnaud et al. (1998) or Takahashi and Fujino (1977) each snow grain consists of one single crystal. Thus the ice in natural snow can be considered in many cases as monocrystalline ice. Indeed, the crystallographic texture of snow is not often quantified and no classification of crystallographic textures for different snow types exists.

Another property of the base material might be relevant for the creep behaviour of snow: the primary creep of ice. Ice starts to deform in primary creep with a decreasing creep rate (hardening) until after about 1% strain secondary creep with a constant creep rate is reached

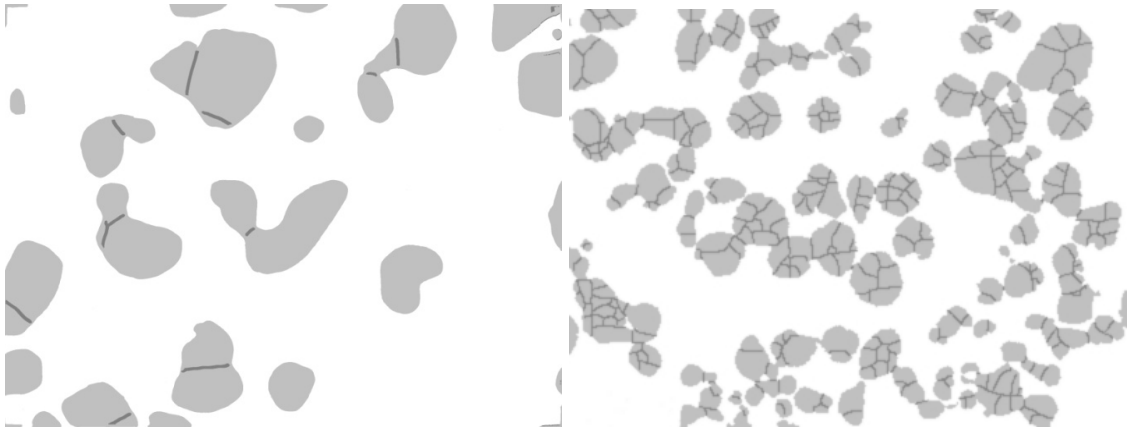

a) b)

Figure 3.1: Sectional view (4-mm wide) of two snow types and their crystallographic texture: natural round grained snow (a) and artificial fine round grained snow. Air in white. Ice in gray. Crystallographic grain boundary in dark gray. In figure a) each snow grain corresponds to one single crystal, while each snow grain in figure b) is a polycrystal.

(Schulson and Duval, 2009). This hardening during primary creep has its origin in dislocation dynamics (Duval et al., 1983; Miguel et al., 2003). Snow also shows a hardening behaviour. The origin of snow hardening is unclear. It can be caused by the hardening of the ice or by the change of its microstructure during deformation.

The microstructure of snow is multifaceted: densities range from less than 50 kg/m^3 for fresh snow to more than 600 kg/m^3 for firn and the grain shapes vary from plates over spheres to faceted particles or concave crystals like depth hoar (Libbrecht, 2005). This variety causes a wide range of macroscopic snow properties. Measured snow viscosities range from about 10 to 10^7 MPa s at a temperature of -10°C (Kojima, 1967). Even for snow with equal density and temperature the viscosity can vary by factor 100 (Kojima, 1967). The microstructure of snow is therefore essential to understand the macroscopic properties. During snow compaction the density increases and the microstructure changes. How the changing microstructure influences the viscosity and the hardening behaviour of snow is not well understood. For low density snow it has been suggested that the influence of microstructure can be captured using an open cell foam of polycrystalline ice (Kirchner et al., 2001) following the general ideas of creep of cellular materials (Andrews et al., 1999; Gibson and Ashby, 1988). However, the foam model implies a viscosity which solely depends on the volume fraction, leaving the geometry of the unity cell invariant during compaction. This implies a hardening solely caused by density where topological changes of the ice network are not accounted for. This seems questionable for low density snow. Topological changes were for example quantified by Edens and Brown (1991) who determined increasing coordination numbers for increasing snow densities. Therefore many models of snow densification exist which consider topological changes of the snow structure (e.g. Alley, 1987; Johnson and Hopkins, 2005). However, these models are based on the assumption of grain boundary sliding and grain rearrangements. Though certain characteristics of snow densification can be explained by these models none of these models is able to predict measured snow viscosities without a free parameter. The weaknesses of these models are simplified assumptions about the geometry of the snow structure. The grain boundary viscosity is treated

as a free parameter and not a measured material parameter. Alley (1987) finds best-fit grain boundary viscosities between 30 and 70 MPa s, while Johnson and Hopkins (2005) use grain boundary viscosities between 10^{-3} and 55 MPa s in their discrete element model of snow but still miss measured snow viscosities by three orders of magnitude.

The open questions are on one hand the effect of the geometrical arrangement of the microstructure, and on the other hand the mechanical behaviour of the ice. We focused here on these two aspects.

To this end we observed the changing microstructure of creeping snow with time-lapse micro tomography. For the experiments snow with densities between 200 to 400 kg/m^3 was compressed under constant stresses of 2 or 10 kPa with deformation rates in the range of 10^{-6} to 10^{-7} 1/s at -10°C during 10 days. We observed hardening with an exponent close to the common Andrade creep law (Miguel et al., 2003). To further elucidate the mechanisms of snow densification, the tomography images were used for microstructurally based creep simulations. The simulations use finite elements, because we assumed dominating intracrystalline deformations. In contrast a discrete element model is well suited to simulate granular material and intercrystalline deformations as used by Johnson and Hopkins (2005). To achieve a numerically tractable model for large enough snow volumes, the snow structure was approximated by beam elements. Thereby the number of elements was reduced by two orders of magnitude compared to tetrahedral or octahedral meshes. Grain boundary sliding was not considered in the model. Furthermore we assume that the ice in snow behaves like monocrystalline ice in secondary creep. Because our experiments were conducted in almost isothermal conditions, we did not simulate effects of snow metamorphism. The measured viscosities were used to validate the simulations. We found good agreement between modelled and measured macroscopic snow viscosities. Thus the assumption of dominating intracrystalline deformation mechanism with monocrystalline ice behaviour can be used to successfully model the creep behaviour of snow. An alternatively used polycrystalline material model overestimates the measured viscosities by an order of magnitude. Furthermore we found that topological changes of the microstructure are the main origin of snow hardening; the hardening is clearly underestimated by foam theory.

3.2 Experiments

We observed the changing microstructure by micro tomography during creep experiments. Two samples of different density were measured. Additionally, we carried out four creep experiments outside the computer tomograph to collect additional creep data.

3.2.1 Samples

Round grained snow with three different initial densities was used for a total of six experiments: 200 kg/m^3 for sample 1, 350 kg/m^3 for sample 2 and 185 kg/m^3 for samples 3.1 to 3.3 (Table 3.1). Round grained snow consists of sintered round ice grains. This snow is very homogeneous compared to other snow types. The single snow grains consist of single crystals for this type of snow as can be seen in Figure 3.1 a).

	Density (kg/m^3) initial / final	SSA (1/mm) initial / final	Specific genus ($1/mm^3$) initial / final	Number of beams/mm^3 initial / final	Simulated volume (mm^3)
Sample 1	205 / 240	24.0 / 23.0	7.0 / 11.57	41.7 / 55.9	95.5
Sample 2	270 / 345	14.5 / 12.4	6.42 / 9.63	33.3 / 29.3	119.4
Sample 3	180 / 240	25.8 / 18.1	-	-	-

Table 3.1: Material parameters of the snow samples. All samples consisted of rounded snow. SSA is the specific surface area, i.e. the ice surface area divided by ice volume. Initial values are determined at the beginning of the experiment and final values at the end of the experiment.

3.2.2 Time-lapse tomography of creeping snow

The snow samples were put into a cylindrical sample holder with a diameter of 35 mm and a height of 100 mm. A cylindrical weight was placed on top of the snow sample and was guided by the sample holder. The sample holder was positioned in a desktop X-ray micro computer tomograph (μCT) (Scanco Medical, Switzerland), which is located in a cold lab at a temperature of $11^{\circ}C$. Sample 1 had a height of 30 mm and a diameter of 35 mm equal to the diameter of the sample holder, thus the sides of sample 1 were constrained. Sample 2 had a height of 5 mm and 16 mm diameter. Thus it was smaller than the sample holder and the sides of sample 2 were not constrained. The weight imposed a pressure of 2 kPa on sample 1 and 10 kPa on sample 2. This corresponds to typical pressures in a snowpack. A pressure of 2 kPa for example corresponds to a pressure below 1 m of snow with a density of 200 kg/m^3. Under this load the samples deformed with strain rates between 10^6 to 10^7 1/s. Sample 1 was compressed during 5 days and reached a strain of 12%. Sample 2 reached a strain of 17% in 19 days. During compression the samples were scanned 9 times. To minimise the amount of data and the scanning times, only the section 3 mm to 6 mm above the bottom of sample 1 was scanned with a resolution of 15 μm. Sample 2 was scanned over the total sample height of 5 mm with a resolution of 18 μm. To avoid that the CT-images get blurred due to the continuous compression of the snow, the structure should move as little as possible during the scan. The minimal possible scan time was 20 minutes. During this time, the plane 6 mm above the bottom of the sample moved 10 μm at a strain rate of 10^6 1/s. This displacement was smaller than the resolution of the CT-images and did not blur the images.

To have additional data for viscosity, the same experiment was repeated three times (samples 3.1 to 3.3), but without computer tomography. Instead of observing the microstructure, only the macroscopic strain was captured by a digital camera with a temporal resolution of one hour.

3.2.3 Evaluation of CT-images

The raw CT-data were reconstructed using a cone-beam algorithm, resulting in a three-dimensional grey-scale (16 bit) volume image (in the following we use “image” for “volume image”). For the analysis of the images, the grey-scale images were transformed to binary images, where

each voxel is assigned to either the ice-phase or the air-phase of the snow microstructure. To this end the images were segmented by thresholding. To reduce the image noise, the images were first median filtered using a 3 x 3 x 3 kernel. The temporal series of binary images of the deforming snow microstructure were used as geometric input for finite element simulations and to determine the compression strain during the experiment. Furthermore the genus of the microstructure was determined from the images. The genus is the maximum number of cuttings without disconnecting the structure.

The strain was determined by image registration. Two images were shifted until parts of the images are congruent. Here we used the technique to determine the shift between two successive CT-images. The difference between the shift of the top slice and the bottom slice of a 3D image determines the deformation between top and bottom and hence the strain. To be able to determine the strain rates $\dot{\epsilon}_t$ from the measured strains we first fitted a power law to the measured strains and then determined the temporal derivative. Given the known stress σ on the sample we can determine the viscosity η_t of the snow for each time step:

$$\eta_t = \frac{\sigma}{\dot{\epsilon}_t} \tag{3.1}$$

Even though snow is not an ideal viscous material with a linear relation between strain rate and stress, this viscosity is a useful measure to characterise and compare the macroscopic properties of a certain snow. Also in literature this value is commonly used (e.g. Johnson and Hopkins, 2005; Kojima, 1967; Lehning et al., 2002). However, this value has to be used with caution. Only viscosities obtained at similar stresses can be compared. The true relation between stress and strain rate in snow is non-linear (Scapozza and Bartelt, 2003).

3.3 Simulations

The CT-images of the snow structure were furthermore used as geometric input for finite element simulations of the viscosity of the snow samples. The beam model was generated from the 3D CT-images using the programming language IDL (IDL 6.4, ITT Visual Information Solutions). Afterwards the model (including mesh, boundary conditions and material properties) was imported to the commercial FE software package ANSYS where the model was solved.

3.3.1 Mesh

We used beam elements to approximate the structure of the snow. Beam elements are computationally much more efficient than conventional solid hexahedron elements, in case the structure can be approximated as a framework. Beam models were already successfully applied to simulate porous structures like trabecular bone (Pothuaud et al., 2004) and metal foams (Stauber et al., 2004). However, snow is more tortuous than a foam or trabecular bone, and the thickness of the elements more variable. To account for these characteristics we assigned different thicknesses to each beam and split tortuous segments into several adjoining beams.

The procedure to create the beam model from the 3D CT-images works as follows: In a first step a skeleton of the structure is created using a 3D thinning algorithm (Tao and Anup, 2007). The thinning algorithm preserves the connectivity. The structure is eroded layer by

layer until only a skeleton of voxels in the centre of the structure is left. In a second step the beams are assigned to the skeleton voxels. A simple approach would take each skeleton voxel as an endpoint of a beam. However, the number of beam elements can be strongly reduced. The Reumann-Witkam algorithm creates from a sequence of adjoining points a line. We applied without loosing much precision a modified Reumann-Witkam algorithm (Shi and Cheung, 2006) to the skeleton voxels, so that each beam covers a certain line segment of the skeleton. Thereby the precision parameter *e* limits the maximum distance between skeleton and beam elements like in a standard Reumann-Witkam algorithm. Additionally the parameter *a* is introduced to limit the maximum thickness difference in a skeleton segment covered by one beam. The structural thickness is determined by assigning the Euclidean distance transform (Soille, 1999) of the original image to each skeleton voxel. This distance is the distance from a skeleton voxel to the nearest air-voxel in the original image. In a last step the radii of the beams are determined. The root mean square of the radii of a skeleton segment is assigned to the corresponding beam. If the cross-sectional area is a circle, this approach conserves the area. For all other shapes the cross-sectional area is underestimated. Therefore the beam model is strictly valid only for structures with circular cross-sections. We compensated the underestimation of the cross-section by multiplying with a volume-conserving factor such that the total beam volume corresponds to the total ice volume in the original image. This factor ranges from 1.8 to 2.1.

3.3.2 Material model

We used two alternative material models to simulate the creep behaviour of the snow samples: a polycrystalline and a monocrystalline model. The parameters of the material models are adjusted to the temperature of -11$^\circ C$ and are valid for the range of stresses in the ice network during the experiments. The stresses in the ice network can be estimated by dividing the stress on the snow samples (10 kPa) by the relative density (0.2). This gives a stress of 50 kPa, for the unrealistic case that all ice in the snow was optimally arranged and carries the same load. In fact the stresses are not equally distributed over the ice network and much higher stresses are expected to occur. The elastic behaviour for both models is described by a Young's modulus of 10 GPa and a Poisson's ratio of 0.3 (Schulson and Duval, 2009).

Polycrystalline model

The secondary creep of polycrystalline ice is described by Glen's law:

$$\dot{\epsilon}_p = B_p \, \sigma^{n_p} \, , \tag{3.2}$$

with $B_p = 10^{-7}\,\mathrm{MPa}^{-n_p}/s$ and n_p=3 for stresses between 0.1 and 10 MPa and B_p=5·10^{-8} MPa$^{-n_p}$ $/s$ and n_p=2 for lower stresses at a temperature of -10$^\circ C$ (Schulson and Duval, 2009). The measured strain rates for a given stress and temperature differ by a factor of 10 (Schulson and Duval, 2009). Especially for low stresses (<200 kPa) also the exponent differs between different experiments. Values between 2 and 3 can be found in literature. The parameters chosen here are therefore not completely certain.

Monocrystalline model

In fact the snow consists of randomly orientated single ice crystals, like polycrystalline ice, but the grains are not laterally constrained. Therefore we decided to use also a monocrystalline material model for the beams. In this model each beam behaves like a single ice crystal with a random orientation. The viscosity of monocrystalline ice depends strongly on the orientation of the crystal lattice. The c-axis in ice is perpendicular to the basal plane. The optimal orientation for the fastest compression of a single crystal is at an angle of 45° between force vector and c-axis, because then the shear stress on the basal plane is maximal. At -10°C the steady-state creep rate of a single crystal with this orientation is given by

$$\dot{\epsilon}_m(45°) = B_m \, \sigma^{n_m} \ , \tag{3.3}$$

with $B_m = 10^{-4}$ MPa$^{-n_m}$ $/s$ and n_m=2 (Schulson and Duval, 2009).

From this equation we can derive the creep rate of a single crystal with the angle α between force vector and c-axis:

$$\dot{\epsilon}_m(\alpha) = \begin{cases} 2^{n_m+1} B_m \, \sigma^{n_m} \, sin^{n_m+1}(\alpha) \, cos^{n_m+1}(\alpha), & 3° < \alpha < 87° \\ B_{mp} \, \sigma^{n_m}, & 0° < \alpha < 3°, \ 87° < \alpha < 90° \end{cases} \tag{3.4}$$

with $B_{mp} = 10^{-8}$ MPa$^{-n_m}$ $/s$ (Schulson and Duval, 2009).

Only where the angle of the c-axis of the single crystal to the force direction is between 0° – 3° and 87° – 90° other deformation mechanisms than basal glide contribute significantly to the deformation. For these orientations the creep rate is set to the minimum creep rate for non-basal glide. This material model was implemented by defining 36 different material models for 36 different, equally distributed angles between 0° and 90°. Each beam was then randomly assigned to one of these material models. Hence each beam simulates the behaviour of a single crystal with random orientation.

3.3.3 Boundary conditions

The boundary conditions for the simulation were chosen to correspond as well as possible with the experimental conditions. The bottom of the simulated cut-out was fixed in all directions. For sample 1 the movement of the sides was suppressed in normal direction to the sides. For sample 2 the sides were unconstrained like in the experiment. The movement of the top was suppressed in horizontal direction, while in vertical direction a velocity was prescribed. The velocity was chosen to correspond with the measured strain rates during the experiment. Prescribing a velocity is easier than prescribing a force. Even though a force was prescribed in the experiment, it is appropriate to prescribe a velocity in the simulation and compare the resulting simulated force with the given force of the experiment.

3.3.4 Solution

The FE model was imported to the commercial FE software package ANSYS. Beam elements based on Timoshenko beam theory were used. This beam type is suitable for analyzing slender

to moderately thick beam structures. Shear deformation effects are included and creep models are supported by this element type. The solution settings for the nonlinear solution were automatically optimised. This included the choice of the solver, the choice of the time steps and the convergence tolerances. The deformation velocities were applied stepped. This means that the deformation velocity is constant over the simulated time interval and not ramped. The length of the time interval was varied between 1000 and 5000 s to be in a steady-state of the creep deformation. The simulation of a structure with 10000 elements took about 2 hours on a 2.66 GHz Intel Pentium processor with 2 GB memory.

3.3.5 Postprocessing

The simulated viscosity was calculated as follows. The simulated reaction forces in compression direction of all constrained nodes at the top or at the bottom of the sample were summed up. This sum divided by the area of the simulated cut-out gives the compressive stress on the sample. The ratio between simulated compressive stress and prescribed strain rate is the viscosity of the simulated structure (Equation 3.1).

3.4 Results and discussion

In this section we will first perform a sensitivity analysis to quantify the uncertainties and error sources of the model. Then we discuss the simulations and compare them with the measurements. Based on the comparison, we discuss the model assumptions about the behaviour of the ice in snow. Finally we discuss the influence of microstructure evolution on snow hardening and the applicability of foam theory on snow.

3.4.1 Sensitivity to model parameters

The quality of the beam model depends on several parameters, as the size of the simulated volume (representative volume element), the quality how well beams approximate the snow structure, the influence of the boundary conditions, the length of the simulated time interval and the parameters of the material model.

The size of the simulated volume needs to be large enough to represent the macroscopic properties of the sample. For small, round grained snow the representative volume element with respect to heat conductivity has an edge length of about 5 mm (Kaempfer et al., 2005). The simulated volume of sample 1 has dimensions of 5.82 mm $\times$ 5.82 mm $\times$ 2.82 mm and 5.8 mm $\times$ 5.8 mm $\times$ 3.6 mm for sample 2. These volumes should be large enough to represent the mechanical properties of the snow sample. As a rough test we compared the results of sample 1 with a cubic cut-out with an edge length of 2.61 mm. The result differed by less than 10%.

The representation by beam elements was checked by comparison with discretisations using tetrahedral and octahedral meshes. Tetrahedral and octahedral meshes reproduce the geometry much more directly and precise at the cost of a much higher number of elements. The tetrahedral mesh was created by ANSYS ICEM CFD and simulated by ANSYS. The octahedral mesh was created and simulated by IPLFE (van Rietbergen et al., 1995). Figure 3.2 shows the tetrahedral and the beam mesh of the same snow structure. Linear elastic simulations of this structure gave

a Young's modulus of 41 MPa by ANSYS and 31 MPa by IPLFE. The Young's modulus of the beam system is between 32 MPa and 110 MPa depending on the choice of the parameters e and a. Thus for this structure the results of the beam mesh are close to the reference results for small e and a. However, the sensitivity of the results to e and a is high. The results varied by a factor 3 for different e and a. We used a value of 2.5 for a and a value of 0.1 mm for e, as this was a good compromise between exact representation of the structure and a small number of elements.

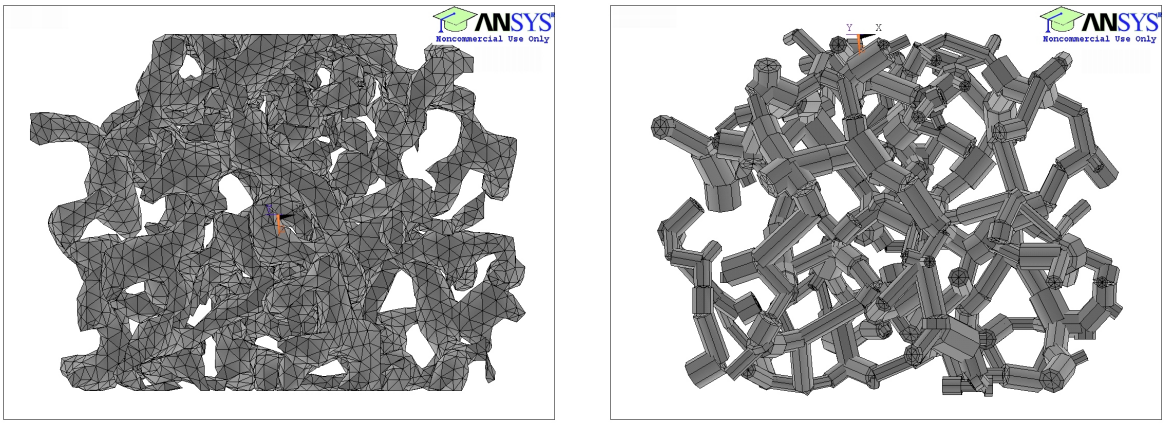

a) b)

Figure 3.2: Comparison of tetrahedral mesh (24187 elements) and beam mesh (383 elements) of the same snow structure. This cut-out of sample 1 is a cube with 2 mm side length.

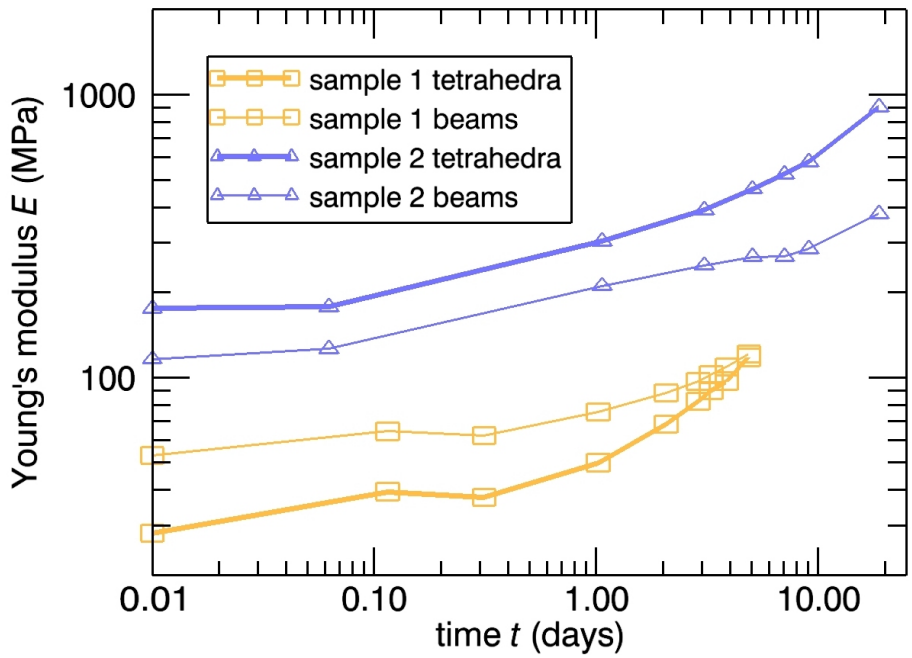

Figure 3.3: Comparison of simulation results based on the tetrahedral and beam mesh for sample 1 and sample 2.

The representation by beams becomes less appropriate with decreasing porosity. An extreme case is firn or ice with air pores, which can hardly be approximated by beams. Sample 1 has a

low density of 200 to 230 kg/m^3. The results of the beam model are close to the reference data (Figure 3.3). But the increase of the Young's modulus from step 0 to step 9 was not covered to the same extent as in the reference model (Figure 3.3). While the Young's modulus increased by a factor 2.5 in the reference model, the increase in the beam model was only factor 1.9. For sample 2, which had a higher density, this difference was even more distinct: the Young's modulus of the reference model increased by a factor 5.2, while the beam model determined an increase of only 3.2. For higher densities (sample 2) the beam model underestimates the Young's modulus, while it overestimates it for lower densities (sample 1). This difference can be explained by the dependence of the beam representation on density. To consider this difference, we adjusted the resulting stress of the beam model with a correction factor. The correction factor is the ratio between Young's modulus simulated by the reference model and Young's modulus simulated by the beam model.

The influence of the boundary condition on the simulation results is estimated by comparing the results after applying both boundary conditions, described in Section 3.3.3. One boundary condition restricts any movement of the sides in normal direction. For the other boundary condition the sides are unrestricted. The effective conditions during the experiments were somewhere between these two extremes. The difference of the simulation results is about 10%.

The time interval needs to be long enough to be in a steady-state of the creep deformation and short enough to not substantially change the microstructure. To check which time interval for the creep simulation is suitable, we varied the time interval until convergence. The time interval needed to be long enough so that the creep deformation was dominant and the elastic deformation could be neglected. Figure 3.4 shows the simulated viscosity during different time intervals for different strain rates. The creep rates in the experiments range from 10^{-6} to 10^{-8} 1/s. For a creep rate of 10^{-6} 1/s the forces converge after around 200 s and for a creep rate of 10^{-8} 1/s the forces converge after 3000 s. To be on the safe side we used a time interval of 5000 s for most simulations. For a strain rate of 10^{-6} 1/s the strain after 5000 s is 0.5%. This is small enough to not substantially change the structure during the simulation. For time intervals of 5000 s and 10000 s the simulated viscosities vary by less than 2%.

The material models were the most uncertain parameter of the simulation. The exponent of the creep law does not vary a lot and is always between 2 and 3 in literature (Schulson and Duval, 2009). But the pre-factors for poly- and monocrystalline material models vary by factor 10 in literature. By choosing the logarithmic average of the pre-factors from literature the chosen value can be 3 times too large or 3 times too small. Fortunately the sensitivity of the simulation results is small to this pre-factor: Increasing this pre-factor by factor 3 changed the simulated viscosity by a factor 0.7. And decreasing the pre-factor by factor 3 increased the simulated viscosity by a factor 1.5.

The mentioned error sources multiply to an uncertainty of about a factor 2 for the simulation results. The material model was the most uncertain parameter. Some uncertainties were difficult to estimate. Therefore we could not determine an exact confidence interval. However, at least an order of magnitude of the uncertainty of the model could be estimated. Most parameters, like the pre-factor of the material model, just influence the order of magnitude of the simulation results but not the relative evolution of the results over time.

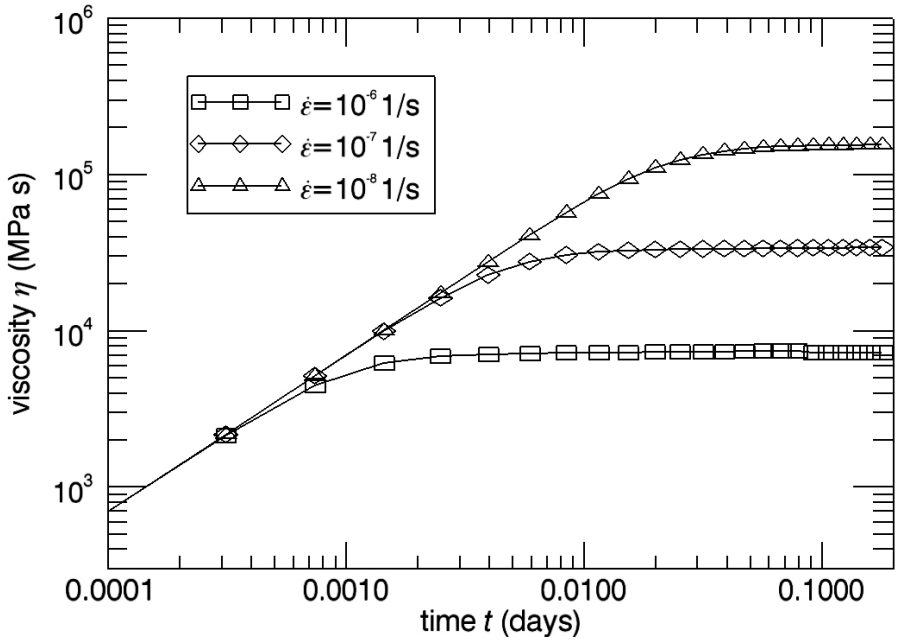

Figure 3.4: Dependence of simulated viscosities on simulated time interval for different strain rates.

3.4.2 Comparison of simulated and measured results

During the creep experiments the snow samples were scanned several times by μCT. Thereby the evolution of the snow structures was observed. By using a cut-out of each CT-image as input for the creep simulation, we obtained the evolution of the simulated viscosities. The same cut-outs were also used to measure the strain during the experiments by the method described in Section 3.2.3. From the time evolution of the strains we can determine the strain rate and finally the viscosity. To determine a smooth time derivative of the strain we first fitted a power law to the measured strain values (Figure 3.5). The deviations of the fitted from the measured strain values at the beginning (sample 1) and at the end (sample 2) may result from experimental difficulties where the sample had to be removed from the CT. Small vibrations during this procedure cannot be ruled out. The fit is used to extract a smooth evolution of the measured viscosity by the method described in Section 3.2.3, the fit is subsequently used for comparison with the simulations. For all simulations of one time series all parameters including the material model were kept constant. Thus the changes of the simulated viscosity over time were only caused by the changing microstructure.

By comparing simulated and measured viscosities we can check whether the simulated viscosities are the same as the measured viscosities and whether the evolution of the simulated and measured viscosities matches. Thereby the exponent and the pre-factor of the material models can be verified. Changing the exponent in the material model changes the evolution of the simulated viscosity, while a change of the pre-factor shifts all simulated viscosities by the same magnitude.

First we have a look at the exponent of the material model. In Figure 3.6 the change of the measured viscosity is compared with simulations using different exponents for sample 1 and

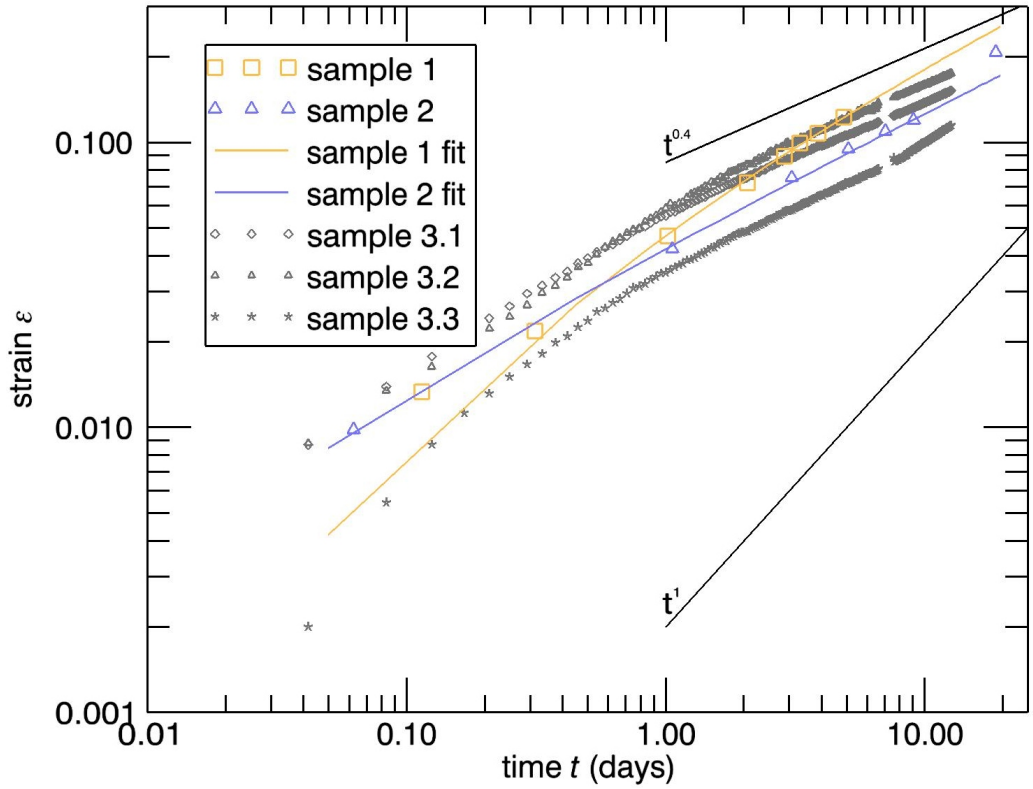

Figure 3.5: Strain over time for sample 1, sample 2 and reference experiments with sample 3. The hardening follows a power law with exponent 0.4. The measured strains are fitted by $\epsilon(t) = a\,(b+t)^n - c$. The fitted strains are used to determine the strain rates and the measured viscosities.

sample 2. An exponent of 2 gives the best agreement between simulated and measured viscosity evolution for sample 1. However, for sample 2 we find that an exponent somewhere between 2 and 3 gives the best agreement between simulated and measured viscosity. These exponents are in the small range of values realistic for ice. In experiments with mono- or polycrystalline ice typically exponents between 2 and 3 were determined.

Next we will compare the magnitude of the measured and simulated viscosities. The different pre-factors of the mono- or polycrystalline material models have a much bigger impact on the simulated viscosities than the exponents. In Figure 3.7 the different material models are compared for sample 1 and sample 2. The simulated viscosities using the material model for monocrystalline ice was close to the measured viscosities, while the results of the simulations with the polycrystalline ice material model were about 10 times too large.

Sample 2 had a higher density and viscosity than sample 1. The approximation of high density snow by beams can be problematic. But the agreement between simulation and measurement is rather good. Therefore we conclude that the model was able to simulate the creep behaviour of round grained snow with densities between 200 and 400 kg/m^3.

These results show for the first time that mechanical properties of snow can be modelled successfully using fundamental mechanical parameters from ice and a detailed representation of the microstructure.

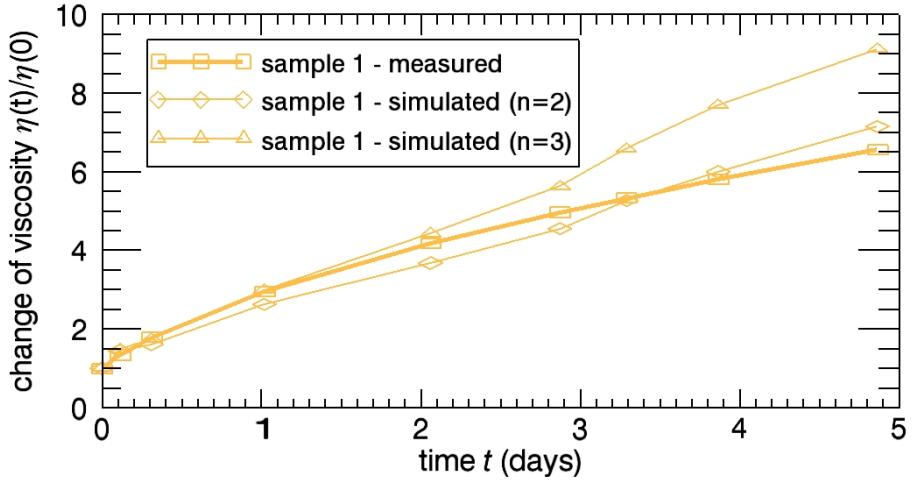

a)

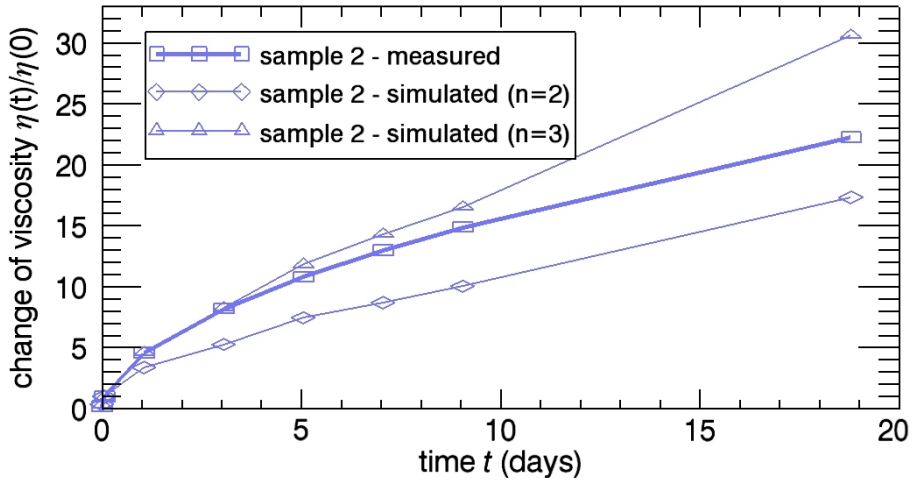

b)

Figure 3.6: Comparison of the change of viscosity over the experiment for different exponents in the material model. Figure a) for sample 1 and figure b) for sample 2.

3.4.3 The creep behaviour of ice in snow

We used three assumptions about the creep behaviour of ice in our model, namely that ice in snow behaves like monocrystalline ice, that grain boundary sliding has no effects on snow viscosity and that ice in snow deforms like monocrystalline ice in secondary creep. We will now discuss the correctness and the relevance of these assumptions based on the verified simulation results.

The assumption that the ice in snow behaves like monocrystalline ice is based on crystallographic observations of snow. As described in Section 3.4.2 we could confirm this assumption for the snow types we investigated: The simulated viscosities for the monocrystalline material model matched the measured viscosities while the simulated viscosities for the polycrystalline material model were more than one order of magnitude higher. The high viscosity of polycrystalline ice compared to the viscosity of monocrystalline ice is caused by the mutual blocking of the single crystals. A crystal in polycrystalline ice which is weaker due to its orientation cannot deform independently from its neighbouring grains. In contrast the single crystals in snow have

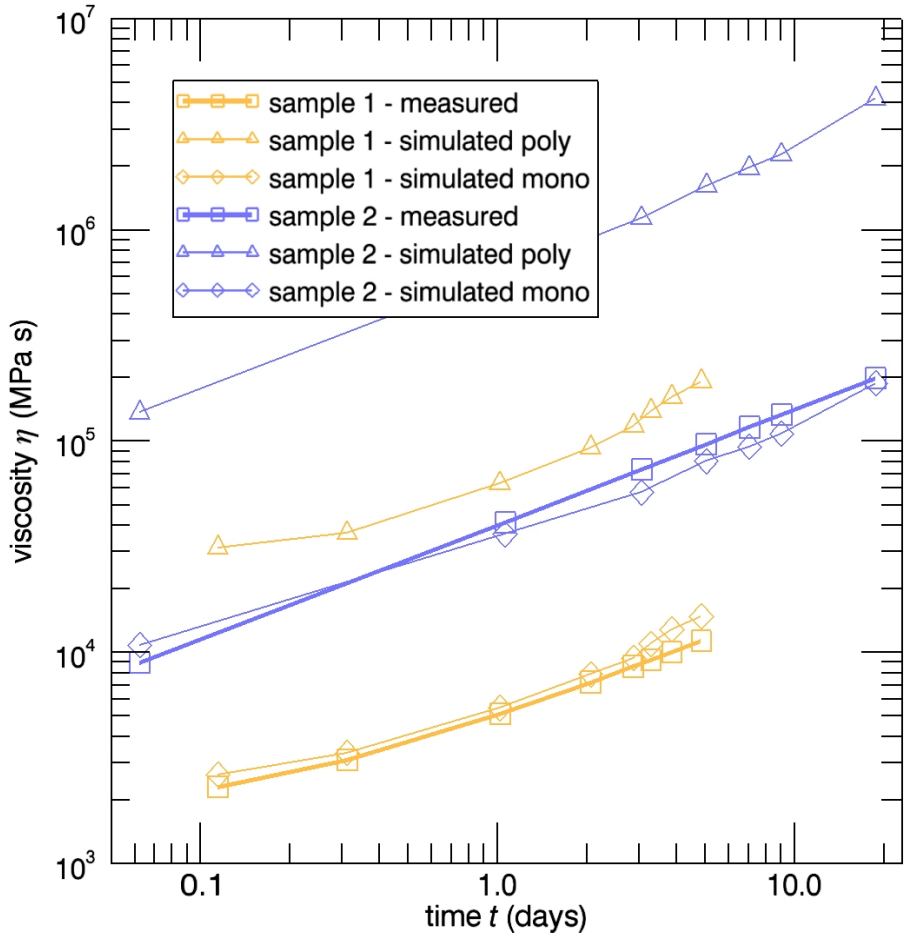

Figure 3.7: Comparison of simulated viscosities using different material models for sample 1 and sample 2.

a much higher freedom to deform independently from their neighbouring grains. This is true as long as the density is low and the grains in snow are single crystals as in Figure 3.1 a).

An interesting hypothesis is that snow types with different crystallographic texture behave differently. For the artificial snow in Figure 3.1 b) each grain is a polycrystal. This could dramatically change its mechanical properties. The viscosity of such snow could be one order of magnitude higher than for monocrystalline snow (Figure 3.7). Also the orientation of the single crystals in snow could be important for the creep behaviour of snow, since the creep behaviour of ice single crystals is highly anisotropic (Equation 3.3). We assume random orientations of the single crystals in our model. If the single crystals in snow have a preferred orientation this would have a huge impact on the creep behaviour of the snow. Takahashi and Fujino (1977) investigated the crystal orientation in snow and found that the orientation is not always random.

All these statements about the impact of the crystallographic texture on snow properties are somewhat hypothetical. But we showed that the crystallographic texture in snow is a potential key to some unsolved problems in snow mechanics.

Grain boundary sliding is believed to be the dominant deformation mechanism in snow with densities lower than 550 kg/m^3 (Johnson and Hopkins, 2005). According to the established opinion grain boundary sliding should occur during our experiments. It is disputed whether

grain boundary sliding is a relevant deformation mechanism during creep deformation of snow. Our model does not consider grain boundary sliding but successfully simulates the creep behaviour of snow. Still, this is not a strong argument against grain boundary sliding, it could be possible that part of the deformation is caused by grain boundary sliding and the remaining part by intracrystalline deformation. In the model only the intracrystalline deformation is considered. Still the model results can match the experimental result if the material law used for the intracrystalline deformation is "softer" than in reality, so that it somehow includes both grain boundary sliding and the intracrystalline deformation. Since the parameters for the material model of ice are uncertain, it is not possible to conclude from the model that grain boundary sliding does not occur in snow. But the model results definitely support the assumption that grain boundary sliding is not a relevant deformation mechanism.

A stronger hint against grain boundary sliding than by the model is given by the 3D-images of the deforming snow structure captured during the experiments. Rearrangement of particles is supposed to go along with grain boundary sliding during the deformation of snow. But no rearrangement of particles was observed. The deformation resembles the compression of a sponge or foam and not a granular medium.

These two hints and the literature let us conclude that grain boundary sliding and grain rearrangement did not occur during our experiments. Furthermore it seems questionable whether grain boundary sliding is a relevant mechanism for low deformation rates at all. Also the intensively discussed decrease in creep rate at a relative snow density of about 0.6 during snow densification fits to this picture of intracrystalline deformation in snow (Ebinuma and Maeno, 1987; Johnson and Hopkins, 2005). At this point the structure becomes too dense to allow independent deformations of the single grains.

The hardening in snow during compression could be caused by the hardening of the ice crystals or by the changing snow structure. We have captured the changing snow structure during its deformation by micro-tomography and used the images as geometric input for our model. By using a constant, secondary, creep rate we excluded the hardening of ice. Since the modelled viscosity matched the measured results well, we concluded that the influence of the ice hardening was negligible compared to the influence of the structural hardening. Therefore it is appropriate to use a simple monocrystalline material model with a constant creep rate.

A counter-argument could be that a too large exponent in the material model is the reason. The higher the exponent the more hardening is modelled (see Figure 3.6). However, the realistic value for ice used makes such a reason unlikely.

This conclusion might not be valid for snow of higher density, because the behaviour of such snow comes closer and closer to the behaviour of ice. Furthermore this conclusion could be wrong for time scales smaller than days. The temporal resolution of our experiment is too low to draw conclusions about the processes in the first hours of the experiment. Therefore we carried out comparative creep experiments with a temporal resolution of 1 hour. And indeed the hardening behaviour changed after about 10 hours (Figure 3.5). Probably the ice was in primary creep during the first hours of these experiments.

An interesting remark is that the hardening of snow follows a power law with exponent 0.4 (Figure 3.5) similar to the exponent in Andrade creep. Andrade creep occurs in crystals (e.g.

Schulson and Duval, 2009) or polymers (e.g. Ward and Pinnock, 1966) for example. Even though the hardening mechanisms take place on different scales in these materials, similarities in the mechanisms may exist.

3.4.4 Mechanism of snow hardening by microstructure evolution

Snow shows a pronounced hardening behaviour during its densification. During the experiments the viscosity of the snow samples increased by more than a factor 5 for a density increase of only 10%. This increase in the viscosity cannot be explained when considering snow as a foam of ice. Kirchner et al. (2001) suggested to consider snow as an open foam of ice. By applying the foam model from Gibson and Ashby (1988), he found that viscosity should increase with density to the power of 6.5 for snow densities between 200 and 550 kg/m^3. He verifies this hypothesis with measurements of strength and Young's modulus from literature. These measurements indeed change with the power of 6.5 of the density. He argues that strength and Young's modulus are notoriously difficult to measure and in fact are measurements of viscosity. This argument does not correspond with our measurements of viscosity. According to Kirchner, snow viscosity increases by factor 1.86 for a density increase of 10%. This is much smaller than our experimental and simulated results (see Figure 3.8). The reason for this discrepancy is that foam theory does not consider an important mechanism of snow densification, namely the creation of new connections in the ice network. The existence of these new connections can be proven visually by comparing CT-images of the snow samples from the beginning and the end of the experiment or by calculating the genus of the ice network from the CT-images. The change in the genus, the connectivity, is about 50% for a density increase of 10% (see Table 3.1). The new connections have a huge impact on the behaviour of the snow. Stresses are more evenly distributed over the ice network due to the new connections.

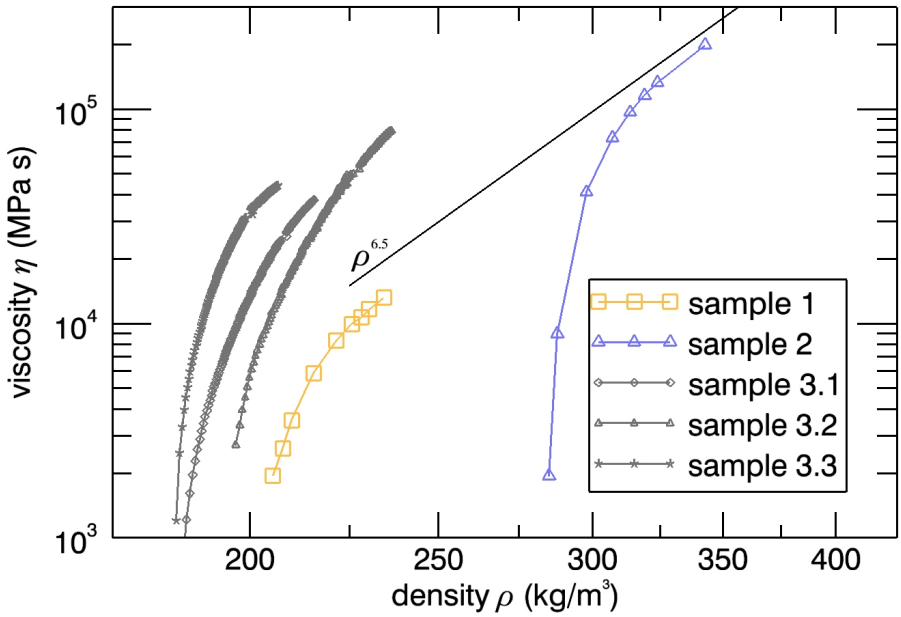

Figure 3.8: Increase of viscosity over density for sample 1, sample 2 and the reference experiments (sample 3). The increase of viscosity is much larger than proposed by Kirchner et al. (2001) (power law with exponent 6.5).

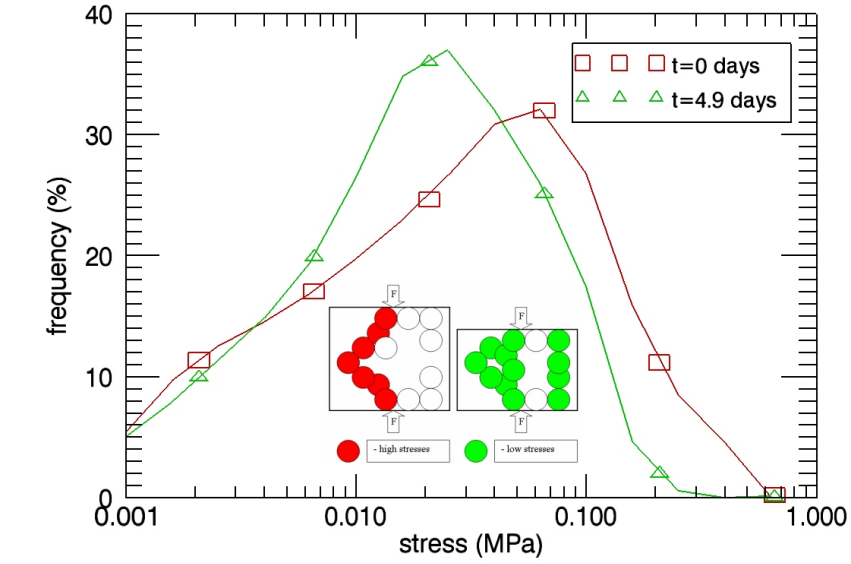

a)

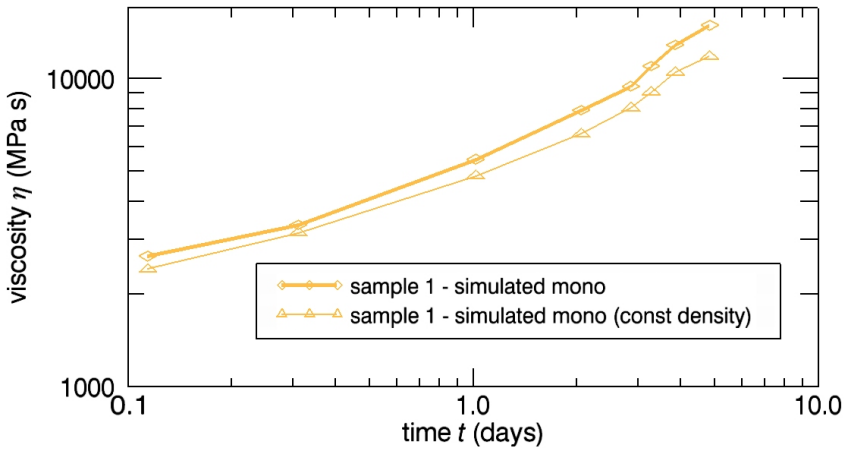

b)

Figure 3.9: Mechanisms of snow hardening. Figure a) shows the compressive stress distributions in the simulated snow structures at the start and end of the experiment. The sketch shows the principle of hardening during snow densification by new connections. Figure b) shows two simulation results of sample 1. The upper curve corresponds to normal simulations with the monocrystalline material model like in Figure 3.7. The other curve corresponds to the same material model but the density was kept constant over time.

This is shown in Figure 3.9 a) by comparing the stress distributions of the simulated snow samples. The distribution of the axial stresses at the beginning of the experiment (squares) was wider with higher stresses than at the end of the experiment (triangles). In the beginning of the experiment only a small fraction of the ice network was load bearing. This fraction was under high stresses. At the end of the experiment new connections were formed causing a more even distribution of stresses. The principle of this mechanism is illustrated in the sketch in Figure 3.9 a). The new connections and the resulting more even distribution of the stresses over the ice network considerably increase the viscosity of the snow. This can be seen in Figure 3.9 b). Simulated viscosities of sample 1 using the monocrystalline material model are shown. The lower curve corresponds to simulations where the density was kept constant over time by re-

ducing the cross-sections of the beams. The simulated viscosity increase was therefore only caused by the changing ice skeleton (new connections). The influence of the density increase was excluded. But the viscosity increases almost as much as for the simulation where the density increase was included (upper curve in Figure 3.9 b). We can therefore conclude that the evolution of the ice skeleton and its new connections had a significant impact on the behaviour of snow during densification. As these mechanisms are not considered in foam models, the idea of snow as a foam of ice is inappropriate to describe snow behaviour over a wide range of densities. However, the evolution of the viscosity as a function of density (Figure 3.8) seems to approach a power law with exponent 6.5. The figure suggests that after an initial phase, where new connections in the structure play a major role, the densification might eventually follow the behaviour suggested by Kirchner et al. (2001). However, longer creep experiments are necessary to proof this assumption.

3.5 Conclusions

Based on micro-tomographic images, a finite-element beam model was developed. The model successfully approximates the complex microstructure of snow. The beam model reduces the number of elements by two orders of magnitude compared to common meshes. Therefore the beam model enables computationally expensive creep simulations of large snow structures. For the first time the mechanical response of snow was successfully modelled and verified based on snow microstructure from 3D CT-images. Based on these simulations, we conclude that the ice in snow behaves like monocrystalline ice. The crystallographic texture of snow has a huge impact on its viscosity and grain boundary sliding was not the dominant mechanism during compression. The crystallographic orientation of the snow grains is an important property. A deeper understanding of the material behaviour may not only require detailed microstructural data, but also at least a frequency map of the grain orientation. The dominant deformation mechanism in our experiments and simulations was intracrystalline creep. This suggests that grain boundary sliding might be much less relevant than usually postulated.

The changing microstructure was identified as one of the dominant hardening mechanisms in snow, while the hardening of ice as the base material was negligible. The most relevant structural changes were the creation of new connections, which could be quantified by determining the genus of the structure. The structural modifications were accompanied by a more uniform stress distribution and a reduction in peak stress. This is unlike in foam, where the creation of new connections is not considered.

Chapter 4

Mechanics of the ski-snow contact

Two outstanding questions of the ski-snow friction are considered: the deformation mode of the snow and the real contact area. The deformation of hard, well sintered snow in a short time impact has been measured with a special linear friction tester. Four types of deformations have been identified: brittle fracture of bonds, plastic deformation of ice at the contact spots, elastic and delayed elastic deformation of the snow matrix. The latter is the dominant deformation in the ski-snow contact. Based on the measured loading curves the mechanical energy dissipation of snow deformation in skiing on hard snow has been determined and found negligible compared to the thermal energy dissipation. A mechanical model consisting of ice spheres supported by rheological elements (a nonlinear spring in series with a Kelvin element) is proposed to model the deformation of snow in the ski-snow contact. The model can describe the delayed elastic behaviour of snow. Coupled with the complete topographical description of the snow surface obtained from X-ray micro computer tomography measurements, the model predicts the number and area of contact spots between ski and snow. An average contact spot size of 110 μm, and a relative real contact area of 0.4% has been found.

4.1 Introduction

It is well known that the slipperiness of ice and snow is due to the formation of a thin meltwater film (Ambach and Mayr, 1981; Bowden and Hughes, 1939; Colbeck et al., 1997; Glenne, 1987; Tusima and Yosida, 1969). The frictional heat generated by the rubbing of ice asperities against a slider's base melts the ice and the resulting meltwater lubricates the interface. In very cold conditions when the heat is not sufficient to melt the ice, snow is similar to sand with a high dynamic frictional coefficient of 0.3 (Bowden, 1953). In most natural conditions, however, meltwater lubrication occurs and snow and ice exhibit frictional coefficients as low as 0.01 making skiing, sledging, and skating possible.

Snow is a sintered material consisting of mono-crystalline ice grains, which are bonded together (Colbeck, 1998). The ice crystals form in the atmosphere. After they fall to the ground they immediately start to sinter together and quickly form a 3D foam-like structure that we call snow. At this stage a process called snow metamorphism starts. During snow metamorphism the size and shape of the ice crystals change. In addition the bonds between the individual crystals grow stronger by sintering. This converts the initially fragile snow into a denser and stronger solid porous material. Depending on how far the metamorphism proceeded, snow densities range from 50 kg/m^3 for freshly fallen snow to 800 kg/m^3 for firn. The latter is close to the density of ice (920 kg/m^3). In Figure 4.2 and 4.3 the 3D microstructure of a high density snow and its surface is visualised. The surface consists of the same type of grains as the rest

of the snow. Only under certain conditions special surface layers, like surface hoar or ice crust occur. In this paper we do not consider such surfaces.

Skiing involves complex and interesting scientific phenomena that attracted the attention of many researchers over the past 100 years (e.g. Colbeck, 1994; Glenne, 1987; Lind and Sanders, 1996). Since the pioneering work of Bowden and Hughes (1939), who proposed the idea of meltwater lubrication and introduced polytetrahydrofourene (PTFE) as a superior ski base material (Bowden, 1955), the theory of ski friction has been developed to a high degree on a phenomenological basis. The effects of temperature (Buhl et al., 2001), load (Buhl et al., 2001), speed (Colbeck, 1988), snow type (Hamalainen, 1986), and ski base material (Bowden, 1955; Colbeck and Perovich, 2004) on the frictional coefficient of a ski were studied experimentally. In addition qualitative relations were established on an empirical basis. More recently, a fundamental approach to understand the basic physical processes involved in ski friction was started by Glenne (1987) and Colbeck (1994). The latter reviewed the individual mechanisms that contribute to the resistance of a ski sliding on snow (Colbeck, 1994). These include the plowing of snow in front of the ski, snow compaction below the ski, deformation and fracture of asperities rubbing against the ski, shearing of the meltwater film, drag by dirt particles, and possibly capillary attachments between snow grains and ski base. Currently, these processes, but especially their interactions are poorly understood and a comprehensive description of the ski-snow friction is missing. An attempt to numerically model the friction of a flat polyethylene slider on ice including all physical processes was recently made by Baurle et al. (2007). They concluded that the most critical parameter in the formation of the meltwater film and thus the frictional coefficient is the real area of contact.

We address two outstanding questions of the ski-snow friction: the deformation mode (elastic, plastic, or brittle) of the snow during the contact, and the real contact area between snow and ski base. This is studied by displacement-controlled loading experiments of hard packed snow samples. Therefore a ski base is pressed vertically on the snow samples. The analysis of the resulting force-displacement curves gives insight into the dimensions of the occurring forces, displacements and consequently the mechanical energy dissipation during skiing. Before and after the loading experiment a high resolution 3D image of the snow microstructure is captured by X-ray computer tomography (Schneebeli and Sokratov, 2004). By comparing these images we can visualise the snow deformation. This visualisation and the analysis of the force-displacement curves allow a precise identification and quantification of different deformation modes. Furthermore we use the 3D images to characterise the snow surface. The radius and the distribution of the snow grains at the surface are important parameters in the ski-snow contact. In a last step a model of the ski-snow contact is set up. The mechanical response of each grain is modelled by rheological elements. Combining this with the distribution of the grains at the surface, we can model the measured force-displacement curves. The parameters of the rheological element are determined using the Hertzian theory of elastic contacts (Johnson, 1985) and a finite element simulation of the mechanical response of the snow structure. The modelled stresses at the contacts exceed the strength of ice by far, so that following simple approximation for the real contact area can be justified: the real contact area is the ratio between normal force and strength of ice (Bowden and Tabor, 1950). With this approximation the model predicts besides the number also the size of the contact patches. These are the most important

input parameters of a frictional heat simulation.

While our experiment is a vertical impact, in reality the snow grains rub against the ski and experience a shear force in addition to a normal force. Due to the low frictional coefficient, the normal force is much bigger than the shear force and therefore we can neglect the shear deformation in respect of the real contact area and the deformation mode. However, this approximation is valid only in the beginning of the contact. When the accumulated frictional heat melts the top of the ice grains, the contacts get lubricated and the real contact area increases. The amount of meltwater also increases, but it is constantly squeezed out from the contacts. In this region the real contact area is primarily determined by the melting-squeezing mechanism not by the deformation of the grains (Baurle et al., 2007). The polishing effect of the meltwater lubrication is very pronounced. The relative contact area after the passage of a ski was determined from micrographs of the snow surface. It was found to be around 2-4% (Baurle et al., 2007; Colbeck, 1994; Huzioka, 1962). This is one order of magnitude higher than the contact area of 0.4% we determined in our experiments without frictional melting.

4.2 Experiments

4.2.1 Snow sample preparation

The goal was to prepare reproducible snow samples with structural and mechanical properties similar to that of the snow on racing ski tracks. This corresponds to high density, well packed and well sintered snow with relatively small grains. We used finely grained fresh snow stored for several months in a freezer at -40$^{\circ}C$. Grains with diameters between 250 and 500 μm were sieved into the sample holder in a cold room at T_{air}=-6$^{\circ}C$. The sample holder consisted of a 35 mm diameter solid cylindrical base and a hollow cylinder that fits snugly, but can slide easily up and down on the base. This is illustrated in Figure 4.1. The snow was compacted to a density of 500 kg/m^3 in the sample holder. A flat ultra high molecular weight polyethylene (UHMWPE) sheet was used as an impactor. UHMWPE is the base material of modern skis. During compaction the hollow cylinder slides down on the base. Holes drilled into the cylinder prevent pressure build-up in the pore space of the snow. After compaction the snow was allowed to sublimate for approximately one hour to smoothen the snow surface. It was then covered to prevent further sublimation and placed into a chamber where it was stored at -3$^{\circ}C$ for 24 hours to obtain a high strength, well sintered sample. In total, 16 samples were prepared.

4.2.2 Tomography measurements of the snow surface

It is possible to obtain a high resolution 3D image of the snow structure with X-ray tomography (Schneebeli and Sokratov, 2004). A μCT 80 X-ray micro computer tomograph (μCT) from Scanco Medical (Bassersdorf, Switzerland), placed in a cold chamber, was used to characterise the snow surface and to visualise the deformation of snow grains. A special adapter allowed placing the sample holder into the μCT. Images with 18 μm nominal resolution were taken of the top 3 mm of the snow samples. The duration of a scan is approximately one hour. For image processing and stereological characterisation the raw sinograms of the μCT were transformed into 16-bit images. To reduce the noise, the stacked images were median filtered using a 3 x 3 x 3 kernel and Gaussian filtered using a 5 x 5 x 5 kernel with σ=1.2. Finally these images were

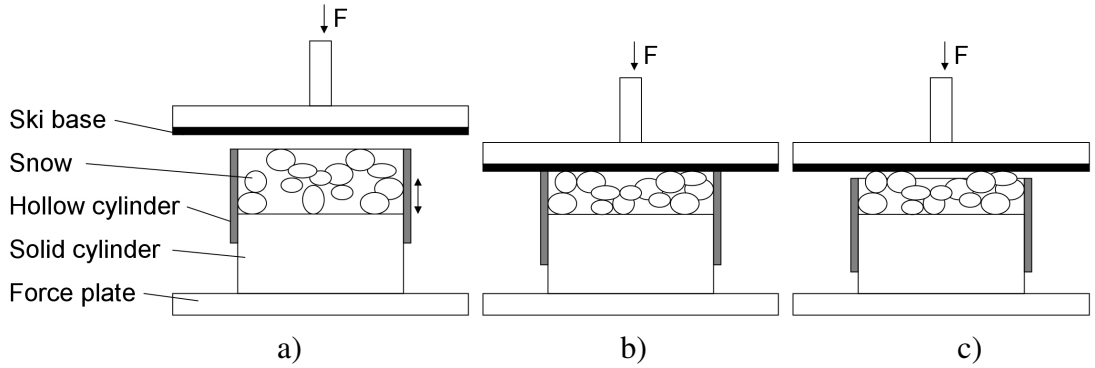

Figure 4.1: Sketch of the experimental setup used for sample preparation (a,b) and the loading experiments (c). For sample preparation low-density snow (a) is compacted to high-density snow (b) by pressing the ski base on the snow. During compaction the hollow cylinder is pushed down by the ski base. It is guided by the solid cylinder. In the experiments the snow is impacted with the ski base. The hollow cylinder is pushed down a bit before running the experiment (c) to avoid contact with the ski base.

segmented by thresholding, resulting in a binary image of the snow microstructure. Images were taken before and after the impact experiment. To determine the location and magnitude of the snow deformation, the displacement field between the two images was calculated using particle image velocimetry (Pudasaini and Hutter, 2007). Therefore the displacement vector of each voxel is determined by cross-correlating a neighbourhood of the voxel in both images. In addition to this analysis, the 3D images were transformed to 2D surface profiles in order to calculate different roughness properties including average roughness, height distribution, surface density of grains, and bearing area ratio. Out of the 16 snow samples 10 were scanned and analysed with the μCT.

4.2.3 Impact loading experiments

The experimental set-up for the experiments was basically the same as for the sample preparation (Figure 4.1c). The snow samples were loaded with a short time vertical impact. The complete loading-unloading cycle took about 100 ms which roughly corresponds to the passage of a 2 m long racing ski sliding with 20 m/s. The experiments were performed by a linear friction tester (LFT) placed in a cold chamber where temperature was kept at -6$^{\circ}C$. The LFT consists of two high power and high precision computer controlled linear drives that can be programmed to realise any 2D movements. In these specific experiments the horizontal drive is fixed while the vertical drive is programmed to apply an impact on the snow sample placed under the drive. A 2 mm thick flat UHMWPE sheet is glued to the face of the vertical drive and acts as an impactor. UHMWPE is the material of modern ski bases. The sheet overlaps the snow sample in order to impact the whole sample.

The force and displacement are recorded during the experiment with a high sampling rate. The force is measured with 0.1 N resolution by a Kistler Model 9254 piezoelectric force plate (Kistler, Switzerland) placed under the snow sample. It measures all three force components simultaneously. The displacement is measured with 1 μm resolution by a linear encoder (Renishaw, UK).

The samples were repeatedly impacted several times. By repeating the impact we were able to observe whether the mechanical behaviour of the sample changed and we were able to observe the recovery of the samples. We varied the impact load from 10 N which corresponds to 12 kPa (the maximum pressure under a stationary ski) to 140 N. For the maximal load of 140 N the deformation of the samples was around 20 m. The sample height was 5 mm. Relating the deformation to the sample height we obtain a strain of 0.004 and a strain rate of 0.04 1/s.

4.3 Results and discussion

UHMWPE has a higher mechanical strength than ice, but a lower Young's modulus (Kim and Keune, 2007; Petrovic, 2003). As a result the ski base deforms elastically during the ski-snow interaction while the ice fails when the stress exceeds its compressive strength. This makes the skis wear resistant and long lasting.

Let us consider the impact of a flat UHMWPE sheet (slider) on hard snow. What would we expect as a result of such an impact: First, the top ice grains come into contact with the slider. As long as the load on the grains is not too excessive the contacts are elastic. The area of the contact patch can be calculated from the Hertzian contact theory. Since the grains are part of a flexible snow matrix, they are not fixed in space. They are pushed down by the contact force. As the contact force increases the grains start to fail. Either the contact pressure reaches the compressive strength of ice, or their bonding in the matrix is not strong enough. In the former case the ice yields until the contact stress drops below the compressive strength. In the latter case the bonds that support the grains yield, and the grain is displaced from the surface as a whole. The failure of grains continues until the number of grains in contact and the real contact area is high enough to support the load. We tried to visualise the deformation of the grains in the snow with the μCT.

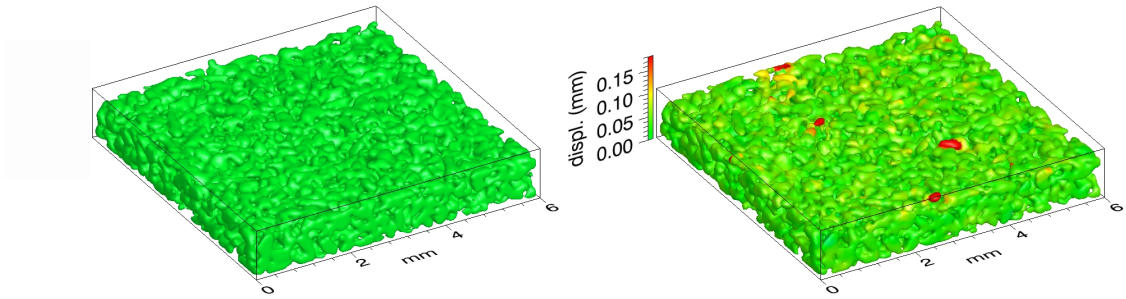

a) b)

Figure 4.2: 3D image of a 6 x 6 mm^2 section of the snow surface before (a) and after (b) the loading experiment. The absolute displacements between the two images, calculated by particle image velocimetry, are colour-coded in Fig. b. No considerable deformation can be seen as a result of the 150 kPa impact. Only isolated grains (in red) that originally rise above the average surface level deform considerably.

The 3D images of the surface of a snow sample before and after an impact experiment are shown in Figure 4.2. The absolute displacements of most surface points are around zero. Except for a very few surface grains no deformation is visible. This confirms our expectation that on hard snow the ski-snow interaction is limited to the very top of the snow. All of the grains

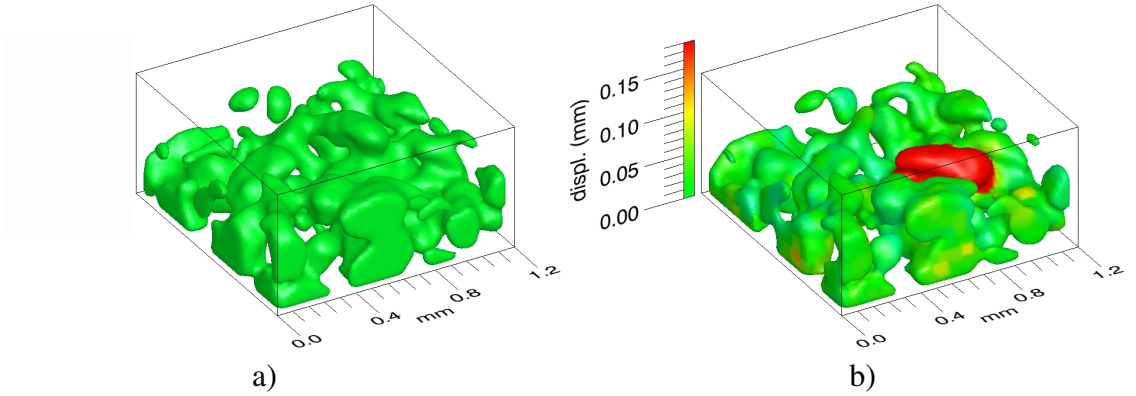

Figure 4.3: Close-up of the deformation of a grain that originally rises well above the surface (image a). It fails under the impact and falls down (image b). In its new position it is below the average surface level indicating brittle failure. Another evidence of brittle failure is that the immediate neighbourhood of the grain shows zero deformation. For a plastic deformation we would expect a smooth transition similar to the deformation pattern shown in Figure 4.7.

that show a visible permanent deformation originally rise well above the average surface level. These grains come into contact with and loaded by the slider first. They experience excessive loads. Their bonds fail and they fall down. One example of such a grain is shown in Figure 4.3. In its final position the top of this grain is under the surface. This shows that its bonds failed completely by brittle failure and the grain fell down instead of having been pushed down by the slider. The sharp transition from the big displacement of the grain to no displacement of the neighbouring grains confirms this. Beside the brittle failure of the bonds the grain itself might deform plastically and forms new bonds in its new position. The grain does not carry any load after failure. The cracking of the bonds of these grains was also observed in the loading experiments: In Figure 4.4 the oscillations in the force in the initial phase of the loading are caused by the brittle failure of the bonds. This occurred only in the first loading of the sample, subsequent loadings showed a smooth increase of the force. The failure of these weakly bonded surface grains is a permanent deformation.

Another expected permanent component of the deformation is the failure of ice on the top of the grains. This deformation is too small to be visible on the μCT images, but it appears in the loading experiments as a shift between the first and subsequent loadings. In Figure 4.4 it is labelled as phase B. It is approximately 5-10 μm. Due to the low number of grains actually in contact with the ski base very high local stresses develop on the top of the grains. The stress far exceeds the compressive strength of ice (around 10 MPa at high deformation rates (Kim and Keune, 2007; Petrovic, 2003)). As a result a localised failure of the ice is inevitable. The failure mechanism is probably a mixture of plastic flow, micro-cracking, and possibly pressure melting depending on the actual stress and strain rate experienced by the grain. Failure of the ice continues until the average stress drops below the strength of ice.

The permanent deformations of the snow discussed above only appear in the first loading of a snow sample. After this first impact the surface is ‘prepared’ to take the load without further permanent deformation. In subsequent loadings the force rises and drops smoothly. This can be observed in the force-displacement curve of the second impact in Figure 4.4. This smooth force-

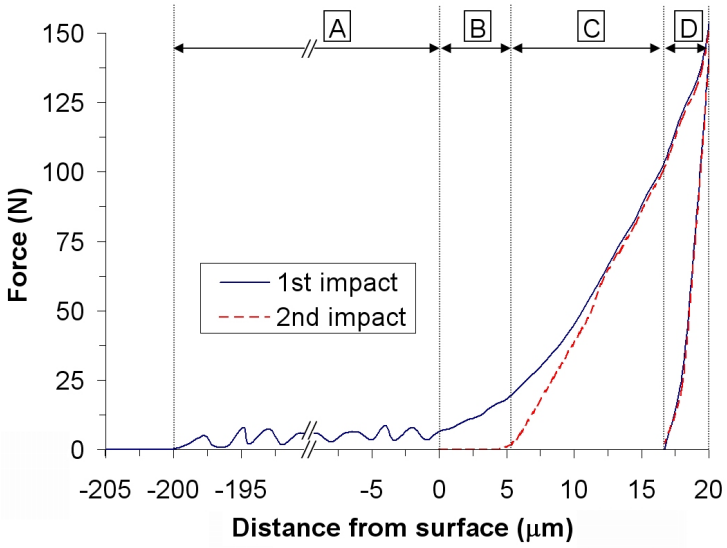

Figure 4.4: Schematic force-displacement curves of two subsequent impact experiments with the same maximum force. Four different deformation modes (A-D) can be identified. The first impact shows an oscillation of the force from -200 to 0 μm (A). This is the brittle failure of surface grains. The surface is defined as the point from which the force signal starts to rise continuously. After the maximum force is reached an elastic recovery of 3 μm occurs during the unloading of the sample (D). The point where the second impact touches the new surface gives information about the delayed elastic recovery of the snow matrix (C) and the total permanent deformation (A + B) of the snow. Thereof about 5 μm are caused by the flattening of the grains which are in contact with the ski (B).

displacement curve is plotted in Figure 4.5. The curve shown is the average of measurements

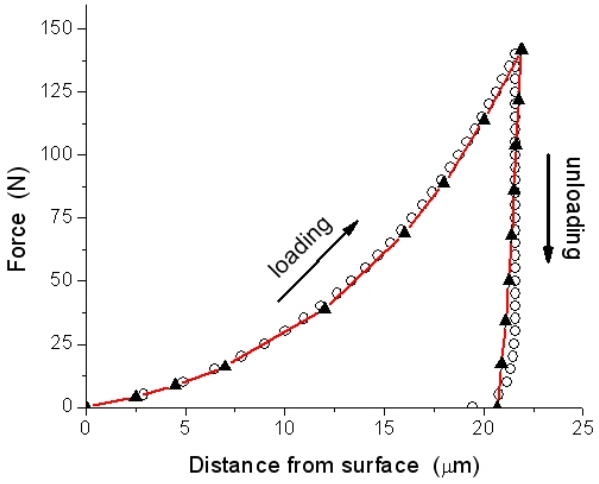

Figure 4.5: Average measured force-displacement plot of the impact loading of 10 hard snow samples (open circles). The grey band shows the variation of the measured loading curves (approximately 20%). The whole loading-unloading cycle takes approximately 100 ms. Subsequent loadings of a sample follow exactly the same curve. The calculated plot based on our model shown in Figure 4.6 is also shown (*solid triangles and line*).

on 10 different samples. Different samples showed 20% deviation which is quite reasonable in experiments with snow. Two interesting features are immediately noticeable. One is the small deformation. The snow is very hard, the total deformation is only 22 μm at 140 N (corresponds to 150 kPa). Another interesting result is that the loading and unloading follow different paths. The loading curve forms a hysteresis loop. This indicates permanent deformation in the snow. Subsequent loadings of a sample, however, closely follow the same curve. The position of the surface where the force starts to rise remains exactly the same. It seems that the sample recovers the strain after unloading and regains its undeformed state. In Figure 4.4 this recovery is labelled as phase C. This behaviour is well known in ice mechanics. It is referred to as primary creep or delayed elasticity (Sanderson, 1988). It has never been studied for snow. Only for crushed ice Singh and Jordaan (1999) describe this behaviour. It is expected to be more pronounced in snow than in case of polycrystalline ice since it is known to be greatly enhanced with increased porosity (Sinha et al., 1979). Nevertheless it is very surprising that delayed elasticity present at such a high strain rate (0.04 1/s) and that the deformation is fully recovered. This is a clear indication how significant delayed elasticity can be in snow. In ice one would expect brittle failure at this strain rate. Polycrystalline ice behaves brittle at strain rates higher than 10^{-3} 1/s (Sanderson, 1988). Unlike in ice, however, the grains have a high mobility in the snow matrix. They can freely move by grain boundary sliding, which is the underlying mechanism of delayed elasticity (Sanderson, 1988; Sinha et al., 1979). The high mobility of the grains then leads to an effective stress relaxation mechanism, and hence improved delayed elasticity.

The reverse creep of delayed elasticity is slower than the withdrawal of the impactor in our experiments. As a result the unloading part of the curve shows the purely elastic part of the deformation. This is only 2-3 μm and includes both the elastic deformations of the ski base and the snow matrix.

Pressure melting and premelting of the ice cannot explain the observed hysteresis in the loading curve. In case of pressure melting a melting-refreezing cycle of the top of the loaded snow grains could result in a hysteresis, but in reality the ice fails well before it could melt. According to the Clausius-Clapeyron equation the melting point of ice changes with pressure as 13.35 MPa/K. All of our experiments were conducted at -6°C. Lowering the melting point of ice to -6°C requires around 80 MPa which is eight times higher than the compressive strength of ice (10 MPa) at high strain rates.

It has been shown by different experimental techniques that a naturally occurring quasi liquid layer (QLL) exists on the surface of ice close to the melting point (Wettlaufer, 1999a). However, the thickness of the QLL in water vapour is very small compared to the displacements in our measurements. Even for ice with a high impurity content (which is known to enhance premelting) it does not exceed 100 nm at -6°C (Wettlaufer, 1999b). In addition, the relative humidity in our cold rooms during the experiments was between 30-50%. In such a low humidity we do not expect to have a QLL on the surface of the top snow grains (Petrenko, 1997).

Nano- and microindentation experiments on ice show a recovery of the ice surface similar to our observations. In nanoindentation the heeling of the surface is attributed to the flow of the QLL (Pittenger et al., 2001). As we mentioned above, in the dry air of our cold rooms we do not expect a QLL present at -6°C. In addition, the length scale of these experiments is very

different. The small volume of the imprint of the microscope tip is filled up quickly, but it is insufficient to account for the 20-30 μm deformation in our experiments. In microindentation of ice the indent is filled very slowly (on the time scale of hours) by newly growing ice grains (Golovin et al., 2000). In our experiments the snow is recovered after 1 minute, a very different time scale. While we cannot exclude that some of the processes discussed above present in our experiments, delayed elasticity seems to be the dominating underlying mechanism of the hysteresis observed in our loading experiments.

The energy dissipated through snow deformation in skiing can be estimated from the loading curve shown in Figure 4.5. The total energy dissipation of a ski, P is simply $P = \mu v F_n$ where μ is the frictional coefficient of the ski on snow, v is velocity, and F_n is the normal load. For a racing ski μ=0.1, v=20 m/s, and F_n=400 N which yields 800 J/s. The area of the hysteresis loop ($860 \cdot 10^{-6}$ J) corresponds to the energy lost to compaction of around 10^3 mm^2 of snow. A 7-cm wide ski, moving with 20 m/s, compacts $1.4 \cdot 10^6$ mm^2/s of snow. Hence the energy lost to snow compaction of this ski amounts to approximately 1 J/s, 0.1% of the total energy dissipation. Therefore, snow deformation can be neglected on a hard ski track leaving thermal energy dissipation the dominant process.

Based on our impact experiments it is possible to construct a mechanical model of the ski-snow contact which will serve as an input to thermal simulations for calculations of meltwater generation. The model includes only the non-permanent part of the deformation, namely the elastic deformation of the ski base and snow, and the delayed elastic deformation of the snow. Figure 4.6 shows the schematic representation of the model. The mechanical behaviour of the

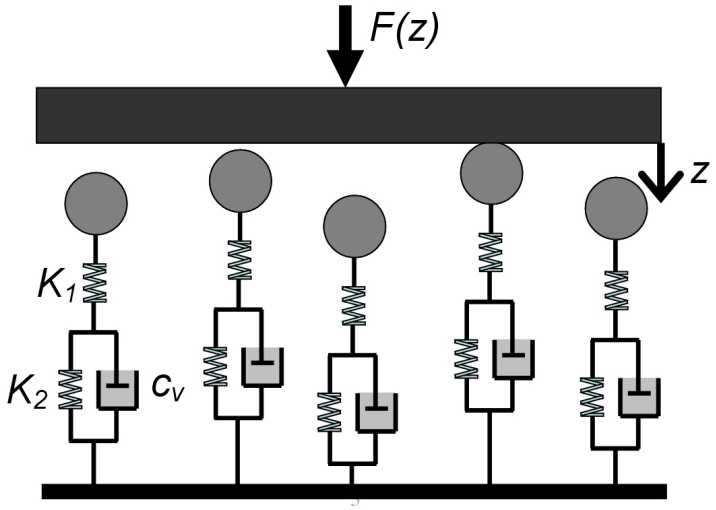

Figure 4.6: Schematic presentation of the mechanical model of the ski-snow interface. Only surface grains are considered all having the same (average) radius. The grains are supported by elastic springs and dashpots that represent the snow matrix.

surface grains and their support by the snow matrix is modelled with rheological elements. Each grain is supported with a spring (K_1) and a Kelvin element (K_2, c_v) in series. This is the simplest rheological model which can describe the desired deformation mode. The spring element (K_1) includes the two elastic components of the deformation: the contact between the

top of the grains and the ski base, and the elasticity of the snow matrix. The former can be calculated from the Hertzian theory of elastic contacts (Johnson, 1985):

$$F_n(\delta) = \frac{4}{3} E^* \sqrt{R} \delta^{3/2} \tag{4.1}$$

Here the normal force, F_n is expressed as a function of deformation, δ. E^* is the effective combined modulus and R is the combined radius of UHMWPE and ice, respectively. R includes the radius of the ice spheres that come into contact with the flat UHMWPE ski base ($R_{UHMWPE}=\infty$). This contact radius was determined from the μCT images. An algorithm was used that fits a sphere to the top section of all surface grains. Therefore not the whole grain, only its top part is used to obtain the radius. A value of 0.18 mm was obtained which is surprisingly close to the average radius of the ice grains used in the sample preparation (0.175 mm). With this, and the Young's moduli of 9100 MPa and 1200 MPa for ice and UHMWPE, respectively, equation 1 becomes $F_n(\delta) = 680.52\ Nmm^{-3/2}\ \delta^{3/2}$. The implementation of this nonlinear relation requires a nonlinear spring (K_1) in the mechanical model shown in Figure 4.6.

In addition to the contact between ski base and ice grains the spring element in the model includes the purely elastic component of the deformation of the snow matrix. This was calculated with finite element simulations. A 1.8 x 1.8 mm^2 section of the 3D μCT images of the snow samples were converted into a discrete finite element mesh with ANSYS ICEM CFD. The mesh was then used to calculate the stiffness of 50 randomly chosen surface grains of the snow with the commercial finite element software ANSYS. In these simulations a load is applied on the top of a surface grain and the resulting displacement is calculated by linear structural analysis. The result of a typical simulation is shown in Figure 4.7. The average stiffness of the grains was found to be 0.53 N/μm, a surprisingly high value. In order to check the validity of the simulations we calculated the Young's modulus of a sample with a density of 520 kg/m^3. We obtained 1200 MPa which corresponds well with measured values (Shapiro et al., 1997). In addition we verified that the dependence on system size is negligible.

The Kelvin element (K_2, c_v) in the model is responsible for the delayed elasticity and the majority of the deformation. Since no measurements of delayed elasticity exist for snow in the literature the parameters of the spring and dashpot (i.e. the spring constant, K_2 and damping coefficient, c_v) are unknown. They must be determined by fitting the model to the measured loading curve. This requires the height distribution of the grains on the snow surface. We determined this from the μCT images with an algorithm that finds the coordinates of the peak of each surface grain. The number of grains per unit area as a function of depth, $n(z)$ is plotted in Figure 4.8. The curve has a maximum at around 0.09 mm, half the average grain radius. Note the scale of the x axis. The resolution of the μCT is 18 μm, only slightly smaller than the total deformation of the snow. Therefore, the fitted curve must be used to extrapolate values close to the surface. With this the total force $F(Z)$ as a function of depth Z can be calculated from

$$F(Z) = A \int_0^Z \frac{dn}{dz}(z) f_Z(z) dz\ , \tag{4.2}$$

where A is the area of the sample and $f_Z(z)$ denotes the force exerted by a single grain originally being in a depth of z and finally pushed down to Z. The total force was calculated numerically.

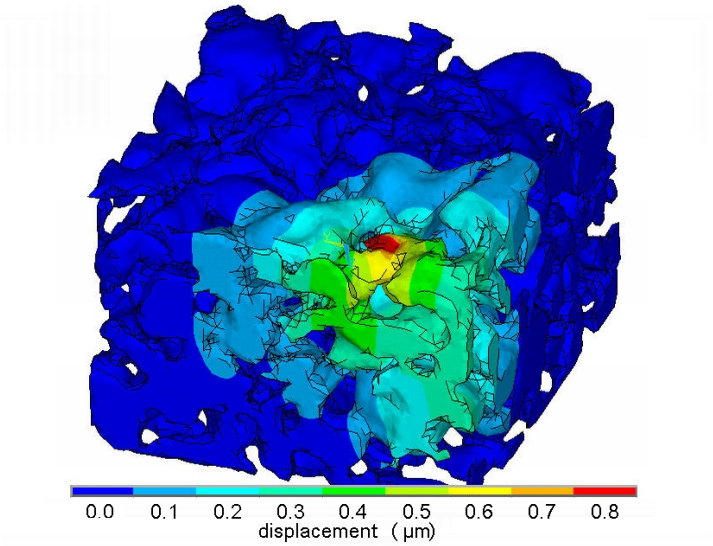

Figure 4.7: Contour plot of the vertical displacement of a typical finite element simulation of the stiffness of surface grains in the snow. It was calculated with a linear structural analysis in the finite element program ANSYS. A realistic load of 0.3 N was applied on this grain. With the simulated displacement of 0.8 μm, a stiffness of 0.375 N/μm results for this grain.

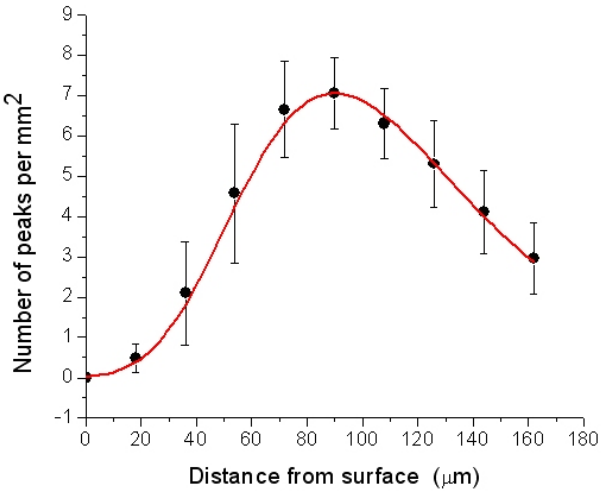

Figure 4.8: The number of peaks per unit area in the snow samples as a function of depth. It was calculated from the μCT images. Error bars show standard deviation. The red line represents the best fit of a Weibull distribution.

Since the displacement of the impactor follows a nonlinear curve over time the deformation rate the grains experience depend on the depth z. Therefore, the function $f_Z(z)$ is different for each Z and it must be calculated individually for each Z. In practice, we calculated $f_Z(z)$ with ANSYS for eight different Z values. To this end a transient analysis was performed on the rheological model in Figure 4.6. The real displacement of the UHMWPE impactor over time in the experiments was applied on the model and the reaction force calculated. The total force

could then be calculated for the eight Z values.

The parameters of the Kelvin-element in the model (K_2 and c_v) are unknown. They were determined by fitting the calculated to the experimental loading curve. The fit shown in Figure 4.5 was obtained with the following parameters of the Kelvin element: K_2=26.2 N/mm and c_v=550 kg/s, respectively. The unloading part of the curve could be determined in the same way using the displacement of the impactor during withdrawal. The parameters of the Kelvin element are material constants of the snow. They describe the delayed elasticity of hard snow.

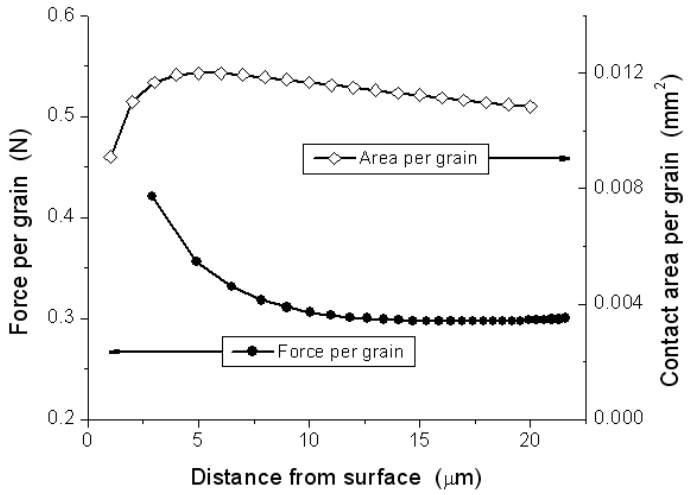

Figure 4.9: Force per grain (solid symbols) and contact area per grain (open symbols) as a function of depth. Both force and area have a relatively constant value.

The force on a single grain can be obtained by dividing the total force by the number of grains shown in Figures 4.5 and 4.8, respectively. It is shown in Figure 4.9. In the beginning of the loading (i.e. close to the surface) only a few grains are in contact with the ski. The force per grain is enormous. This is when grains and bonds in the snow fail. As more and more grains come into contact with the ski the force per grain decreases and eventually reaches a constant value of 0.3 N. This force is still remarkably high. The Hertzian contact theory predicts an average stress of 50 MPa in the contact patch, if the deformation was purely elastic. As the strength of ice is considerably below 50 MPa, the ice on the top of the grains certainly fails. The failure will increase the area of the contact patch until the average stress drops below a critical value. Assuming that this critical stress is the penetration hardness of ice, which is approximately three times the compressive strength (Johnson, 1985), the real contact area can be calculated from the ratio of normal force to penetration hardness. This approach is similar to the calculation of the real contact area between metals (Bowden and Tabor, 1950). The resulting real contact area of one grain is shown in Figure 4.9. A value of 0.011 mm^2 corresponds to a contact patch radius of 55 μm. The relative real contact area between snow and ski is found to be around 0.4%. This is the contact area at the front part of the ski right after the front impacts the snow. It will increase when melting starts. The values found here are reasonable and correspond well with those measured or estimated by others (Colbeck, 1994; Huzioka, 1962).

An estimation of the permanent deformation of the top of the snow grains after the first

impact can also be made from the contact area per grain. A lower and upper limit of the deformation can be given from simple geometrical considerations. The top of the grain is flattened by the high load until a contact patch radius of 55 μm is reached. This can be achieved by either pushing the ice aside to form a plateau or by shaving the top of the grain completely off. The former approach gives a lower limit of the deformation, and results in 4 μm. The latter predicts 9 μm, and it is an upper limit. These estimates are very close to the 5-10 μm permanent deformation observed in the experiments (phase B in Figure 4.4).

4.4 Conclusions

The ski-snow contact is a complicated mechanical process. Even without sliding the effect of the impact of a ski on the snow is very complex. Four types of deformation have been identified during a high speed impact on hard snow with a maximum pressure of 150 kPa:

- The brittle failure of the bonds of some surface grains that come into contact with the ski first. These grains are displaced from the surface and do not bear any load after failure.
- Highly localised failure of the ice on the top of the grains at the contact with the ski. This type of failure continues until the contact stress drops below the strength of ice and it is 5-10 μm. It is probably a mixture of plastic flow and micro-cracking.
- Elastic deformation of the ski base and snow matrix. The former is 2-3 μm, the latter is around 0.5 μm, practically negligible.
- Delayed elastic deformation of the snow matrix. This deformation is fully recovered after unloading. It is approximately 20 μm.

The first two types of deformation are permanent, while the two other are fully recoverable.

A mechanical model consisting of basic rheological elements was constructed that describes the recoverable part of the snow deformation. The model can properly describe the deformation of the snow as a result of an impact. Coupled with the topography of the snow surface obtained from μCT measurements, the number and area of the contact spots can be determined. A remarkably constant value of 0.3 N as the force on one grain during the loading, and 0.4% relative real contact area between ski and snow were found. These values serve as important input parameters in the thermal simulation of meltwater lubrication.

Chapter 5

Modelling the brittle failure of snow

5.1 Introduction

The failure of snow plays a major role during the release of avalanches. Several studies have investigated the failure behaviour of snow (e.g. McClung, 1979; Narita, 1983; Sommerfeld, 1974). A detailed study about snow fracture was performed by Narita (1983). He investigated the dependence of tensile strength on temperature, strain-rate and snow density. As an important result snow exhibits two different fracture behaviours depending on the strain rate. For strain rates below 10^{-4} 1/s snow behaves ductile and large deformations precede ultimate failure. For higher strain rates snow fails in a brittle manner. The characteristics of brittle fracture are very small plastic deformations and a planar fracture surface perpendicular to the stress direction (Hahn, 1976). Even though the important influencing factors for the fracture of snow have been investigated in detail, a detailed understanding of the mechanisms during the failure of snow on the scale of the microstructure is still lacking. Open questions are: Where does the microstructure fail? Can we predict critical loads for failure? Can we deduce the strength of snow from microstructural characteristics? Answers to these questions will improve the understanding of snow fracture and avalanche release. To this end, we observed snow samples before and after fracture tests by micro tomography (μCT). The μCT-images are used to visualise the fracture plane and serve as input for a fracture model. The fracture model is adapted from the beam model, which is described in Chapter 3. As an extension of the beam model, a fracture criterion based on the strength of ice is introduced. The first results show good agreement between simulation and experiment. However, more experiments are needed to further verify the simulation results.

5.2 Experiments

The experimental procedure contains the following steps, all carried out at a temperature of $-8°C$: sample preparation, first μCT-scan, tensile fracture test and second μCT-scan. These steps are explained in the following.

For sample preparation two different snow types were used: round-grained snow with densities between 220 and 265 kg/m^3 and compressed, refrozen wet snow with densities between 350 and 410 kg/m^3. About 40 mm high cylindrical samples were cut out of a big homogenous snow block by a hollow cylinder with an inner diameter of 13 mm. To obtain snow samples with different density and strength some samples were compressed inside the hollow cylinder. The stronger the sample the easier is the handling during the experiments. Next, the cylindrical snow samples with a diameter of 13 mm were carefully placed in a cylindrical sample holder

(Figure 5.1) with an inner diameter of 13.5 mm and a height of 43 mm. This sample holder has an adapter to place it into a micro computer tomograph. To allow a tensile fracture experiment, the bottom and top of the sample needs to be fixed for force transmission. By injecting a drop of water through a hole at the bottom of the sample holder the snow sample freezes to the bottom of the sample holder. The top of the sample is frozen to an aluminium plate. Finally, a 2 mm deep notch is cut into the sample perpendicular to the force direction to weaken the sample and prescribe the region of stress localisation. The sample holder also has a notch to allow cutting a notch into the snow sample.

The first μCT-scan captures the prepared sample before conducting the fracture test. This scan provides a 3D image of the intact microstructure. A 5 mm high region around the notch is scanned. Instead of scanning the entire sample, only a region around the notch needs to be scanned to capture the emerging fracture surface.

The tensile fracture test is conducted by pulling up the aluminium plate at the top of the sample and thus applying a tensile force. The force is measured by a spring scale and successively increased during about 1 s until brittle fracture. Brittle fracture occurs for strain rates higher than 10^{-4} 1/s. Strain rate is neither controlled nor measured during the simple experiment. However, from the absence of plastic deformation and from the characteristics of the fracture surface we can conclude that the snow sample failed in a brittle manner. The maximal measured force is defined as fracture force. The cross-sectional area of the sample minus the area of the notch is defined as apparent fracture area. The fracture force divided by the apparent fracture area gives the tensile strength of the sample.

The second μCT-scan captures the lower part of the broken snow sample. The same cut-out as during the first scan is captured. By comparing the images of the first and second CT-scan the fracture surface can be identified.

The μCT-scans were performed by a desktop X-ray micro computer tomograph from Scanco Medical (Bassersdorf, Switzerland), which is located in a cold lab at a temperature of -8$^{\circ}C$. The resolution of the μCT-images is 30 μm.

Experiments to determine the fracture strength of materials usually use unnotched samples, since stress concentrations at the notch influence the test results. The influence of the notch on the results of this experiment will be discussed later.

5.3 Simulations

A micromechanical finite element model was developed which simulates the fracture of snow, using the commercial FE software package ANSYS. The model is based on the microstructure of the snow samples and material parameters of ice. It requires a geometric description of the microstructure (mesh), a material model, boundary conditions and solution-controls. These components of the model are explained in the following.

The description of the microstructure is based on the μCT-image of the intact microstructure. The microstructure is approximated by beams following the same procedure as explained in Chapter 3 for the creep simulation. The whole μCT-image is used for the simulation. This is a cylinder with diameter of 13 mm and a height of about 5 mm, which amounts to a volume of

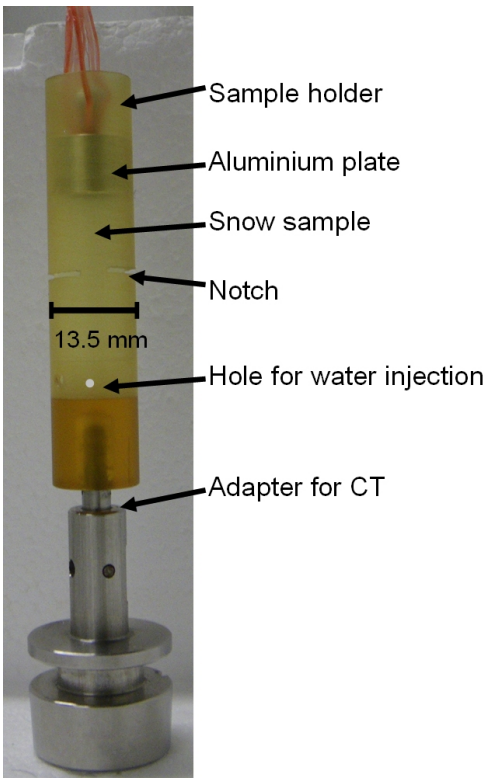

Figure 5.1: Sample holder

660 mm^3. Figure 5.2 shows the lateral view of such a simulation volume with 22000 beam elements. Figure 5.3 a) shows the original μCT-image of the same sample. The notch on the right side of the sample is visible in both figures. Simulating the entire cross-section of the sample enables the verification of the model, including potential notch effects. The approximation of the microstructure by beam elements permits the simulation of relatively large volumes, since the number of elements is reduced by up to two orders of magnitude compared to common octahedral or tetrahedral meshes, which were used in previous finite element models of snow (Schneebeli, 2004; Srivastava et al., 2010).

The material model is based on material parameters of monocrystalline ice like the model in Chapter 3. During ideal brittle behaviour, materials deform elastically until fracture. Therefore the material model requires values for Young's modulus and a fracture criterium. The Young's modulus of monocrystalline ice (10 GPa) (Schulson and Duval, 2009), the tensile strength of monocrystalline ice (4 MPa) (Schulson and Duval, 2009) and the compressive strength of monocrystalline ice (20 MPa) (Schulson and Duval, 2009) are used in this model. The strength of monocrystalline ice depends on the crystal orientation and varies by about a factor two for different orientations. For simplicity we used the arithmetic mean of these values.

As boundary conditions the node displacements at the bottom of the simulated cut-out are set to zero and for the top a constant vertical upward velocity of 10^{-3} mm/s is prescribed. Since the material model is linear elastic, the prescribed velocity has no influence on the simulation results.

Finally, the solution-controls manage how the equations are solved numerically. The system is solved iteratively in several time steps. After each time step the stresses in the beams are

checked. If the maximum stress in a beam exceeds the critical stress, i.e. 4 MPa for tension or 20 MPa for compression, the beam is removed from the model. In Figure 5.2 the red beams reached the critical stress and will be removed for the next time step. The simulation stops when the bearing reaction drops to zero. The bearing reaction is the sum of the forces which act on the restricted nodes of the bottom or top of the sample. The smaller the time steps the fewer beams are removed during one time step and thus the more accurate the simulation. However, smaller time steps increase the computing time. Thus a trade-off between computing time and accuracy must be found. A sensitivity analysis has shown that for more than around 100 time steps, the simulation results converge and 200 and 900 time steps were finally used for the simulations. The computing times on a 64-bit desktop PC with Intel 2 Duo processor and 8 GB RAM varied between four and ten hours, depending on the number of time steps and on the model size, i.e. the number of nodes and beam elements.

The most important output of the simulation is the maximal bearing reaction. This force divided by the apparent fracture area corresponds to the simulated tensile strength of the snow sample. In the following the simulated strength will be compared with the measured strength to verify the simulations.

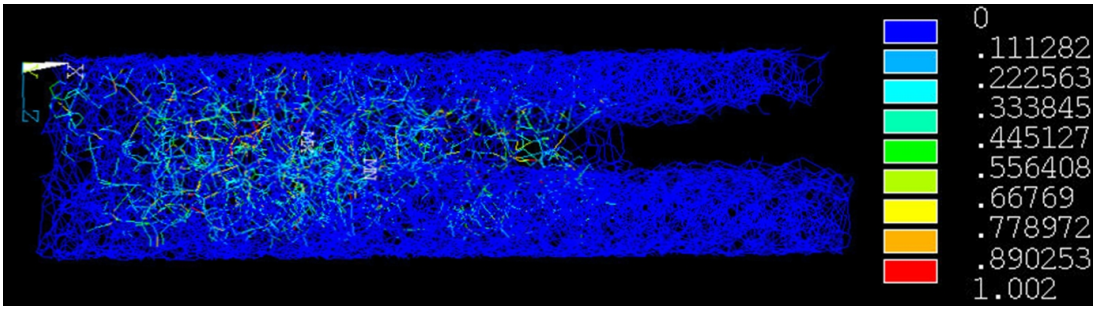

Figure 5.2: Lateral view of a beam mesh with 22000 beam elements and 9000 nodes. This mesh approximates the notched snow microstructure shown in Figure 5.3 a). The diameter of the cylindrical volume is 13 mm. The simulated stress distribution after one time step is visualised colour-coded. The values correspond to the ratio between maximal stress in a beam and critical stress. Thus all red beams will be removed at the next time step.

5.4 Results and discussion

A total of 14 samples were prepared for the experiment. However, only five samples fractured at the notch and could be used for further analysis. All other samples fractured outside the scanned region and therefore could not be used for further analysis. The main results of this study are the modelled tensile strengths, their verification with measured strengths and the analysis of the fracture surface from the μCT-images. These results are presented in the following.

The fracture surface can be visualised by comparing the μCT-images from the first and second μCT-scan. Figure 5.3 shows the entire scanned region before and after the fracture test. On this scale the fracture surface appears like a smooth plane perpendicular to the stress direction - a typical characteristic of brittle fracture (Hahn, 1976). By successively zooming in, more details of the fracture surface become apparent. In Figure 5.4 the microscopic roughness of the

fracture surface is revealed and in Figure 5.5 the fracture of two bonds is shown. It is known that fractures choose the path of least resistance. In snow this path seems to go around the grains through the bonds, resulting in a roughness on the scale of the grains. Bonds in snow are mostly crystallographic grain boundaries (as shown in Chapter 2). Beside the neck shape, grain boundaries in snow are characterised by a sharp grain boundary groove (Colbeck, 1998). Both characteristics turn grain boundaries into an attractive starting point for fracture. From this starting point we assume that the fracture propagates on the basal or prismatic plane through a crystal like in polycrystalline ice (Schulson and Duval, 2009) and not along the grain boundary. However, this is only a hypothesis. A crystallographic observation of the fracture surface is necessary to clarify these points.

Beside the fracture surface, the μCT-images revealed potential microstructural changes in that part of the microstructure which did not fracture. By comparing the microstructure before and after fracture in Figure 5.4, it is shown that the intact part of the microstructure did not change. The shape and position of single grains below the fracture surface (dashed line) remain the same. This suggests that no visible plastic deformation occurred during the experiment which in turn suggests that the experiment results in brittle failure.

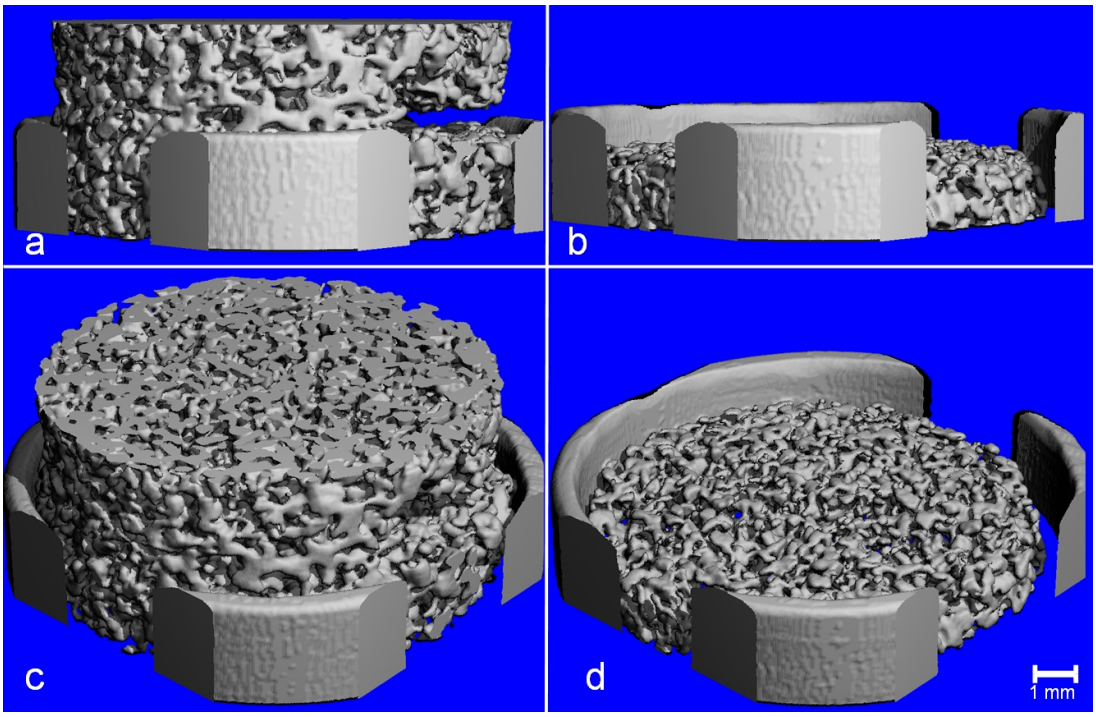

Figure 5.3: μCT-images of the whole scanned region of the densest sample before (a, c) and after (b, d) fracture. In Figure 5.3a) the notch is shown.

To verify the fracture model, simulated and measured tensile strengths are compared in the following. Simulated and measured tensile strengths of the five successful samples are plotted in Figure 5.6 against density. The simulated and measured strengths plotted over the same density correspond to the same sample. Except from the sample with the highest density the simulations agree well with the measurements. The origin of the outlier is unclear. One possible explanation is that the beam model approximates higher density snow less accurate than lower density snow. This was already shown in Chapter 2. Another explanation is that the outlier

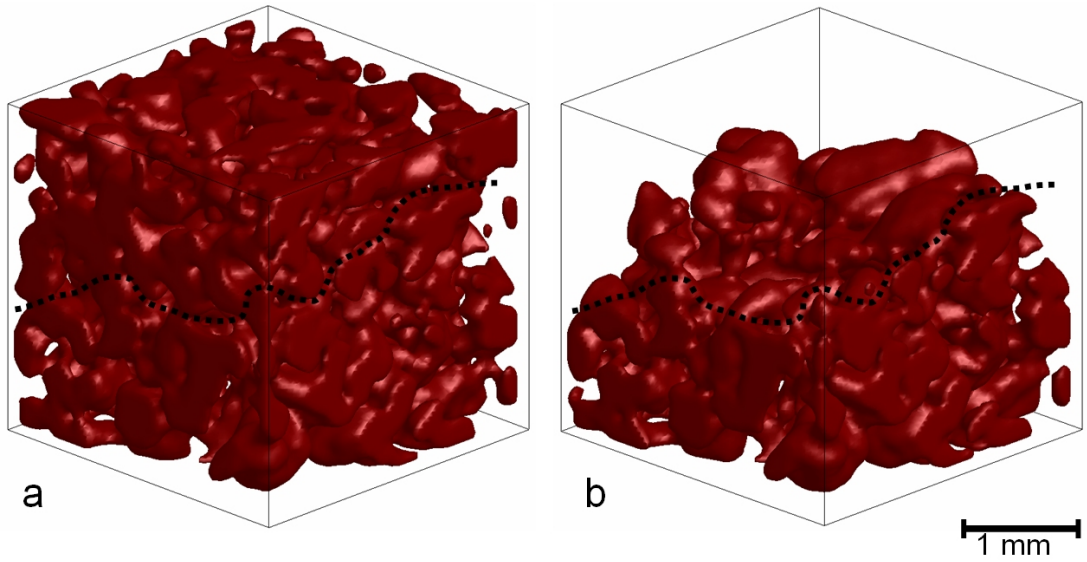

Figure 5.4: Cut-out of sample with a density of 365 kg/m^3 before and after fracture. The dashed line indicates the intersection of the fracture surface with the bounding box.

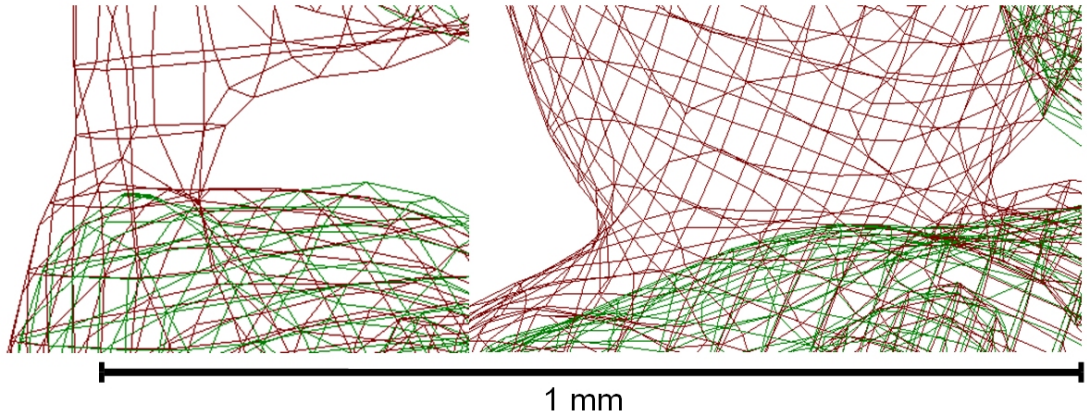

Figure 5.5: Two μCT-images of bonds between snow grains, which fractured during the experiment. The red mesh shows the microstructure before fracture. The green mesh shows the microstructure after fracture.

is not a real outlier, but rather shows the scatter between simulation and measurement. More experiments and simulations are necessary to better evaluate the accuracy of the model.

To compare our simple experiment with experiments from literature, results of brittle fracture tests from Narita (1983) are additionally plotted in Figure 5.6. Uncertainties of our experiment are the unknown strain rate, possible size effects of the small specimen diameter and the unknown influence of the notch. Narita (1983) investigated the tensile fracture of snow in detail. He found that the tensile strength is independent of strain rate for brittle failure. Since our samples fail in a brittle manner, the influence of strain rate is negligible. The influence of the other two uncertainties is more difficult to estimate. However, since the difference between Narita's (1983) and our results is small, we conclude that the fracture test, we performed, is reasonable and capable to determine realistic, macroscopic properties of snow. In fact, we do not focus on the exact determination of the fracture strength of snow, but rather on the connection between

microstructure and fracture strength and the development of a reliable micromechanical model for snow. In future work this model could be applied to investigate the effects of a notch or size effects of snow. Furthermore the model could be applied to determine the strength of different snow types. Especially the strength of fragile snow types, which are difficult to handle in experiments, could be determined by the model.

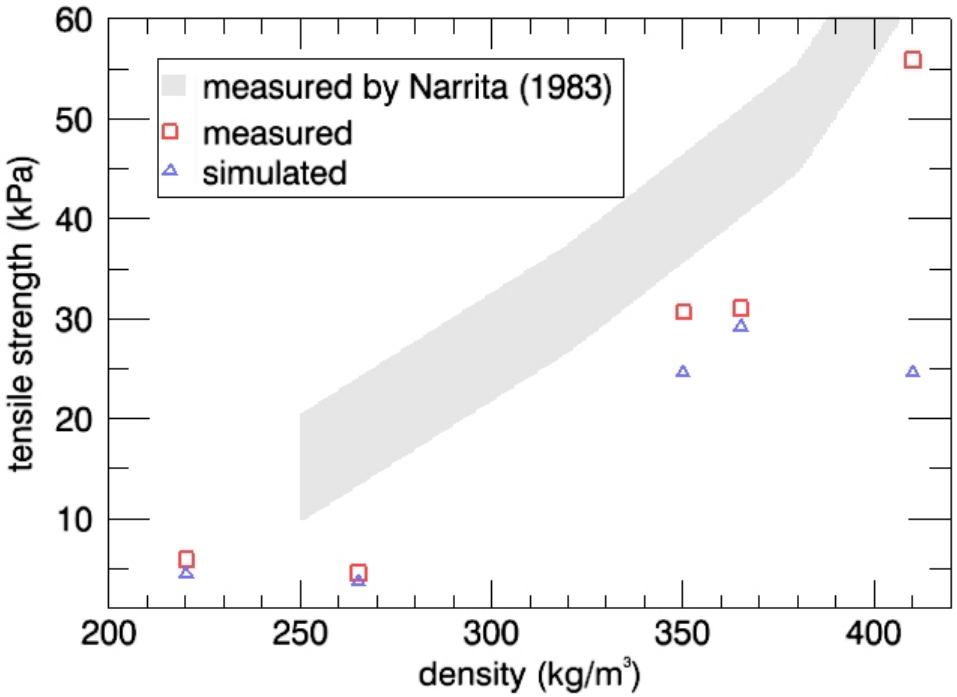

Figure 5.6: Comparison of measured and simulated tensile strength of five snow samples. The two samples with a density lower 300 kg/m^3 consist of round grained snow. The three samples with densities above 350 kg/m^3 consist of compressed and refrozen wet snow. As a comparison, results of brittle fracture tests from Narita (1983) are plotted.

5.5 Conclusions

A promising micromechanical fracture model for snow was presented. The model is adapted from a model originally built for creep simulations. The first results show good agreement between simulation and experiment. However, for the confident application of this model more experiments for verification are necessary.

The μCT-images before and after the fracture test enabled to visualise the fracture surface in snow. It was shown that the fracture surface is rough on the scale of 100 μm to 1 mm and goes around the grains through the bonds. In snow the bonds, i.e. necks, are mostly crystallographic grain boundaries. However, it is still unclear if the fracture surface follows exactly the grain boundaries (intercrystalline fracture) or cuts single crystals (transcrystalline fracture).

Chapter 6

Outlook

The thesis presented several approaches to bring together the microstructure and mechanical properties of snow, with the goal to improve the understanding of the mechanical behaviour of snow. The main achievement was the development of a verified model of the macroscopic behaviour of snow based only on its microstructure and the behaviour of ice. This model in combination with creep and fracture experiments permitted to improve the understanding of the creep and brittle behaviour of snow. However, not all open questions could be addressed in this work. In the following I will describe how some of these open questions could be answered in future work.

- As described in Chapter 1.5 the main problem in snow mechanics is the lack of reliable mechanical constitutive equations that allow confident predictions for a wide range of snow types and load cases. In this thesis only a small range of snow types and load cases was considered. The focus was on the development and verification of the different models. For most experiments round-grained snow was used. This type of snow is easily available and easy to handle for experiments. In future work the models could be applied to different problems with different snow types and different load cases. In Chapter 5 it was already shown that a model, originally built for creep simulations, can be used to simulate the brittle failure of snow. In a next step the model could be applied to different snow types. Especially, modelling the strength of weak layers is of great importance. Weak layers are the weakest snow layers in a snowpack. Avalanches are usually released by fracture of these layers. Weak layers often consist of faceted crystals or buried surface hoar crystals. Modelling these snow types will be challenging. One important step in modelling snow presented in this thesis was the approximation of the microstructure by beam elements to reduce the computing time of the simulations. However, it is doubtful whether facetted crystals can be approximated by beam elements. This can be tested in a first step by comparing simulations of the Young's modulus of weak layers using tetrahedral and beam elements. The tetrahedral mesh is a very precise approximation of the microstructure and can be used here as a reference. If the simulation results with beam and with tetrahedral mesh differ strongly, other approaches to reduce computing time must be found. This could be a different way to simplify the microstructure, more computational power or an improved implementation of fracture simulations.

- The simulations of the creep behaviour of snow using a monocrystalline material model resulted in viscosities ten times smaller than by using a polycrystalline material model. In Figure 3.1 it is shown that both mono- and polycrystalline grains exist. It would be interesting to verify the simulation results, i.e. to show that snow made of polycrystalline

ice grains shows a different creep behaviour than snow consisting of monocrystalline ice grains. This could be shown by a creep experiment as explained in Chapter 3.2 but with these two different snow types. Ideally, we use two different snow types with the same structure but different crystallographic texture for this experiment. Polycrystalline ice grains form when water droplets freeze quickly like during the production of artificial snow by snowguns. In the lab this type of snow can be produced by injecting water droplets in liquid nitrogen. A sintered collection of these ice grains is expected to have a similar microstructure as natural round-grained snow, which consists of monocrystalline ice grains. If the simulation results are reliable the artificial snow creeps slower under the same load than the natural round-grained snow.

- Another problem directly related to the previous one is the characterisation of the crystallographic texture of different snow types. In Chapter 3 the importance of the crystallographic texture of snow was shown. However, the crystallographic texture of snow has never been systematically investigated. One question is whether all natural snow types consist of monocrystalline grains while artificial snow types consist of polycrystalline grains. In this thesis this was assumed based on a small number of observations. The method to detect single crystals in snow works as follows and should be repeated with a set of different natural and artificial snow types: by sublimating a cross section of snow for a few minutes a groove forms at the crystallographic grain boundaries. This groove can be imaged (Figure 3.1). Beside the size of the single crystals their orientation also has an impact on the behaviour of snow. In this thesis the crystal orientation was assumed to be random in the investigated snow type based on observations of Takahashi and Fujino (1977). Other snow types like surface or depth hoar are expected to have a preferred crystal orientation. Due to the highly anisotropic behaviour of ice single crystals, a preferred orientation of the ice single crystals in snow is expected to cause a highly anisotropic behaviour in snow. This could be a possible explanation why depth hoar layers densify slower than other snow layers in the snow pack.

- A long-term creep experiment (strain > 0.3) in future work could help to clarify two open questions: Does the deformation mechanism during densification change at the transition from snow to firn at a density of about 650 kg/m^3? And does snow densification follow the behaviour suggested by Kirchner et al. (2001) after an initial phase? This was suggested in Figure 3.8, but could not have been proven because of a too short experiment. Kirchner did not consider the creation of new connections in the microstructure - a mechanism responsible for the pronounced hardening behaviour of snow (as shown in Chapter 3.4.4). However, maybe the creation of new connections plays a major role only in the beginning of the densification and afterwards can be described by Kirchner's model. The first question is especially interesting for the transition from snow to firn. It is assumed that the deformation mechanism changes at a density of about 650 kg/m^3. This density corresponds to the density of the random close packing. At this point rearrangement of grains should become impossible and further densification is possible only by deformation of the grains. However, this was never investigated in a controlled creep experiment. To perform a creep experiment over a wide density range within a reasonable time frame

the load should be as large as possible without causing fracture, and temperature should be close to 0°C, since ice creeps faster the warmer it is. A problem which might occur in a long-term creep experiment is the superposition of creep and metamorphism. This point will be discussed in the next paragraph.

- It is known that snow can densify by two different mechanisms: creep or metamorphism. Unknown is the impact of metamorphism on densification. Metamorphism can have two different impacts on densification: First, the structure changes by metamorphism. With the structure also viscosity and thus the creep rate changes. Furthermore mass is transported by metamorphism, this mass transport could result in a densification of the structure. To investigate the influence of metamorphism on densification, creep experiments (like explained in Chapter 3.2) with and without metamorphism could be compared. Metamorphism can be switched off in snow by filling the pore space by a liquid (e.g. silicon oil) (Hobbs and Mason, 1964). This way vapour diffusion, the dominant mechanism during metamorphism, is suppressed. Another possibility to investigate the impact of metamorphism on densification is to vary the velocity of metamorphism during different creep experiments. Two different types of metamorphism are distinguished: equilibrium and kinetic metamorphism. Kinetic metamorphism is driven by temperature gradients which induce vapour fluxes in the snow structure. The larger the temperature gradients the higher the fluxes and thus the faster the metamorphism. By applying different temperature gradients on snow the velocity of metamorphism varies. The question is whether the rate of densification also varies.

- The question whether grain boundary sliding or intracrystalline deformation is the dominant deformation mechanism in snow is still not clearly answered. Observing the changes in the microstructure by microtomography during deformation should permit to conclude which mechanism dominates. This approach was already applied on the data from the creep experiment explained in Chapter 3.2. A relative displacement of neighbouring grains as expected for grain boundary sliding was not observed. However, the main problem was that the deformation was superimposed by metamorphism. Thus it was not possible to conclude with confidence where the deformation takes place. A creep experiment with a liquid-filled snow sample, as explained in the previous paragraph, could be used to avoid metamorphism and thus to better investigate how snow deforms. The spatial resolution of the CT-images should be as high as possible to visualise even small deformations.

- In this thesis only compressive creep experiments are described. In future work also tensile creep experiments and the change of microstructure could be investigated. Bader et al. (1939) observed a hardening behaviour during tensile creep experiments. In this thesis the hardening during compression of snow was explained by new connections forming in the snow structure. Is this also the reason for the hardening during tensile deformation?

- The methods to simplify the microstructure of snow described in this thesis could be applied to find structural parameters, which characterise snow. As explained in Chapter 1 the characterisation of snow by density and snow type is not satisfying. Snow properties

vary by up to a factor 10 for the same snow type and density (Kojima, 1967). Several structural parameters (specific surface area, grain size, bond size, coordination number or tortuosity) could be correlated with measured properties.

- The mechanisms and the behaviour during the fast deformation of snow are not well understood. According to Kirchner et al. (2001) so far no reliable data for the elastic properties of snow exist. The reason is that even for very high deformation rates the elastic deformation is superimposed by creep deformations. This was also shown in Chapter 4: We identified delayed elasticity, i.e primary creep, as the dominant deformation mechanism during a fast impact on the snow surface. This deformation is slowly recovered. A combination of grain boundary sliding and elastic deformation of the grains is expected to cause delayed elasticity. However, this assumption requires further confirmation.

References

Abbatt, J. P. D., Interactions of atmospheric trace gases with ice surfaces: Adsorption and reaction, Chemical Reviews, Volume 103, pp. 4783–4800, 2003.

Agrawal, K. C., Mittal, R. K., Influence of microstructure on mechanical properties, in Agrawal, K. C. (editor), SNOWSYMP-94 (International Symposium on Snow & Related Manifestations), 26-28 Sep., 1994, 74–86, Snow & Avalanche Study Establishment, Manali (H.P.), Manali, India, 1994.

Alley, R. B., Firn densification by grain-boundary sliding - a 1st model, Journal De Physique, Volume 48, pp. 249–256, 1987.

Ambach, W., Mayr, B., Ski Gliding and Water Film, Cold Regions Science and Technology, Volume 5, pp. 59–65, 1981.

Andrews, E. W., Gibson, L. J., Ashby, M. F., The creep of cellular solids, Acta Materialia, Volume 47, pp. 2853–2863, 1999.

Arnaud, L., Gay, M., Barnola, J. M., Duval, P., Imaging of firn and bubbly ice in coaxial reflected light: a new technique for the characterization of these porous media, Journal of Glaciology, Volume 44, pp. 326–332, 1998.

Bader, H. P., Haefeli, R., Bucher, E., Thams, C., Neher, J., Eckel, O., Der Schnee und seine Metamorphose, 3rd edition, Kümmerly & Frey, Zürich, 1939.

Baldwin, C. A., Sederman, A. J., Mantle, M. D., Alexander, P., Gladden, L. F., Determination and characterization of the structure of a pore space from 3D volume images, Journal of Colloid and Interface Science, Volume 181, pp. 79–92, 1996.

Barnes, P., Tabor, D., Walker, J. C. F., Friction and creep of polycrystalline ice, Proceedings of the Royal Society of London Series a-Mathematical and Physical Sciences, Volume 324, pp. 127–136, 1971.

Baurle, L., Kaempfer, U., Szabo, D., Spencer, N. D., Sliding friction of polyethylene on snow and ice: Contact area and modeling, Cold Regions Science and Technology, Volume 47, pp. 276–289, 2007.

Bellaire, S., Pielmeier, C., Schneebeli, M., Schweizer, J., Stability algorithm for snow micropenetrometer measurements, Journal of Glaciology, Volume 55, pp. 805–813, 2009.

Bowden, F. P., Friction on Snow and Ice, Proceedings of the Royal Society of London Series a-Mathematical and Physical Sciences, Volume 217, pp. 462–478, 1953.

Bowden, F. P., Friction on Snow and Ice and the Development of Some Fast-Running Skis, Nature, Volume 176, pp. 946–947, 1955.

Bowden, F. P., Hughes, T. P., The mechanism of sliding on ice and snow, Proceedings of the Royal Society of London Series a-Mathematical and Physical Sciences, Volume 172, pp. 0280–0298, 1939.

Bowden, F. P., Tabor, D., The friction and lubrication of solids, Clarendon Press, Oxford, 1950.

Brown, R. L., Volumetric constitutive law for snow based on a neck-growth model, Journal of Applied Physics, Volume 51, pp. 161–165, 1980.

Brown, R. L., A review of past research on the mechanical properties of snow, in Agrawal, K. C. (editor), Proceedings SNOWSYMP - 94 (International Symposium on Snow and Related Manifestations), Manali, India, 1994.

Brzoska, J.-B., Coleou, C., Lesaffre, B., Borel, S., Brissaud, O., Ludwig, W., Boller, E., Baruchel, J., 3D visualization of snow samples by microtomography at low temperature, European Synchrotron Radiation Facility Newsletter, 22–23, 1999.

Buhl, D., Fauve, M., Rhyner, H., The kinetic friction of polyethylene on snow: the influence of the snow temperature and the load, Cold Regions Science and Technology, Volume 33, pp. 133–140, 2001.

Colbeck, S. C., The Kinetic Friction of Snow, Journal of Glaciology, Volume 34, pp. 78–86, 1988.

Colbeck, S. C., A Review of the Friction of Snow Skis, Journal of Sports Sciences, Volume 12, pp. 285–295, 1994.

Colbeck, S. C., Sintering in a dry snow cover, Journal of Applied Physics, Volume 84, pp. 4585–4589, 1998.

Colbeck, S. C., Najarian, L., Smith, H. B., Sliding temperatures of ice skates, American Journal of Physics, Volume 65, pp. 488–492, 1997.

Colbeck, S. C., Perovich, D. K., Temperature effects of black versus white polyethylene bases for snow skis, Cold Regions Science and Technology, Volume 39, pp. 33–38, 2004.

Culligan, K. A., Wildenschild, D., Christensen, B. S. B., Gray, W. G., Rivers, M. L., Tompson, A. F. B., Interfacial area measurements for unsaturated flow through a porous medium, Water Resources Research, Volume 40, p. 12, 2004.

De Montmollin, V., Shear tests on snow explained by fast metamorphism, Journal of Glaciology, Volume 28, pp. 187–198, 1982.

De Winter, J., Wagemans, J., Segmentation of object outlines into parts: A large-scale integrative study, Cognition, Volume 99, pp. 275–325, 2006.

Duval, P., Ashby, M. F., Anderman, I., Rate-controlling processes in the creep of polycrystalline ice, The Journal of Physical Chemistry, Volume 87, pp. 4066–4074, 1983.

Ebinuma, T., Maeno, N., Particle Rearrangement and Dislocation Creep in a Snow-Densification Process, Journal De Physique, Volume 48, pp. 263–269, 1987.

Edens, M. Q., Brown, R. L., Changes in microstructure of snow under large deformations, Journal of Glaciology, Volume 37, pp. 193–202, 1991.

Fierz, C., Armstrong, R., Durand, Y., Etchevers, P., Greene, E., McClung, D., Nishimura, K., Satyawali, P., Sokratov, S., The international classification of seasonal snow on the ground, Technical report, 2009.

Föhn, P., Camponovo, C., Krüsi, G., Mechanical and structural properties of weak layers measured in situ, Annals of Glaciology, Volume 26, pp. 1–6, 1998.

Fukue, M., Mechanical performance of snow under loading, Technical report, Tokai University, 1979.

Fukuzawa, T., Narita, H., An experimental study on the mechanical behavior of a depth hoar under shear stress, in Proceedings International Snow Science Workshop, Breckenridge, Colorado, U.S.A., 4-8 October 1992, 171–175, 1993.

Gibson, L. J., Ashby, M. F., Cellular solids: structure and properties, first edition, Pergamon Press, Oxford, 1988.

Glenne, B., Sliding Friction and Boundary Lubrication of Snow, Journal of Tribology-Transactions of the Asme, Volume 109, pp. 614–617, 1987.

Goldsby, D. L., Kohlstedt, D. L., Reply to comment by P. Duval and M. Montagnat on "Superplastic deformation of ice: Experimental observations", Journal of Geophysical Research-Solid Earth, Volume 107, p. 17, 2002.

Golovin, Y. I., Shibkov, A. A., Shishkina, O. V., Effect of complete restoration of the ice surface after indentation in the temperature range 243-268 K, Physics of the Solid State, Volume 42, pp. 1287–1289, 2000.

Golubev, V. N., Frolov, A. D., Modelling the change in structure and mechanical properties in dry-snow densification to ice, Annals of Glaciology, Vol 26, 1998, Volume 26, pp. 45–50, 1998.

Good, W., Thin sections, serial cuts and 3-D analysis of snow, in Davos Symposium on Avalanche formation, movement and effects, Volume 162, Volume 162, pp. 35–47, IAHS Publ. 162, 1987.

Goujon, C., Barnola, J. M., Ritz, C., Modeling the densification of polar firn including heat diffusion: Application to close-off characteristics and gas isotopic fractionation for Antarctica and Greenland sites, Journal of Geophysical Research-Atmospheres, Volume 108, p. 10, 2003.

Grannas, A. M., Jones, A. E., Dibb, J., Ammann, M., Anastasio, C., Beine, H. J., Bergin, M., et al., An overview of snow photochemistry: evidence , mechanisms and impacts, Atmospheric Chemisty and Physics Discussion, Volume 7, pp. 4165–4283, 2007.

Gregory, A., State, A., Lin, M., Manocha, D., Livingston, M., Interactive surface decomposition for polyhedral morphing, The Visual Computer, Volume 15, pp. 453–470, 1999.

Gubler, H. U., Determination of the mean number of bonds per snow grain and of the dependence of the tensile strength of snow on stereological parameters, Journal of Glaciology, Volume 20, pp. 329–341, 1978.

Hahn, H. G., Bruchmechanik, first edition, B. G. Teubner, Stuttgart, 1976.

Hamalainen, T., Influence of snow hardness on ski friction, Commentationes Physico-Mathematicae, Volume 76, pp. 1–17, 1986.

Hansen, A. C., Brown, R. L., An internal state variable approach to constitutive theories for granular materials with snow as an example, Mechanics of Materials, Volume 7, pp. 109–119, 1988a.

Hansen, A. C., Brown, R. L., An Internal State Variable Approach to Constitutive Theories for Granular-Materials with Snow as an Example, Mechanics of Materials, Volume 7, pp. 109–119, 1988b.

Heggli, M., Frei, E., Schneebeli, M., Snow replica method for three-dimensional X-ray microtomographic imaging, Journal of Glaciology, Volume 55, pp. 631–639, 2009.

Hobbs, P., Mason, B., The sintering and adhesion of ice, Philosophical Magazine, Volume 9, pp. 181–197, 1964.

Hoffman, D., Salience of visual parts, Cognition, Volume 63, pp. 29–78, 1997.

Huthwelker, T., Ammann, M., Peter, T., The uptake of acidic gases on ice, Chemical Reviews, Volume 106, pp. 1375–1444, 2006.

Huzioka, T., Studies on the resistance of a snow sledge, 5. Friction between snow and a plastic plate, Low Temperature Science, Volume A20, pp. 159–180, 1962.

Ignat, M., Frost, H. J., Grain-boundary sliding in ice, Journal De Physique, Volume 48, pp. 189–195, 1987.

Ioannidis, M. A., Chatzis, I., On the geometry and topology of 3D stochastic porous media, Journal of Colloid and Interface Science, Volume 229, pp. 323–334, 2000.

Jamieson, J. B., Johnston, C. D., Evaluation of the shear frame test for weak snowpack layers, Annals of Glaciology, Volume 32, pp. 59–68, 2001.

Johnson, J. B., Hopkins, M. A., Identifying microstructural deformation mechanisms in snow using discrete-element modeling, Journal of Glaciology, Volume 51, pp. 432–442, 2005.

Johnson, K. L., Contact Mechanics, Cambridge University Press, Cambridge, 1985.

Joshi, S., Mahaja, P., Upadhyay, A., Study of layered snow under shear and tension, in Gleason, A. (editor), Proceedings ISSW 2006, International Snow Science Workshop, 165–173, Telluride, Colorado, USA, 2006.

Kaempfer, T. U., Schneebeli, M., Sokratov, S. A., A microstructural approach to model heat transfer in snow, Geophysical Research Letters, Volume 32, pp. 1–10, 2005.

Katz, S., Leifman, G., Tal, A., Mesh segmentation using feature point and core extraction, The Visual Computer, Volume 21, pp. 649–658, 2005.

Kim, H., Keune, J. N., Compressive strength of ice at impact strain rates, Journal of Materials Science, Volume 42, pp. 2802–2806, 2007.

Kinosita, S., Compression of snow at constant speed, Physics of Snow and Ice: proceedings, Volume 1, pp. 911–927, 1967.

Kirchner, H. O. K., Michot, G., Narita, H., Suzuki, T., Snow as a foam of ice: plasticity, fracture and the brittle-to-ductile transition, Philosophical Magazine a-Physics of Condensed Matter

Structure Defects and Mechanical Properties, Volume 81, pp. 2161–2181, 2001.

Kojima, K., Densification of seasonal snow cover, Physics of Snow and Ice: proceedings, Volume 1, pp. 929–952, 1967.

Kry, P. R., Quantitative stereological analysis of grain bonds in snow, Journal of Glaciology, Volume 14, pp. 467–477, 1975a.

Kry, P. R., The relationship between the visco-elastic and structural properties of fine-grained snow, Journal of Glaciology, Volume 14, pp. 479–477, 1975b.

Kwiecien, M. J., Macdonald, I. F., Dullien, F. A. L., Three-dimensional reconstruction of porous media from serial section data, Journal of Microscopy, Volume 159, pp. 343–359, 1990.

Lebensohn, R. A., Montagnat, M., Mansuy, P., Duval, P., Meysonnier, J., Philip, A., Modeling viscoplastic behavior and heterogeneous intracrystalline deformation of columnar ice polycrystals, Acta Materialia, Volume 57, pp. 1405–1415, 2009.

Lehning, M., Bartelt, P., Brown, B., Fierz, C., Satyawali, P., A physical SNOWPACK model for the Swiss avalanche warning: Part II. Snow microstructure, Cold Regions Science and Technology, Volume 35, pp. 147–167, 2002.

Liang, Z., Ioannidis, M. A., Chatzis, I., Geometric and topological analysis of three-dimensional porous media: Pore space partitioning based on morphological skeletonization, Journal of Colloid and Interface Science, Volume 221, pp. 13–24, 2000a.

Liang, Z., Ioannidis, M. A., Chatzis, I., Permeability and electrical conductivity of porous media from 3D stochastic replicas of the microstructure, Chemical Engineering Science, Volume 55, pp. 5247–5262, 2000b.

Libbrecht, K. G., The physics of snow crystals, Reports on Progress in Physics, Volume 68, pp. 855–895, 2005.

Lind, D., Sanders, S. P., The physics of skiing, Springer-Verlag, New York, 1996.

Matzl, M., Schneebeli, M., Measuring specific surface area of snow by near-infrared photography, Journal of Glaciology, Volume 52, pp. 558–564, 2006.

McClung, D. M., In-situ estimates of the tensile strength of snow utilizing large sample sizes, Journal of Glaciology, Volume 22, pp. 321–329, 1979.

Mellor, M., A review of basic snow mechanics, in Snow mechanics symposium, 251–291, IAHS-AISH, 114: 251-291, Grindelwald, Switzerland, 1975.

Meysonnier, J., Philip, A., Capolo, L., Mansuy, P., Experimental studies of the viscoplasticity of ice and snow, in Kolymbas, D., Viggiani, G. (editors), Mechanics of natural solids, Springer, Berlin, 2009.

Miguel, M. C., Andrade, J. S., Zapperi, S., Deblocking of interacting particle assemblies: from pinning to jamming, Brazilian Journal of Physics, Volume 33, pp. 557–572, 2003.

Mowers, T., Budd, D., Quantification of porosity and permeability reduction due to calcite cementation using computer-assisted petrographic image analysis techniques., American As-

sociation of Petroleum Geologists Bulletin, Volume 80, p. 14, 1996.

Nakaya, U., Matsumoto, A., Simple Experiment Showing the Existence of Liquid Water Film on the Ice Surface, Journal of Colloid Science, Volume 9, pp. 41–49, 1954.

Narita, H., An experimental study on tensile fracture of snow, Contributions from the Institute of Low Temperature Science, Volume 32, pp. 1–37, 1983.

Nicot, F., Constitutive modelling of snow as a cohesive-granular material, Granular Matter, Volume 6, pp. 47–60, 2004.

Ogawa, N., Flin, F., Brzoska, J., Representation of two curvatures of surface and its application to snow physics, Memoirs of the Hokkaido Institute of Technology, Volume 34, p. 7, 2006.

Ohser, J., Schladitz, K., 3D Images of Materials Structures - Processing and Analysis, 1st edition, Wiley-VCH, Weinheim, 2009.

Oswald, S., Kinzelbach, W., Greiner, A., Brix, G., Observation of flow and transport processes in artificial porous media via magnetic resonance imaging in three dimensions, Geoderma, Volume 80, pp. 417–429, 1997.

Petrenko, V. F., Study of the surface of ice, ice/solid and ice/liquid interfaces with scanning force microscopy, Journal of Physical Chemistry B, Volume 101, pp. 6276–6281, 1997.

Petrovic, J. J., Mechanical properties of ice and snow, Journal of Materials Science, Volume 38, pp. 1–6, 2003.

Pinzer, B., Dynamics of temperature gradient snow metamorphism, Ph.D. thesis, ETH Zurich, 2009.

Pittenger, B., Fain, S. C., Cochran, M. J., Donev, J. M. K., Robertson, B. E., Szuchmacher, A., Overney, R. M., Premelting at ice-solid interfaces studied via velocity-dependent indentation with force microscope tips, Physical Review B, Volume 6313, pp. –, 2001.

Pothuaud, L., Van Rietbergen, B., Charlot, C., Ozhinsky, E., Majumdar, S., A New Computational Efficient Approach for Trabecular Bone Analysis using Beam Models Generated with Skeletonized Graph Technique, Computer Methods in Biomechanics and Biomedical Engineering, Volume 7, pp. 205 – 213, 2004.

Pudasaini, S. P., Hutter, K., Avalanche Dynamics: Dynamics of Rapid Flows of Dense Granular Avalanches, Springer-Verlag, New York, 2007.

Ree, J. H., Grain boundary sliding in experimental deformation of octachloropropane, Journal of the Virtual Explorer, Volume 2, 2000.

Reiweger, I., Schweizer, J., Dual, J., Herrmann, H. J., Modelling snow failure with a fibre bundle model, Journal of Glaciology, Volume 55, pp. 997–1002, 2009.

Salm, B., Mechanical properties of snow, Reviews of Geophysics and Space Physics, Volume 20, pp. 1–19, 1982.

Sanderson, T. J. O., Mechanical properties of ice: laboratory studies, in Ice mechanics: Risk to offshore structures, 70–103, Graham & Trotman, London, 1988.

Satyawali, P. K., Schneebeli, M., Pielmeier, C., Stucki, T., Singh, A. K., Preliminary characterization of Alpine snow using SnowMicroPen, Cold Regions Science and Technology, Volume 55, pp. 311–320, 2009.

Scapozza, C., Bartelt, P., Triaxial tests on snow at low strain rate. Part II. Constitutive behaviour, Journal of Glaciology, Volume 49, pp. 91–101, 2003.

Schladitz, K., Peters, S., Reinel-Bitzer, D., Wiegmann, A., Ohser, J., Design of acoustic trim based on geometric modeling and flow simulation for non-woven, Computational Materials Science, Volume 38, pp. 56–66, 2006.

Schneebeli, M., Numerical simulation of elastic stress in the microstructure of snow, Annals of Glaciology, Volume 38, pp. 339–342, 2004.

Schneebeli, M., Johnson, J. B., A constant speed penetrometer for high resolution stratigraphy, Annals of Glaciology, Volume 26, pp. 107–111, 1998.

Schneebeli, M., Sokratov, S. A., Tomography of temperature gradient metamorphism of snow and associated changes in heat conductivity, Hydrological Processes, Volume 18, pp. 3655–3665, 2004.

Schulson, E. M., Duval, P., Creep and Fracture of Ice, first edition, University Press, Cambridge, 2009.

Schweizer, J., Laboratory experiments on shear failure of snow, Annals of Glaciology, Volume 26, pp. 97–102, 1998.

Serra, J., Image Analysis and Mathematical Morphology, 1st edition, Academic Press, Inc., Orlando, 1983.

Shapiro, L. H., Johnson, J. B., Sturm, M., Blaisdell, G. L., Snow mechanics - Review of state of knowledge and applications, Technical Report CRREL Technical Rep. 97-3, CRREL, 1997.

Shi, W., Cheung, C., Performance Evaluation of Line Simplification Algorithms for Vector Generalization, The Cartographic Journal, Volume 43, pp. 27–44, 2006.

Shu, X., Huang, B. S., Predicting dynamic modulus of asphalt mixtures with differential method, Road Materials and Pavement Design, Volume 10, pp. 337–359, 2009.

Singh, S. K., Jordaan, I. J., Constitutive behaviour of crushed ice, International Journal of Fracture, Volume 97, pp. 171–187, 1999.

Sinha, N. K., Ehrhart, P., Carstanjen, H. D., Fattah, A. M., Roberto, J. B., Grain boundary sliding in polycrystalline materials, Philosophical Magazine A, Volume 40, pp. 825 – 842, 1979.

Soille, P., Morphological image analysis, Springer-Verlag, Berlin, 1999.

Solymar, M., Fabricius, I. L., Image analysis and estimation of porosity and permeability of Arnager Greensand, Upper Cretaceous, Denmark, Physics and Chemistry of the Earth, Part A: Solid Earth and Geodesy, Volume 24, pp. 587–591, 1999.

Sommerfeld, R., A Weibull prediction of the tensile strength-volume relationship of snow, Jour-

nal of Geophysical Research, Volume 79, pp. 3353–3356, 1974.

Speijer, R. P., Van Loo, D., Masschaele, B., Vlassenbroeck, J., Cnudde, V., Jacobs, P., Quantifying foraminiferal growth with high-resolution X-ray computed tomography: New opportunities in foraminiferal ontogeny, phylogeny, and paleoceanographic applications, GEOSPHERE, Volume 4, pp. 760–763, 2008.

Srivastava, P. K., Mahajan, P., Satyawali, P. K., Kumar, V., Observation of temperature gradient metamorphism in snow by X-ray computed microtomography: measurement of microstructure parameters and simulation of linear elastic properties, Annals of Glaciology, Volume 51, pp. 73–82, 2010.

Stauber, M., Huber, M., van Lenthe, G. H., Boyd, S. K., Müller, R., A Finite Element Beammodel for Efficient Simulation of Large-scale Porous Structures, Computer Methods in Biomechanics and Biomedical Engineering, Volume 7, pp. 9 – 16, 2004.

Steinemann, S., Experimentelle Untersuchungen zur Plastizität von Eis, Ph.D. thesis, ETH, 1958.

Stroeven, P., He, H., Guo, Z., Stroeven, M., Particle packing in a model concrete at different levels of the microstructure: Evidence of an intrinsic patchy nature, Materials Characterization, Volume 60, pp. 1088–1092, 2009.

Takahashi, T., Fujino, K., Crystal orientation of fabrics in a snow pack, Low temperature science. Ser. A, Physical sciences, Volume 34, p. 8, 1977.

Tao, W., Anup, B., A note on 'A fully parallel 3D thinning algorithm and its applications', Pattern Recognition Letters, Volume 28, pp. 501–506, 2007.

Tschirky, F., Brabec, B., Kern, M., Avlanche rescue systems in switzerland: Experience and limitations, in Proceedings of the International Snow Science Workshop, 369–376, Montana State University, Bozeman, U.S.A., Big Sky, Montana, U.S.A, 2001.

Tusima, K., Yosida, Z., The melting of ice by friction, Low Temperature Science, Volume A27, pp. 17–39, 1969.

van Rietbergen, B., Weinans, H., Huiskes, R., Odgaard, A., A new method to determine trabecular bone elastic properties and loading using micromechanical finite-element models, Journal of Biomechanics, Volume 28, pp. 69–81, 1995.

Voitkovsky, K. F., Bozhinsky, A. N., Golubev, V. N., Laptev, M. N., Zhigulsky, A. A., Slesarenko, Y. Y., Creep-induced changes in structure and density of snow, in Rodda, J. C., Kisby, P. (editors), Snow Mechanics Symposium, 171–179, IAHS Proceedings and Reports "Red Books" Publication, International Association of Hydrological Sciences, Grindelwald, Switzerland, 1974.

Wakahama, G., Internal strain and changes in the microscopic texture of snow caused by compression. I. : Compression of thin section of snow by a static load, Low temperature science. Series A, Physical sciences, Volume 19, p. 35, 1960a.

Wakahama, G., Internal strain and changes in the microscopic texture of snow caused by compression. II. : Compression of thin section of snow at a constant speed, Low temperature

science. Series A, Physical sciences, Volume 19, p. 23, 1960b.

Wakahama, G., The role of meltwater in desification processes of snow and firn, in Snow Mechanics Symposium, Volume 114, Volume 114, pp. 66–72, Int Assoc Sci Hydrol Pub, Grindelwald, Switzerland, 1974.

Ward, I. M., Pinnock, P. R., The mechanical properties of solid polymers, British Journal of Applied Physics, Volume 17, p. 3, 1966.

Wettlaufer, J. S., Ice surfaces: macroscopic effects of microscopic structure, Philosophical Transactions of the Royal Society of London Series a-Mathematical Physical and Engineering Sciences, Volume 357, pp. 3403–3425, 1999a.

Wettlaufer, J. S., Impurity effects in the premelting of ice, Physical Review Letters, Volume 82, pp. 2516–2519, 1999b.

Yeong, C. L. Y., Torquato, S., Serial sectioning and digitization of porous media for two- and three-dimensional analysis and reconstruction, Physical Review Letters E, Volume 58, pp. 224–238, 1998.

Zhao, H. Q., Macdonald, I. F., Kwiecien, M. J., Multi-orientation scanning: Necessity in the identification of pore necks in porous media by 3-D computer reconstruction from serial section data, Journal of Colloid and Interface Science, Volume 162, pp. 390–401, 1994.

Zuckerberger, E., Tal, A., Shlafman, S., Polyhedral surface decomposition with applications, Computers and Graphics-Uk, Volume 26, pp. 733–743, 2002.

Acknowledgements

The work presented in this thesis was carried out between 2007 and 2010 during my time at the Institute for Snow and Avalanche Research SLF in Davos. Neither the work nor the life here would have been possible or as pleasant without the help and company of many persons. Thank you all for your support!

I especially want to thank my supervisor Martin Schneebeli for his support and for providing me with inspiring advice through all these years. His friendly and optimistic attitude created a genial and motivating working environment. Further, I would like to thank Professor Bob Svendsen for his interest in my work, for accepting me as a PhD student and thus for the possibility to work with the fascinating material snow. Furthermore I thank Jun.-Professor Svantje Bargmann for her willingness to examine this thesis.

Next I want to thank my fellow workers responsible for the friendly atmosphere at the SLF and in our group. Especially, I would like to express my gratitude to my office neighbour Henning for all his help, for the many discussions we had on various scientific issues and for all his corrections and suggestions after reviewing hardly understandable drafts. The combination of knowledge and helpfulness just in my office was very useful to me and has facilitated my research a lot. Furthermore I would like to thank Denes for all the selfless help and for encouraging me to do this work. I thank my "little" brother Tom for his valuable help with experimental work, data analysis, skiing and simulations during his internship at the SLF. Moreover I thank Stephen, Bernd, Martin, Mathias, Matthias, Magret and Fabienne from the team snowphysics for all the fruitful discussions, corrections, coffee breaks and laboratory assistance.

Many thanks also go to Silvia Dingwall for her excellent language corrections, to Yoni De Witte from the Centre for X-ray Tomography of the Ghent University for providing some 3D image data, and to Benjamin Klusemann and Kerstin Walter for all their help with the details of handing in a PhD thesis at the TU Dortmund. Furthermore the financial support by Bridgestone is gratefully acknowledged.

Last but not least, I would like to thank my parents for all their support and my friends for spending time with me outdoors or in pubs making life here so eventful and pleasant. And finally many thanks to Berna.

Curriculum Vitae

Personal

Name:	Thiemo Claas Theile
Date of Birth:	June 15, 1980
Place of Birth:	Herdecke, Germany
Nationality:	German

Education and Experience

1986-1999	Primary and secondary school, Herdecke, Germany
2000-2007	Diploma studies in Mechanical Engineering, TU Dortmund, Germany
2003-2004	Master studies in Industrial Engineering, Georgia Institute of Technology, Atlanta, USA
2007-2010	Doctoral Student, WSL Institute for Snow and Avalanche Research SLF and Institute of Mechanics, TU Dortmund, Germany